Faculdade de Engenharia da Universidade do Porto

Validation of two types of textile electrodes for electrocardiography and electromyography measurement applications

Pedro Filipe Pereira da Fonseca

DISSERTATION SUBMITTED TO FACULDADE DE ENGENHARIA DA UNIVERSIDADE DO PORTO FOR PARTIAL FULFILMENT OF THE REQUIREMENTS OF THE MASTER IN BIOMEDICAL ENGINEERING

FINAL VERSION

July 2012

The present dissertation was partially funded by FCT: Fundação para a Ciência e a Tecnologia (Portuguese Foundation for Science and Technology), and integrated in the projects BIOSWIM (PTDC/EEA-ELC/70803/2006) and PROLIMB (PTDC/EEA-ELC/103683/2008), under the supervision of:

Professor Doutor Miguel Velhote Correia
Professor Doutor João Paulo Vilas-Boas

Dedication

To all that are dear to me.

Abstract

Wearable systems are a growing trend in multipurpose biosignals acquisition, combining monitoring systems with garments or pieces of clothing in order to obtain inconspicuous wearable devices. The use of textile electrodes in wearable monitoring devices became very popular because of the simplicity and homogeneity provided by embedding them in a piece of fabric or garment, being currently the *de facto* standard in this kind of applications. Textile electrodes can be manufactured using several methods and conductive yarns made of different materials, each one with distinct electrical properties.

In this study, the validation of two types of textile electrodes, one for electrocardiographic (ECG) and another for electromyographic (EMG) applications, was performed using as comparison the standard conventional silver-chloride electrodes. The electrical properties of the three types of electrodes were evaluated by means of skin-electrode impedance measurements, and their measuring capability was assessed by more detailed analyses. The ECG validation procedure included the measurement of ECG biopotentials simultaneously using the ECG textile electrodes and the standard electrodes at rest, so that a direct comparison between morphology, time domain and frequency domain variables of the signals could be done. Identical procedure was used with the EMG textile electrodes, since the biopotentials were also recorded simultaneously with the textile and standard electrodes. To this end both electrode sets were placed on the *biceps brachii* muscle belly at the same time as close as possible and voluntary isometric contractions with three sub-maximal loads were performed.

Results showed that the ECG textile electrodes are capable of measuring ECG signals with identical morphology to those of the standard electrodes. The interval period between consecutive R-waves (IRR) was the same in the signals from both electrodes, and the power-spectrum distribution was also similar. The Bland-Altman diagrams reinforced these results showing a good agreement between both types of electrodes. The EMG textile electrodes showed identical results to those of the standard electrodes at all the sub-maximal loads. Pattern and frequency distribution was very similar, with only a few differences that can be attributed to the fact that the electrodes could not have been placed on the exact same

place. Time-frequency analysis did not show any significant differences between the spectrogram of each electrode's signal, and the Bland-Altman diagrams corroborated that textile and standard electrodes have a good agreement in voluntary isometric contractions.

Resumo

Os sistemas vestíveis são uma tendência crescente na aquisição de sinais biológicos genéricos, combinando sistemas de monitorização com vestimentas ou peças de vestuário de modo a obter dispositivos vestiveis discretos. A utilização de eléctrodos têxteis em sistemas de monitorização vestiveis tornou-se muito popular devido à simplicidade e homogeneidade providenciada pela sua introdução em peças de tecido ou vestimentas, sendo actualmente o tipo de eléctrodo padrão neste tipo de aplicações. Os eléctrodos têxteis podem ser fabricados usando diversos métodos e fibras condutoras de diversos materiais, cada um com propriedades eléctricas distintas.

Neste estudo, a validação de dois tipos de eléctrodos têxteis, um para aplicações electrocardiográficas (ECG) e outro para electromiográficas (EMG), foi realizada usando como comparação os eléctrodos convencionais de cloreto de prata. As propriedades eléctricas dos três tipos de eléctrodos foram avaliadas por meio de medições da impedância pele-eléctrodos, e a sua capacidade de medição foi avaliada por análises mais detalhadas. O procedimento de validação ECG incluiu a medição destes biopotenciais simultaneamente usando eléctrodos têxteis de ECG e os eléctrodos padrão em repouso, de modo a uma comparação directa entre variáveis morfologicas, do dominio temporal e de frequências pudesse ser feita. Procedimento idêntico foi usado com os eléctrodos têxteis de EMG, uma vez que os biopotenciais foram também recolhidos simultaneamente com os eléctrodos têxteis e os eléctrodos padrão. Para este fim, os dois conjuntos de eléctrodos foram colocados simultaneamente sobre a barriga do músculo *biceps brachii*, tão próximos quanto possivel, e contrações isométricas voluntárias com três cargas sub-máximas foram realizadas.

Os resultados mostraram que os eléctrodos têxteis de ECG são capazes de medir sinais ECG com morfologia idêntica à dos eléctrodos padrão. O período de intervalo entre ondas R consecutivas (IRR) foi o mesmo nos sinais de ambos os eléctrodos, e a distribuição de energia no espectro de frequências foi também semelhante. Os diagramas de Bland-Altman reforçaram estes resultados, mostrando uma boa concordância entre os dois tipos de eléctrodos têxteis. Os eléctrodos têxteis de EMG mostraram resultados idênticos aos dos eléctrodos padrão para todas as cargas sub-máximas. O padrão e distribuição das frequências

foi muito semelhante, com apenas algumas diferenças que podem ser atribuidas ao facto de os eléctrodos não poderem ser colocados exatamente no mesmo local. Análise de tempo-frequência não revelou nenhuma diferença significativa nos espectrogramas dos sinais dos eléctrodos têxteis e padrão, e os diagramas Bland-Altman corroboraram que os eléctrodos têxteis e os padrão possuem uma boa concordância durante contracções isométricas voluntárias.

Acknowledgments

To Professor Miguel Velhote Correia, who was always available to clarify my questions even if they took too much of his time, and for the exemplar guidance that allowed me to expand my understanding in various aspects of biomedical signal analysis.

To Professor João Paulo Vilas-Boas for receiving me in his laboratory where I learned much more than I was expecting, and for giving me the opportunity to discover the amazing relationship that engineering and sports sciences can have.

To Professor André Catarino, whose assistance was fundamental during the course of this thesis, for providing the necessary study material and clarify my always numerous questions.

To Dr. Márcio Borgonovo, whose assistance was more important than I can describe, and that always had time and patience to teach me something new.

To the Faculty of Sports of the University of Porto Biomechanics Laboratory team, namely Professor Leandro Machado, Professor Filipa Sousa, Dr. Marcelo Castro, Eng. Sofia Abreu and Dr. Denise Soares, for their constant good mood and for sharing their extensive knowledge and experience.

To all my friends who have been available when I need their help.

To my family, that was my first and most enthusiastic supporters.

To my grandparents and my brother that always expressed their unconditional support and pride.

To my parents, for having been my role models and giving me the opportunities they did not had.

To my girlfriend Sónia Gomes, for her comprehension and support whenever I needed, for always know what to say to keep me in the right path, but above all for believing in me.

Contents

List of Figures

List of Tables

Abbreviations and Symbols

Abbreviation	Description
Amp	Amplification
AVRR	Averaged interval between R-waves
BM	Bridge Method
DC	Direct Current
Deg	Degree
dIRR	Difference between corresponding R-wave intervals
ECG	Electrocardiogram
EMG	Electromyogram
IC	Integrated Circuit
IHCP	Improved Howland Current Pump
IMF	Instantaneous Median Frequency
iRMS	Integral of the Root Mean Square envelope
IRR	Interval between R-waves
MDF	Median Frequency
MSE	Mean Square Error
MVC	Maximum Voluntary Contraction
PDA	Personal Digital Assistant
pRMS	Peak value of the Root Mean Square envelope
PSD	Power Spectrum Density
QD	Quadrature Demodulation
RC	Resistor-Capacitor
RMS	Root Mean Square
RMS	Root Mean Square Error
SD	Standard Deviation
SNR	Signal-to-Noise Ratio
SDRR	Standard Deviation of the interval between R-waves

STFT	Short-Time Fourier Transform
TKEO	Teager-Kaiser Energy Operator
VCCS	Voltage Controlled Current Source

Symbol	**Description**
Z	Impedance Magnitude
φ	Impedance Phase

Chapter 1

Introduction

1.1. Motivation

The measurement of biopotentials is rather common, both in the medical and research contexts, in particular the measurement of the cardiac and muscular activity. For this purpose, it is necessary to use a sensor capable of transforming the ionic currents within the body to electrical signals that can be measured by conventional electronic systems.

Several types of electrodes have been used with different shapes, sizes and fixing mechanisms, but all of them use silver-chloride as a transducer material, generally in a form of a metallic disc. This is due to silver-chloride's good electrical properties and stability when measuring biopotentials. Recently, the market of physiological monitoring systems suffered a paradigm shift with the increase of personal sensorised textile garments. A transversal characteristic to these garments is their use in long-term electrocardiogram and electromyogram physiological measurement. With this new line of technology development based on textile wearable systems, the conventional silver-chloride electrodes present some limitations and disadvantages such as skin irritation, the fact they are not reusable and the heterogeneity of the connections between the electrode and the textile substrate of the garment. This has led to a necessity in research alternative electrodes that could be used in textile garments.

One alternative, popular to the point of becoming the most common (almost standard) in sensorised garments, is the textile electrode. The main reasons for this is their easy integration into the garment's fabric, enabling discreet biopotentials measurements, and being reusable. The diversity of the manufacturing methods and conductive yarns available, plus the lack of standardized fabrication methods led to the existence of several models of

textile electrodes. Although advantageous in some applications, it is still a relatively recent technology. Therefore, whenever a new fabrication method is tried out, the resulting electrode should be characterized in terms of its electrical properties and the recorded signals features, in order to determine if it is a feasible and reliable alternative to the standard silver-chloride electrodes.

1.2. Objectives

The present dissertation aims at performing a validation study of the electrical properties and features of the signals recorded with two types of textile electrodes, one for electrocardiography and another for electromyography, against those of one standard silver-chloride electrode. To this end, the following objectives were established:

- To compare the skin-electrode interaction of the two types of textile electrodes with respect to the standard silver-chloride electrodes;
- To qualitatively and quantitatively compare the electrophysiological signals recorded using the two types of textile electrodes with those recorded using standard silver-chloride electrodes.

1.3. Main Contributions

With this dissertation is expected to provide a better understanding on the electrical and measuring properties of two types of textile electrodes, revealing the particular characteristics of each one and the possibility of using them as an alternative to the conventional standard silver-chloride electrodes.

1.4. Structure

This dissertation is divided into three parts, representing the three stages of research undertaken to validate the two types of textile electrodes.

In the first part, comprised by Chapter 2 and Chapter 3, a review of relevant literature was carried out. Chapter 2 begins by addressing the present state of development of personal monitoring systems, in particular those using sensorial elements based on textile technology. Next, in Chapter 3, the textile electrodes are described in more detail as textile sensors for physiological measurements, from their characteristics and electrical properties, to their manufacturing methods and electrical interaction with the skin.

The second part consists in Chapter 4, in which a brief overview on a voltage-to-current converter is presented in order to introduce the circuit designed to measure skin-electrode impedance. After this, the standard silver-chloride and the textile electrodes used in this dissertation are presented and their skin-electrode impedance are measured and evaluated.

The third and last part is composed by Chapter 5, Chapter 6 and Chapter 7, where comparisons between textile electrodes and standard silver-chloride electrodes were made. This analysis starts in Chapter 5 with the electrocardiography textile electrode signals being morphological, time and frequency compared against the standard silver-chloride electrode signals during measurements at rest. In Chapter 6, a morphological, frequency and time-frequency spectrum comparison is performed to compare the signals recorded using the electromyography textile electrodes during isometric contractions with different sub-maximal loads. To conclude, in Chapter 7 a general discussion and general conclusions of this dissertation are presented.

Chapter 2

Wearable monitoring systems

2.1. Origin of the Sensory Garments

Clothing is a fundamental aspect on people's life, either to protect them against the weather conditions, or to establish an individual identity and personality. When sensory capabilities, or the ability to display and transmit data, are given to clothes they become part of the smart clothing group. They are able to feel and communicate with the surrounding environment, respond to the user status and to stimuli of electrical, thermal, mechanic, chemic, magnetic or other nature (Gilsoo *et al.*, 2011; Tao, 2001). In turn, wearable computational systems can be defined as mobile electronic devices that can be applied in a discreet and comfortable way into a piece of clothing or accessory (Anliker *et al.*, 2004).

After several projects carried out by military and academic entities to create garments with sensorial or computational capabilities, Lind (1997), from the Georgia Institute of Technology, gave the first step toward the creation of textile based systems, in the form of a sensorised shirt called "Sensate Liner". The second stage of development of this shirt was introduced by Gopalsamy (1999), who called it "Wearable Motherboard", a name that became famous. Its main objectives were to monitor vital signs (blood pressure, heart rhythm, respiratory rate, electrocardiographic activity) and, through optical and electronic sensors, detect the penetration of projectiles. At the same time, Schwartz (1999) of the Massachusetts Institute of Technology (MIT) presented the Smart-Vest, a system that allowed the implementation of a microcomputer on a lightweight mesh jacket. This did not explore the sensory potentialities of the textile fabric, using it merely as a support for conventional instruments.

According to Fabrice (2005) it is possible to distinguish smart clothing into two distinct groups. The first group is characterized by having sensors very close to the skin, either by placing them over fabric, or using the fabric itself as a sensory element. These clothes are typically used in biomedical application for physiological measurements. The second group involves the use of sensors and devices in pockets, and although they are not capable of physiological measurements, they allow the integration of micro-radios, microcomputers, flexible screens and keyboards, or even display images and colours. Although distinct, these two groups of smart garments are compatible and complementary. Considering this classification, the work done by Gopalsamy (1999) may be included in the first group, while Schwartz's (1999) would fit in the second.

2.2. Applications

According to Ariyatum (2005), the applications of smart clothing can be categorized as military, medical, communications, entertainment and sports, since they are products with commercial potential, and they fall into the current trends of healthy lifestyle and well-being (Dittmar *et al.*, 2005). Therefore, the growth of each of these sectors is dependent on the associated market demand. Figure 2.1 presents not only some of the main applications of the smart wearable systems, as also classifies them in terms of cost and functionality.

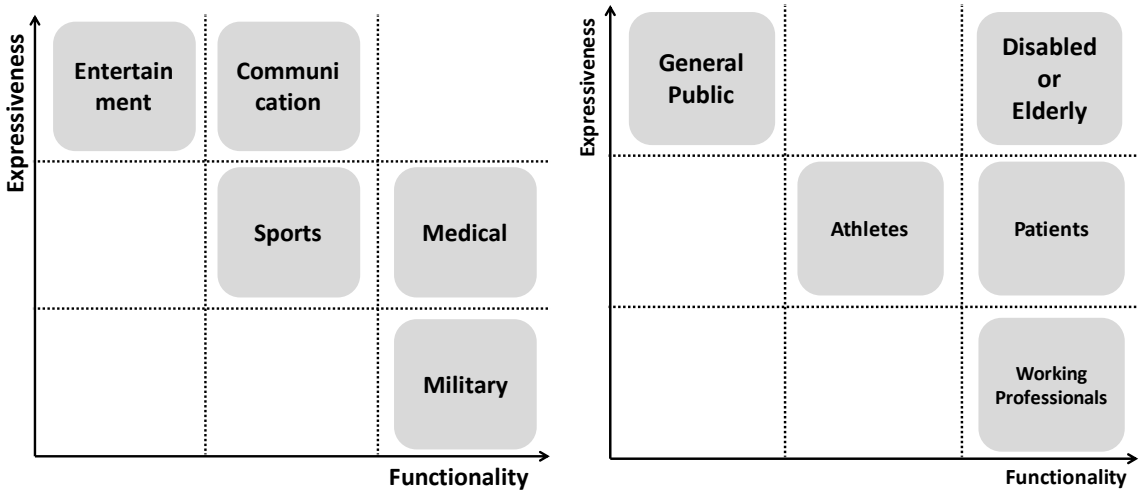

Figure 2.1- Distribution of the smart clothing market according to the (a) product and (b) to the user (reproduced from Suh *et al.*(2010)).

2.3. Textile Sensors: a Trend in Physiological Measurement

The primacy of wearable systems directed to clinical monitoring is attributed to the high costs associated with these services. The use of systems that allows the constant monitoring of an individual without the need to stay in a hospital can reduce the hospitalization time,

the healthcare costs and improve the patient's quality of life (Bifulco *et al.*, 2011). Allying financial issues with the fact that population over 65 years old is increasing, it becomes evident the advantages of using these systems to aid senior citizens who do not have the opportunity to benefit from a permanent personalized health care service.

As Mestrovic (2007) refers, several sensors can be embedded in clothing thus making a wearable system. Despite its name, many wearable systems are not really comfortable and discreet due to the heterogeneity between sensors and clothing. In order to provide a greater integration of the sensors in the garments, it is possible to use textile technology. This allows to manufacture flexible, lightweight, robust and washable textile sensors that can be fully integrated into a garment, increasing comfort and making them more suitable for long-term monitoring (Bifulco *et al.*, 2011; Bourdon *et al.*, 2005; Coosemans *et al.*, 2006; Kirstein *et al.*, 2005; Pola & Vanhala, 2007).

The use of conductive yarns has been studied with the objective of developing fully textile sensors that could be embedded in a common piece of clothing. However, with the exception of the textile electrodes, textile research is fragmented or still in its early stages of development (Bonfiglio & Rossi, 2010).

2.3.1. Respiratory Activity Sensors

The measurement of respiratory activity in wearable systems may be performed using different kinds of sensors. Traditionally, the variation of the thorax diameter (plethysmography) or impedance (pneumography) is measured, but there are also inductive and pressure methods available.

The use of conductive fibres as piezoresistive sensors to measure thoracic and abdominal respiration was explored by Loriga (2005) and Enzo Pasquale (2005), who took advantage of the fact of these fibres behave like strain-gauges to relate changes in their resistance value with the increase and decrease of lung volume. An alternative approach goes by measuring the impedance changes caused by different concentrations of gases inside the lungs. For this purpose, four electrodes are placed on the thorax through which a high frequency current is injected. By measuring the voltage drop induced by the different impedances during the inspiration and expiration phases it is possible to infer about the respiratory activity (Loriga *et al.*, 2005).

The inductive option depends on the use of coils, as the ones used in "Respibelt" (Catrysse *et al.*, 2004), which are made of stainless steel on a lycra substrate and are pressed against the user's chest. When breathing, the coil's circumference and length will change, resulting in an inductance and resistance change, allowing the measurement of both the perimeter and section changes in the thorax and abdomen.

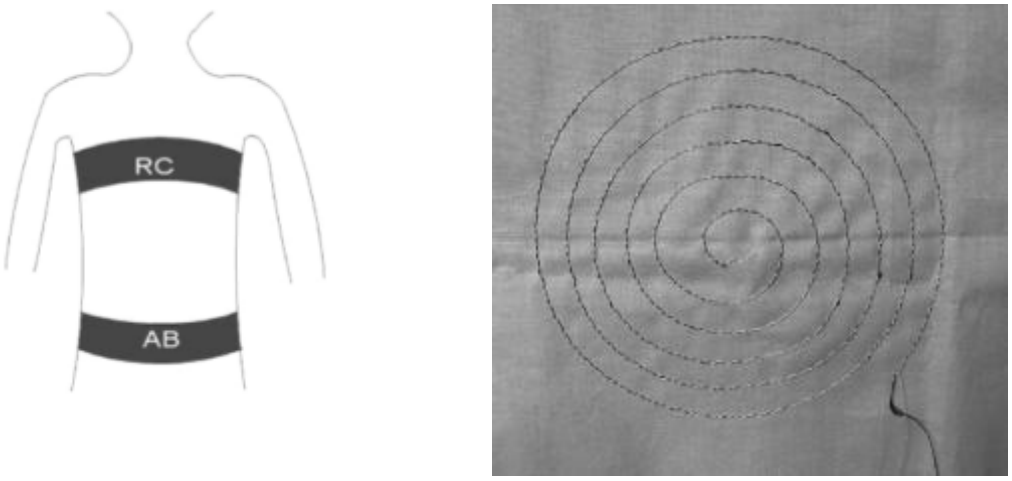

(a) (b)

Figure 2.2 – Representation of two methods to measure respiratory activity using (a) piezoresistive sensors and (b) inductance coils (reproduced from Catrysse *et al.*(2004) and Enzo Pasquale *et al.* (2005))

The use of pressure sensors is based on the variation of pressure exerted by the chest against the sensor, which can be embedded in a shirt or garment. Brady (2005) manufactured a pressure sensor by coating a conductive polymer with polyurethane foam, which made the sensor soft and sensitive to tridimensional forces. When placed between the thorax and a shirt, it is capable of measuring respiratory activity.

2.3.2. Biomechanical Sensors

Monitoring body movements, gestures and positions provides useful information for the classifications of activities, biosignals denoising, and interpretation of physiological states (Tröster, 2005). Often accelerometers, gyroscopes and magnetometers are used to carry out this detection, but it is also possible to explore the conductive properties of fibres for this purpose.

The use of resistive properties of conductive yarns was explored by Gibbs (2004), who embedded them in fabric tight to the articulations, and when they move the changes in the yarns length cause variations of their electrical resistance, which can be correlated with the different angles the articulations performed. Similar work was developed by Giorgino (2006), who sought to make a recognition of full gestures. In turn, Wijesiriwardana (2006) developed a mesh composed by two textile coils capable of inductive angular measurements. When embedded in a fabric sleeve, it allows the measurement of the joints movement without the hysteresis problems associated with resistive sensors. The use of two coils has advantages, because when just one is used it is more vulnerable to changes in position and suffers higher wear.

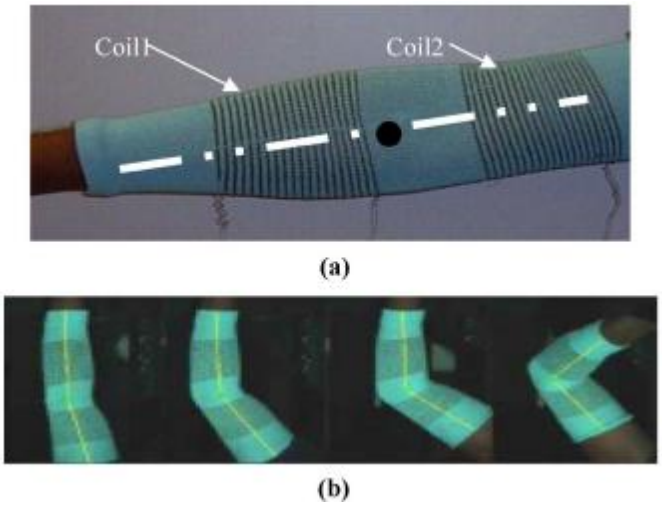

Figure 2.3 – Coils arrangement in the sleeve with the joint (a) extended and (b) flexed in different angles (reproduced from Wijesiriwardana (2006)).

The piezoresistive properties of fabrics to measure biomechanical parameters in rehabilitation were explored by De Rossi (1997). This author, along with Paradiso (2006), presented a piezoresistive sensor obtained by applying a mixture of silicon rubber and graphite to a textile substrate, in order to evaluate the mobility of the wrist, elbow and shoulder during the rehabilitation of stroke patients. While not being able to measure slowly varying signals, the piezoresistive sensors offer an high sensitivity and a wide transduction band (Bonfiglio & Rossi, 2010).

Nevertheless, textile technology faces some limitations in terms of biomechanics detection, which sometimes require other non-textile technologies, such as accelerometers (Rocha & Correia, 2006; Salazar *et al.*, 2010; Sung *et al.*, 2004) and optical fibres (Dunne *et al.*, 2006) .

2.3.3. Chemical Sensors

Textile yarns are not limited to electrical conduction and measuring biopotentials and body movements. It is also possible to use them to detect gases and liquids of various origins, even if they are toxic.

The use of synthetic fibres coated with conductive polymers can be used in a preventive means to detect toxic vapours (Collins & Buckley, 1996) or pathogens resulting from exhalation (Koncar, 2005), or even in more analytical applications like humidity measurements (Norris and Mattes 2007), sweat components detection (Morris *et al.*, 2009) and perspiration monitoring (Salvo *et al.*, 2010). The most studied physiological fluid captured by textile sensors is the sweat. Coyle (2009) studied textile potentialities in detecting sweating rate, pH, sodium concentration and conductivity (Coyle *et al.*, 2010), by developing a textile pump capable of collecting and forwarding sweat to specific sensors.

This work was subordinated to Project BIOTEX, funded by the European Commission, having sports as its main application (Luprano, 2009).

Although there are some promising work in creating chemically sensitive fabrics, some detection methods still rely on optical sensors (Benito-Lopez *et al.*, 2010; El-Sherif *et al.*, 2007). The small size of these methods allow to obtain data from smaller samples, and making them easily embedded in textile based wearable systems (Benito-Lopez *et al.*, 2010).

2.3.4. Textile Electrodes

In the human body, one can find electrically excitable cells, capable of generating an action potential, or biopotentials, that propagates through ionic channels from cell to cell. This phenomenon can be observed in muscular (skeletal and cardiac), cerebral and other tissues, with the use of electrodes.

Although there are many types of electrodes for biopotentials measurement, the non-invasive surface electrodes are very common, in particular the silver-chloride. Their properties are well known, and the low polarization and stable skin-electrode impedance allow the acquisition of good quality signals (Xu *et al.*, 2008). However, they can cause skin irritation due to the use of fixation adhesives and conductive gel (Catrysse *et al.*, 2004); they also have a limited shelf-life and can support bacterial growth (Gruetzmann *et al.*, 2007; Marozas *et al.*, 2011), making its use not recommended for long-term measurements. Besides their advantages and being well established as standard in the scientific and medical communities, their disadvantages have excelled as the main reasons for seeking an alternative in the textile electrodes. The textile electrodes, or textrodes, as sometimes they are called (Van Langenhove & Hertleer, 2004), are manufactured using stainless steel yarns, silver, or other electrical conductor together with conventional textile yarns. Hence, their sensory area presents a much higher ductility than the standard electrode, allowing a better adaptation to the body's contours. Because they are made of textile fibres they can be washed and reused, and their permeability to air and water prevent the occurrence of skin irritations and inflammations (Xu *et al.*, 2008).

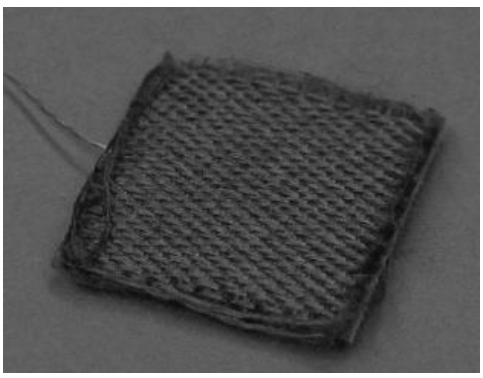

Figure 2.4 – Textile electrode presented by Catrysse (2004).

The acquisition of cardiac potentials with this kind of electrodes has been accurately performed, although with the additional presence of noise, during sleep (Ishijima, 1997), in preventive heart monitoring (Harris & Habetha, 2007) and in neo-natal care (Bouwstra *et al.*, 2009). Currently, textile electrodes are already being commercialized after the FDA approval of the Textronic Inc. (PA, USA) electrodes (Textronic, 2008). The characteristics and properties of these electrodes are widely discussed in Chapter 3.

2.4. Smart Textile Wearable Health Systems

The use of wearable monitoring systems allows a medical doctor, coach or other technician to get real-time data from the wearer's clinical or physical conditions. Furthermore, they allow new possibilities for the media exploitation of events, such as sports or entertainment. Thus, the creation of garments that integrate multiple sensors working in a synergetic way to provide an overall picture of the user status is extremely advantageous. Although wearable systems can generally be used in several environments, as described in section 2.2, currently the large majority of the textile based sensory garments described in the literature are mainly for medical applications: neonatal care, monitoring patients with cardiac conditions, diabetes and others.

2.4.1. Multipurpose Systems

Multi-purpose systems have several sensors distributed over the garment in order to monitor a large number of parameters. By having a high density sensor distribution, these systems can be used for various purposes, giving the user a greater freedom of choice. Although each system present their own distinct characteristics which make them unique, they all exhibit common lines, being the system presented by Linti (2006) a representative example. In this case, the author sought to incorporate multiple sensors in a garment without making it too bulky or warm. Therefore, the author chose to use textile sensors to measure respiratory, heart and sweat rate as well as temperature. These sensors allow the collection of enough information to infer about the user's health status or physical performance.

By using day-to-day monitoring systems, the user is allowed to have a greater awareness of his situation. The VTAM (*Vêtement de Télé Assistance Médicale Nomade*) was designed to incorporate a sensory network capable of performing measurements on a daily basis. It has four dry ECG electrodes, an inductive plethysmography sensor, two temperature sensors, a fall detector based on a bi-axial accelerometer and a GPS module (Noury *et al.*, 2004; Weber *et al.*, 2003). It has also the ability to send alarms, detect position through GPS, detect hyper and hypothermia, as well as the occurrence of brady-tachycardia (Noury *et al.*, 2004).

The Smart Vest (Pandian *et al.*, 2008) is capable of measuring ECG, blood pressure, skin's galvanic response and perform photoplethysmography using sensors embedded and

distributed over the garment in places where they could make better contact with the skin. Communication between sensors is carried on by wires sewn in the garment's fabric. Data acquired by the sensors is collected by a central acquisition board and subsequently sent wirelessly to a remote computer.

2.4.2. Cardiac Monitoring Systems

Regarding the development of wearable systems toward a particular objective, it is easy to verify the prevalence of the cardio-pulmonary monitoring, due to the easy acquisition of ECG and respiratory activity signals. In this matter, the European Commission has intervened by funding some exploratory projects in the textile technology domain, like WEALTHY and MyHeart (Langereis *et al.*, 2007).

The MagIC System (*Maglietta Interattiva Computerizzata*) works on an assumption similar to VTAM, using textile electrodes to measure ECG and respiratory activity, and a portable electronic board with a tri-axial accelerometer and the Bluetooth modules responsible for transmitting data to a remote computer or PDA (Di Rienzo *et al.*, 2010; Di Rienzo *et al.*, 2005). Initially, it was designed to monitor elderly or cardiac patients while confined at environments such as home or the hospital, but it has also been tested during car driving, parachute jumps and in microgravity conditions during a parabolic flight (Di Rienzo *et al.*, 2007).

The MyHeart Project results of the joint effort of a consortium of 33 partners from ten different countries. By analysing the respiratory rate and the ECG, this system seeks to monitor patients with a high-risk of cardiac failure, reducing the mortality rate and at the same time improving the user's quality of life through preventive monitoring (Harris & Habetha, 2007).

The WEALTHY system was designed to monitor intermediate-risk cardiac patients. It is based on the use of textile sensors like electrodes and piezoresistive yarns in order to measure some physiological signals on a daily basis (Paradiso *et al.*, 2005). The textile electrodes are used to measure ECG, although with a reduced sampling rate (250Hz), and impedance pneumography. Data transmission is performed using a short-range wireless system, which sends the data to a remote computer, PDA or cell phone. Figure 2.5 shows a representation of the electrode's and other sensor's distribution in the garment.

Although the majority of the wearable systems seem to be focused on the analysis of vital signs, some researchers have sought to develop applications targeted to other public health issues, like posture problems (Dunne *et al.*, 2006; Giorgino *et al.*, 2006), glucose levels monitoring in diabetic patients (Lim, 2009), and the preventive monitoring of workers suffering from increased tension and musculoskeletal disorders (Langereis *et al.*, 2007; Linz *et al.*, 2007).

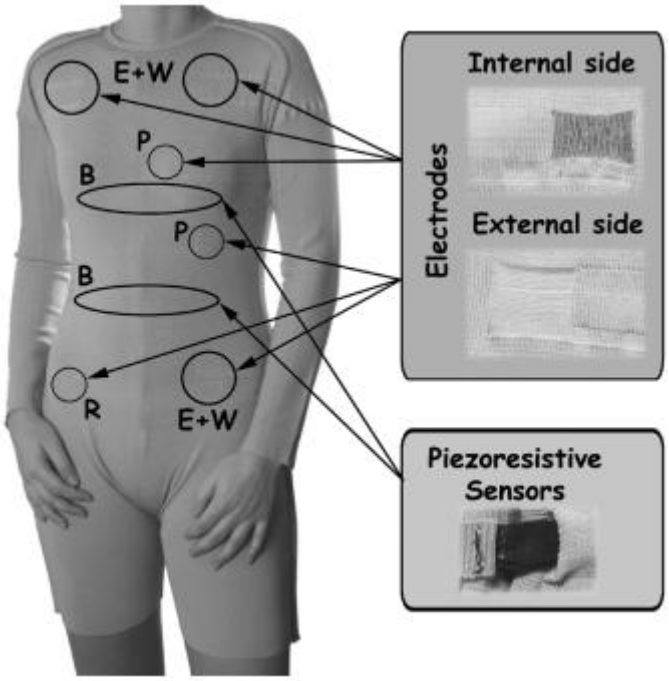

Figure 2.5 – WEALTHY system with the textile electrodes and piezoresistive sensors highlighted (reproduced from Paradiso *et al.* (2005)).

2.4.3. Neonatal care

The non-invasive and comfortable monitoring motto, claimed by wearable systems, is especially important in neonatal care. This starts even before birth, allowing the pregnant woman to follow the health status of her foetus. With this objective, the Smart-Clothing uses textile electrodes and pressure sensors to count foetal movements in low-risk pregnancies, releasing the pregnant woman from this task (Borges *et al.*, 2008).

Once in the incubator, the Smart-Jacket (Bouwstra *et al.*, 2009) aims at providing continuous monitoring of vital signs such as body temperature, ECG, respiratory activity and blood oxygenation of the new-born. These authors claim that the need for wearable systems relates with the fact that the main cause of discomfort to the baby in the incubator is the monitoring system. This happens due to the use of adhesives to hold the sensors, which cause irritation on their still fragile skin, and the cables that connect the sensor to the external monitors, that disturb the baby's sleep. To alleviate these problems, Coosemans (2006) developed a garment comprised by textile sensors that do not require adhesives to hold the sensors in place, and through a coil is not only capable of powering the electronic circuits as it can use it to data transmission. This way the garment truly becomes independent of any kind of physical connection between the baby and the monitoring computer.

2.4.4. Human Locomotion Monitoring Systems

Project BIOSWIM (*Body Interface System based on Wearable Integration Monitoring*) aims at developing a fully autonomous, cable-free, instrumented swimming garment, capable of recording both physiological and biomechanical parameters, fundamental to assess an athlete's performance. Although intended to be used in water, it can also be used in dry land to monitor athletes in other sports and activities.

By means of textile technology, it is possible to measure physiological signals like ECG and EMG, and support other sensors like tympanic temperature, respiratory activity and hydrodynamic pressure. Kinematic parameters are measured with a Wearable Inertial Monitoring Unit (WIMU)(Salazar *et al.*, 2010), enclosing a tri-axial accelerometer and bi-axial gyroscopes, placed close to the centre of mass. The sensors distribution on the garment is depicted in Figure 2.6. WIMU units may also be attached to limb's extremities to monitor their movements.

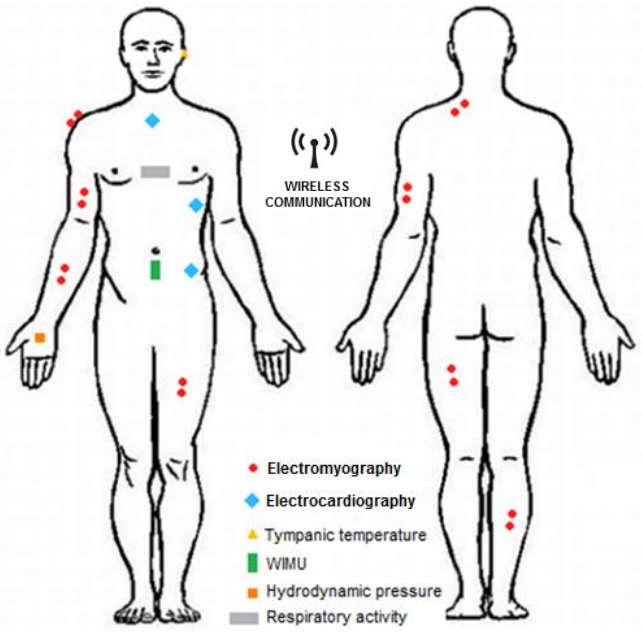

Figure 2.6 – Representation of BIOSWIM sensor distribution on the garment.

All BIOSWIM's measuring systems have reduced dimensions, use conductive fibres instead of conventional copper cables, and have wireless data transmission to a central computer. The use of textile electrodes for measuring biopotentials allow them to be used several times without needing to be changed and, for long term measurements, they do not need conductive gel since natural body sweet moisture them reducing their impedance, therefore reducing the risk of skin irritation. The textile electrodes used to measure ECG and EMG are distinct from each other. The ECG textile electrodes have a larger area than standard Ag-AgCl electrodes in order to minimize skin-electrode impedance, reduce noise and ensure a better skin contact. During a standard ECG measurement, electrodes are usually placed according to the Einthoven Triangle, placing an electrode over the left and right shoulder, and the third

on the right leg. This derivation is used due to its good immunity to motion artefacts caused by trunk movements (Enzo Pasquale *et al.*, 2005). However, during swimming and other sports practice, electrodes placed on the left and right shoulder would experience substantial artefacts due to the arms movements. So, by shifting the electrodes to more stable positions, it is expected to minimize motion artefacts. Therefore, in BIOSWIM garment, the first electrode is placed over the manubrium, the second over the fifth intercostal space of the mid-axillary line and the reference electrode over the iliac crest.

The PROLIMB project has the objective of developing a wearable system capable of recording physical variables related with the human locomotion, even in persons with high physical impairment and disability. It was designed to be used in clinical and laboratory environment, but also in the patient's day-to-day life. The variables recorded to characterize the locomotion include linear and angular movements of the lower limbs, and the surface EMG signals of the thigh and leg (FEUP, 2010; INESCTEC, 2011).

2.5. Concluding Remarks

The recent advances in the development of wearable systems are mostly targeted to health physiological monitoring. This research line has produced several solutions that explore the use of textile technology to monitor not only biopotentials but also respiratory activity and biomechanical parameters, among others. Due to the easiness of its integration into a garment's fabric, textile electrodes have been widely used in wearable systems, with interesting results. The ability to be reused, the washing resistance and comfort have proven to be their strong points, and the main reasons why they are used.

In the future, it is expected that more sensors became textile integrated, and wearable systems became even more comfortable and unobtrusive, while at the same time their functionality increases.

Chapter 3

Electrode Theory

3.1. The Origin of Biopotentials

The biopotentials have their origin in the electrochemical activity of the excitable cell, and in their permeability to Sodium (Na^+), Potassium (K^+) and Chloride (Cl^-) ions. These ions are found in different concentrations in the intra and extracellular environment, and when they cross the cellular membrane, they create a concentration gradient. Due to the sodium-potassium pump, the Na^+ ions leave the interior of the cell in an amount of two to five times the K^+ ions passing to the intracellular environment. So when the ions flux ceases, the cell is said to be polarized because its interior is electrically more negative than the outside, which creates a resting transmembrane potential between -70 mV and -90 mV (Chan, 2008; Khandpur, 2003). When the cell is in a state of equilibrium, its membrane remains polarized, but when a stimulus is able to cause its depolarization, the cell undergoes a change in its equilibrium potential, reaching a value of +20 mV, after which returns to its resting state (Khandpur, 2003). The coordinated propagation of a stimulus can excite adjacent cells, and promote the whole tissue's contraction, as occurs in cardiac and muscular tissue.

Although amplitudes are very small (in the range of μV and mV), measuring biopotentials is possible using electrodes, which act as transducers, converting the body's ionic current to an electric current that can be acquired, amplified and filtered by conventional electronic systems (Rattfalt *et al.*, 2007; Webster & Clark, 2009).

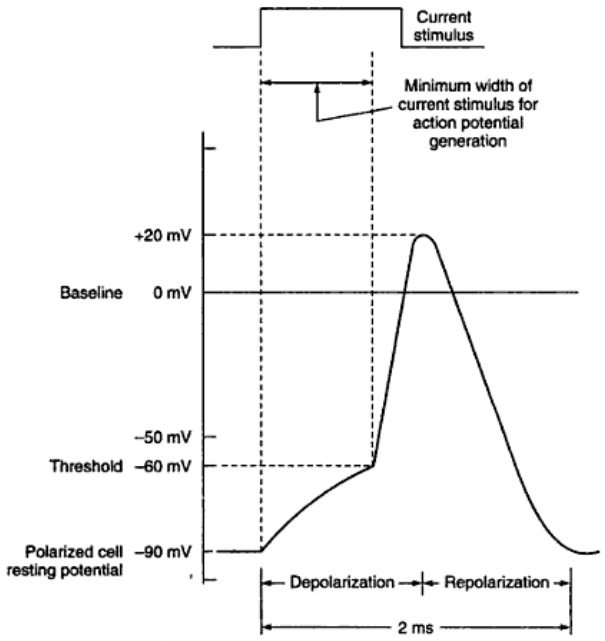

Figure 3.1 - Potential Waveform of an excitable cell (reproduced from Khandpur (2003)).

3.2. Electrodes Classification

Electrodes may be manufactured using different materials which, together with a set of criteria, allow their classification in groups. When evaluating an electrode in terms of conductivity, it can be classified as resistive or capacitive, while in the functional perspective the different levels of polarization determines whether the electrode is suitable for biopotentials acquisition or defibrillation. Other criteria may be used to classify electrodes as dry or wet, flexible or rigid (Xu *et al.*, 2008).

The differences in manufacturing resistive and capacitive electrodes relates right away with the materials used. For resistive electrodes it is necessary to keep a conductive material in contact with the skin, while capacitive electrodes use dielectric materials to establish a capacitive coupling with the skin. The main difficulties associated with resistive electrodes are related to its ability to maintain a good and stable contact with the skin, normally requiring electrolytic gels and fixation adhesives, while the capacitive electrode just have to deal with the intrinsic noise of charge accumulation (Xu *et al.*, 2008).

The polarization of an electrode determines its ability to allow the passage of current between the electrode and the electrolyte. Although in practice it is not possible to get purely polarizable or non-polarizable electrodes, their properties may be obtained in higher or lower degree, depending on the material used in its manufacturing. In theory, non-polarizable electrodes facilitate current passage, making them best suited for biopotentials measurements, while the polarizable electrodes are preferred in electro-stimulation applications (Webster & Clark, 2009; Xu *et al.*, 2008).

3.3. Electrical Characteristics of the Skin-Electrode Interface

The electrical behaviour of an electrode can be modelled using three electronic components arranged in series and/or parallel. The resistors represent the opposition to current flow, the capacitors frequency-dependent reactance, and the power sources the differences of potential.

Since electrodes are used in contact with the skin, the model is not complete if the interface between the electrode and the skin is not considered. Skin has three layers: epidermis, dermis, and subcutaneous layer. The epidermis, in turn, subdivides itself in another three layers: *stratum corneum*, *stratum granulosum* and *stratum germinativum*, where the deeper layers only have vascular components, nerves, sweat glands and ducts, and hair follicles. Thus, the epidermis plays a significant role in the skin-electrode interface, since the other two layers does not have any particular characteristic besides some sweat glands (Xu *et al.*, 2008). Figure 3.2 depicts an electrical equivalent model representation of the electrode and the various skin layers.

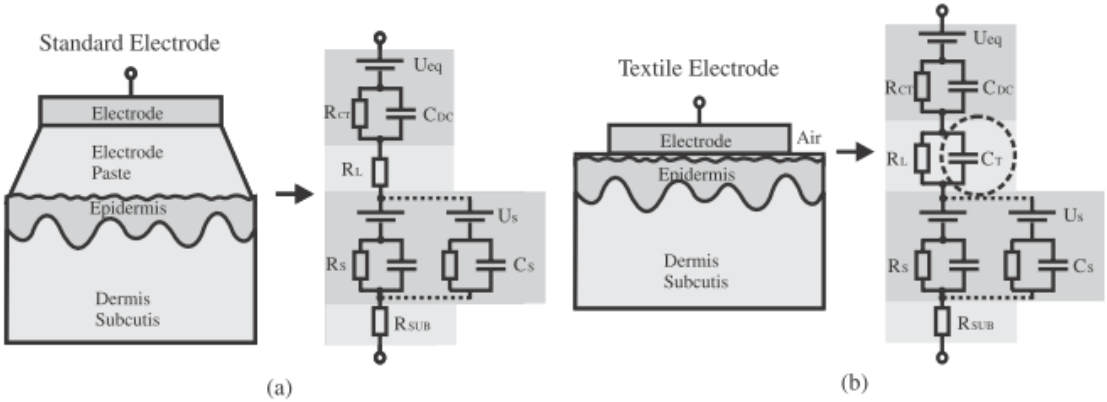

Figure 3.2 – Equivalent electric circuit of the skin-electrode interface of (a) a standard electrode and that of (b) a textile electrode (reproduced from Beckmann & *et al.*(2010)).

The electrical behaviour of an electrode can be represented by a voltage source called half-cell potential (U_{eq}), which is characteristic of the material used to manufacture the electrode. Different materials generate different half-cell potentials, as it can be seen in Table I. This potential is in series with a parallel arrangement of a resistor (R_{CT}) and a capacitor (C_{DC}) that represents the electrode behaviour. Since in the lower frequencies C_{DC} act as an open circuit, its integration in the electrical model has to be done in parallel, in order to allow that even in these situations there is a current flow through R_{CT}. The electrolytic gel, typically present in the standard electrodes, promotes a better contact between the electrode and the skin, but it also represents additional resistance (R_L). The semi-permeability of the *stratum corneum* allows the existence of different ions concentrations in both sides of the membrane, creating a potential U_{eq}. In addition to this potential, the epidermis also behaves similar to a RC parallel circuit due to the presence of

sweat glands and ducts, as well as hair follicles. The dermis, being well irrigated by blood, presents a purely resistive behaviour, thus being represented by R_{SUB} (Beckmann & *et al.*, 2010; Webster & Clark, 2009).

Table I - Electrode potentials of some metals with respect to Hydrogen. (Adapted from Khandpur (2003)).

Metal	Ionic Symbol	Electrode potential
Aluminium	Al^{3+}	-1.66 V
Iron	Fe^{2+}	-0.44 V
Lead	Pb^{2+}	-0.12 V
Hydrogen	H^{+}	0 V
Copper	C^{2+}	+0.34 V
Silver	Ag^{+}	+0.80 V
Platinum	Pt^{+}	+1.2 V
Gold	Au^{+}	+1.69 V

Since the textile electrodes do not need electrolytic gels to operate with good contact conditions, it is possible to substitute the gel by air in the electrical model. The strong capacitive behaviour that the textile electrodes shows justifies the presence of C_T, and sweat and skin's moisture result in a conductive channel (R_L), parallel to this capacitance (Beckmann & et al., 2010).

3.4. Textile Body-Surface Recording Electrodes

The silver-chloride electrodes have been, for many years, the standard for surface biopotentials measurement. Their good conductivity, low impedance and stable skin-electrode impedance, allows them to record accurate signals (Webster & Clark, 2009). The addition of electrodes in garments to monitor physiological parameters has been subject of significant research efforts. However, the use of standard silver-chloride electrodes has the drawback of the heterogeneity between the connection of the electrode and the fabric, as well as the discomfort they can cause in long-term measurements (Gilsoo *et al.*, 2011). When used for long periods, these electrodes stimulate the skin causing skin allergies, the electrolytic gel dehydrates the skin leading to a considerable reduction on the signal's quality, as well as potential bacterial growth (Gilsoo *et al.*, 2011; Marozas *et al.*, 2011; Xu *et al.*, 2008).

In some situations, the standard electrodes may not be the best option, being the textile electrodes a possible alternative. Since they do not require electrolytic gels to promote their conductivity, it is possible to minimize some of the adverse effects of the standard electrodes, and they also have the added value of simplicity when integrating into clothing or other textile structures, making them more comfortable to use (Borges *et al.*, 2008).

3.4.1. Manufacturing Methods

Textile yarns are normally an insulation material however it is possible to endow them with conductive properties through several methods. According to Tröster (2005) it is possible to distinguish three types of conductive threads that can be used to develop textile sensors: (i) fibres filled with carbon or metal particles; (ii) fibres coated with conductive polymers or metal; (iii) thin metal or plastic conductive threads spun with synthetic fibres. The conductive fibres can then be used to manufacture textile electrode through sewing them into a textile substrate (Gilsoo *et al.*, 2011; Pola & Vanhala, 2007). Stainless steel is one of the most popular conductive fibres used in textile electrodes due to their low toxicity and high availability (Coosemans *et al.*, 2005; Merritt, 2008).

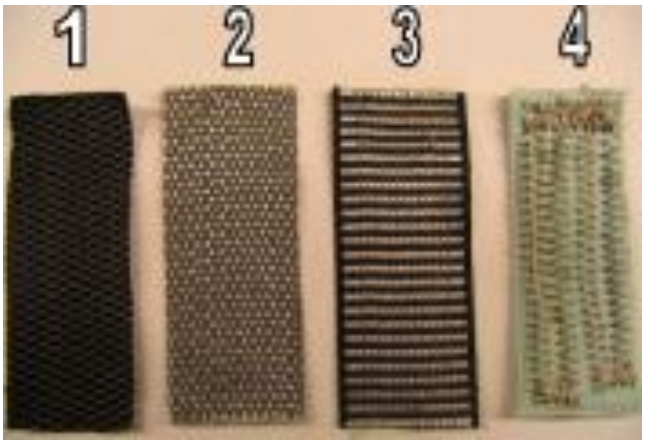

Figure 3.3 – Examples of textile electrodes obtained with different manufacturing techniques: 1) knitting, 2) weaving along the weft, 3) weaving along the wrap, 4) embroidering (Reproduced from Pola & Vanhala (2007)).

In Figure 3.3 are depicted four electrodes manufactured using the three techniques mentioned above. Electrode 1 was knitted, so that the conductive fibres were crossing at an angle on the fabric; the electrode 2 and 3 were obtained by weaving so that the conductive yarns were along the weft and following the wrap, respectively; and electrode 4 was obtained by embroidering with a manual sewing machine, thereby generating random patterns (Pola & Vanhala, 2007). The ratio between conductive and non-conductive fibres should be previously calculated to fit the utilization needs, because when it increases, impedance and signal noise decreases, but also the sweat absorption ability decreases, causing discomfort (Ishijima, 1997).

The characteristics of textile electrodes play an important role in acquiring good quality signals, and are dependent on their dimension properties, raw material, structure and production parameters. These features are reflected primarily in its resistance or susceptibility to motion artefacts and impedance changes.

3.4.2. Artefacts

Motion artefacts are a phenomenon resulting from a momentary charge disturbance in an interface region. It is an undesirable event in biopotentials measurements because it can change the isoelectric line or even mask the desired signal (Khandpur, 2003). This can occur in three different situations: (1) when a polarizable electrode moves relatively to his electrolyte, the movement causes an interface charge disturbance, resulting in the momentary change of the half-cell potential until it can re-establish the equilibrium; (2) if during a measurement using a pair of electrodes, one of them moves while the other remains at rest, a difference of potential will appear between them; (3) if the skin under the electrode suffers any significant change in terms of traction or compression, the skin-electrode interface potential could change momentarily (Webster & Clark, 2009).

Currently, ways to reduce the occurrence of movement artefacts includes: (a) skin preparation through abrasion of the *stratum corneum*; (b) the use of high common mode rejection amplifiers; (c) skin-piercing electrodes (Lay-Ekuakille & Mukhopadhyay, 2010). Excluding option (b), all the other options are invasive or uncomfortable to the human subject.

One of the disadvantages of the textile electrodes relates with their higher susceptibility to motion artefacts (Coosemans *et al.*, 2005). This is due to their increased difficulty in maintaining a stable contact with the skin. By being more polarizable than standard electrodes, it also facilitates the interface charges imbalance during a mechanical disturbance. These stability issues stem from the fact that the electrodes are subject to the same movements of the fabric mesh where they are embedded, from the electrode position, from its adherence to the body, and from the fibre used (Di Rienzo *et al.*, 2010).

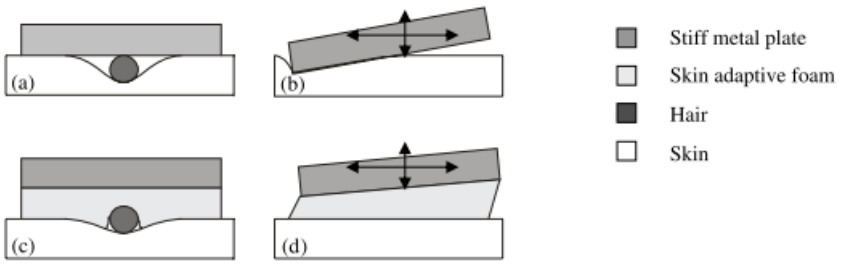

Figure 3.4 – Representation of the behaviour from a ductile substrate electrode comparatively to a rigid electrode (reproduced from Gruetzmann, Hansen *et al.* (2007)).

However, if only the sensory area of the textile electrode is considered, it is possible to verify that its ductile properties are far more advantageous than those of the stiff metal plate from the standard electrodes, when making contact with the skin.

The textile electrode ductility allows it, with an adequate compression, to better adapt to the body's topography, thus maintaining skin contact even in areas with sharp curvatures or the presence of hair (Figure 3.4c). This does not occur with a stiff metal plate electrode,

which creates an air gap that decreases the contact area (Figure 3.4a). Regarding the capability to withstand a small mechanical disturbance, the stiff metal plate electrode would lose contact with the skin more easily (Figure 3.4b), which occurs frequently in curved areas of the body, while the textile electrode would be capable to adapt (Figure 3.4d) (Gruetzmann *et al.*, 2007). This ability of the textile electrode to make a good skin contact is reported by Marozas (2011) who, although did not performed a detailed study on electrodes contact properties, noticed that textile electrodes imprinted themselves in the skin, thus making a better contact than the standard electrodes.

3.4.3. Skin-Electrode Impedance

The opposition that the skin, and even the electrode, presents against the passage of alternated current is called skin-electrode impedance. Its value is usually higher in the low frequencies, becoming smaller as the frequency increases, as depicted in Figure 3.5.

In ambulatory monitoring, in which the patient needs to keep the electrodes placed for long periods of time, to record good quality signals with low noise it is necessary to ensure that the impedance is small. In order to maximize the signal's quality without the need to increase the amplifier's input resistance, the contact impedance should be kept as low as possible, preferably with values lower than 20 kΩ (Xu *et al.*, 2008). To do so, depilation and skin abrasion is performed prior to the electrodes placement.

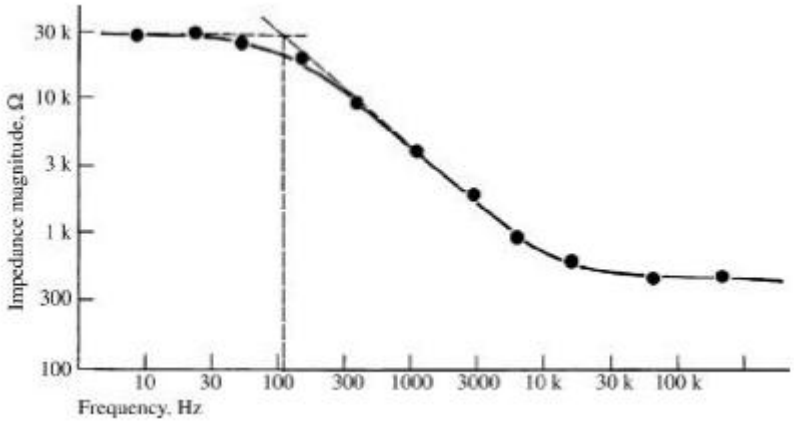

Figure 3.5 – Representative skin-electrode impedance behaviour according to the frequency (reproduced from Webster and Clark (2009)).

However, this is only a temporary solution, since hair starts growing again and the *stratum corneum* regenerates within 24 hours. Therefore, these measures only contribute to the discomfort of the patient and to increase the likelihood of occurring skin irritations.

The skin-electrode impedance is the result of the electrical characteristics of the electrode and the skin over which the electrode is placed. When using electrodes with different characteristics, the skin-electrode impedance should also be distinct. The electrode

impedance is determined by the material from which it was made, by its size and the use, or not, of electrolytic gel.

The standard silver-chloride electrodes properties, with gel, were studied by Rossel (1988), who measured the impedance in several locations of the body, obtaining results ranging from 10 kΩ to 1 MΩ at 1 Hz, to an average impedance of 120 Ω at 1 MHz. In turn, dry textile electrodes presented substantially higher impedances, ranging from 1 MΩ/cm^2 to 5 MΩ/cm^2, comparatively to the 10 kΩ/cm^2 of the standard electrodes (Bifulco *et al.*, 2011; Catrysse *et al.*, 2004). These impedance differences are mainly due to the use of electrolytic gels by the standard electrodes, which moisture the *stratum corneum* and increases its ionic conductivity (Gruetzmann *et al.*, 2007). As the textile electrodes usually do not use this kind of gels, it is expected a higher impedance. But by contrast they are used tightly to the body, and sweat acts as a natural electrolytic gel. Even its ionic conductivity is lower than the electrolytic gels, which is enough to decrease the impedance and noise, allowing the acquisition of good quality signals (Gruetzmann *et al.*, 2007).

By varying the electrode area, its resistance and capacitance will also change, so when increasing a standard electrode area, the impedance and noise will decrease (Marozas *et al.*, 2011; Puurtinen *et al.*, 2006). Comparatively, in dry textile electrode, the noise level is practically the same regardless of the electrode size, but when electrolytic gel is added the noise decreases significantly with the increase of the electrode area (Puurtinen *et al.*, 2006).

3.5. Concluding Remarks

The electrical characteristics of the electrodes and the skin over which they are placed are essential aspects to acquire good quality electrophysiological signals. The silver-chloride electrodes, by having stable electrical characteristics, and for being easily fixated to the body are, for many years, the standard choice for physiological monitoring. However, their disadvantages have led to the exploration of alternatives, especially giving the growing interest in the development of wearable systems. Therefore, the textile electrodes have emerged as a suitable alternative to integrate electrodes in garments, because its conductive fibres can be handled as normal fibres and be washed repeatedly without losing their qualities.

The manufacturing of textile electrodes with different techniques allows obtaining electrodes that are best suited to adapt to the body's curvatures. By making them with different sizes, it is also possible to decrease noise in the recorded signals. The use of textile technology allows the exploration of different concepts, as the brush electrode presented by Hui (2011), that by having several filaments in a brush like structure allows the increase in the effective contact area, and is even capable of moving through hair.

However, unlike the standard electrodes that use adhesives, fixation and contact with the skin are critical in textiles. To keep a good contact with the skin it is necessary that they are embedded in a garment or fabric that keeps an adequate pressure against the body

(Merritt, 2008), having Ottenbacher (2004) suggested the use of a foam material to provide additional pressure between the electrode and the body.

The textile electrodes may not be suitable for every type of physiological measurements, but they are a good alternative to standard electrodes when intended to be used in wearable system.

Chapter 4

Skin-Electrode Impedance Characterization

4.1. Introduction

The characterization of the skin-electrode impedance provides information about the characteristics of an electrode placed on the skin, and gives information for the correct design of an adequate amplifier to record faithfully the biopotentials signals (Baba & Burke, 2008). According to Yuxiang (2006) there are basically two techniques for measuring the impedance of biological tissue: the bridge method (BM) and the quadrature demodulation (QD) method, being the BM the most popular although requiring careful bridge balance. Despite the chosen method, both require an excitation current, and the measurement of a voltage which, through the Ohm's Law, allows the calculation of the impedance:

$$Z = \frac{V}{i} \tag{1}$$

Therefore, by injecting a known current i through a pair of electrodes, and measuring the voltage V across them, it is possible to measure the impedance Z of the interface. Knowing this, it would also be possible to apply voltage and measure current, however Isaacson (1986) stated that noise is reduced when current is injected and voltage measured rather than applying voltage and measuring current.

In this chapter, a brief review on Voltage Controlled Current Sources is conducted as a step for the implementation of a current injector circuit, which was subsequently used to measure the skin-electrode impedance of two different textile electrodes, in comparison to a reference standard silver-chloride electrode.

4.2. Voltage Controlled Current Sources

Electric current may be generated using a voltage controlled current source (VCCS), that is, a voltage-to-current converter that generates a current signal proportional to a voltage input. The main problem of this kind of circuits is to keep the voltage-current proportionality even when the resistive load changes, due to a virtual or real impedance in parallel with the load, called output impedance R_o (Tabuenca, 2009).

The transconductance equation, i.e., the equation that models the conversion of voltage into current, is given by:

$$i_{out} = AV_{in} - \frac{1}{R_o}V_{out} \tag{2}$$

where i_{out} represents the generated current, V_{in} the input voltage supply, A the circuit's gain, V_{out} the output voltage developed by the load in response to i_{out} and R_o the output impedance. By observing both the equation (2) and the Norton equivalent circuit depicted in Figure 4.1, it is clear that R_o value is critical in determining the output current.

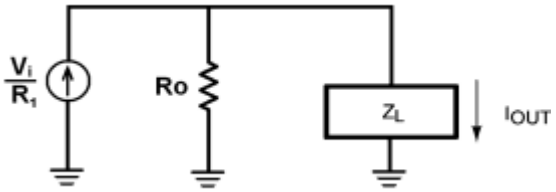

Figure 4.1 - Norton equivalent of a current injector (reproduced from Tabuenca (2009)).

Since a true VCCS has to be independent of V_{out}, the value of R_o must be as high as possible, ideally infinite, in order to all the current be driven into the load (Franco, 2002). The Howland Current Pump is, according to Ross (2003), the VCCS with the highest reported output impedance, achieving 3.8 GΩ at 10KHz (Chen *et al.*, 2010).

4.2.1. Howland Current Pump

The Howland Current Pump was invented by Prof. Bradford Howland, of the MIT, around 1962, and it was not patented, which contributed to its wide use and popularity (Pease, 2008). It has two feedback loops, one to the positive input of an operational amplifier, and other to the negative input, being the current output the result of the contribution of these two inputs, the same as a differential circuit.

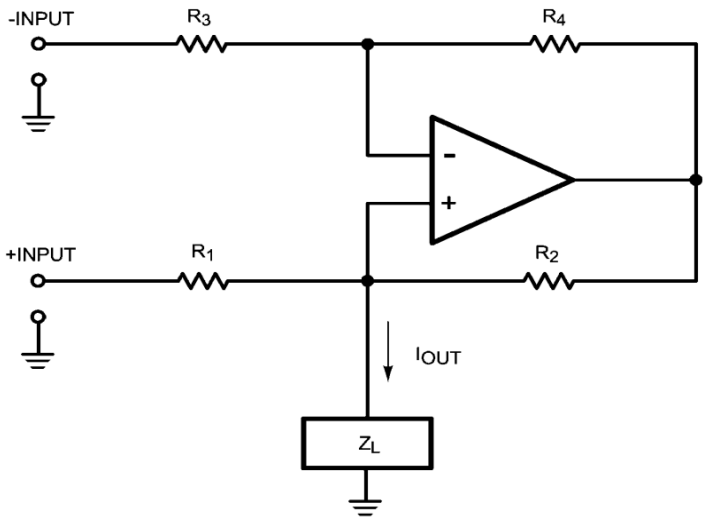

Figure 4.2 - Electronic schematic of the Howland Current Pump (reproduced from Tabuenca (2009)).

This is a bridge circuit, since the current production is possible by the careful balance of the resistors with a ratio of $R1/R2 = R3/R4$ in order to achieve $R_o = \infty$, since the output impedance is give by:

$$R_o = \frac{R_2}{R_2/R_1 - R_4/R_3} \tag{3}$$

If this condition is met, the output current is truly independent of the load, and can be calculated by:

$$i_{out} = \frac{V_{in}}{R_1} \tag{4}$$

The fact that the output current depends on a single resistance, makes its calculations more intuitive and the circuit implementation easier. However, the Howland Circuit has an high energy waste (Al-Obaidi & Meribout, 2011), and a limited output capability restricting its use to low currents and frequencies in the kHz region. To counteract these problems the Howland Circuit was modified, resulting in the Improved Howland Current Pump.

4.2.2. Improved Howland Current Pump

The Howland Current Pump was first modified in 1994, with the introduction of a fifth resistor, being henceforth named Improved Howland Current Pump (IHCP) (Stiz *et al.*, 2009). This modification prevents the unnecessary high current drop on R_1, which forced the circuit to waste more energy than that it produced at the output terminal (Franco, 2002).

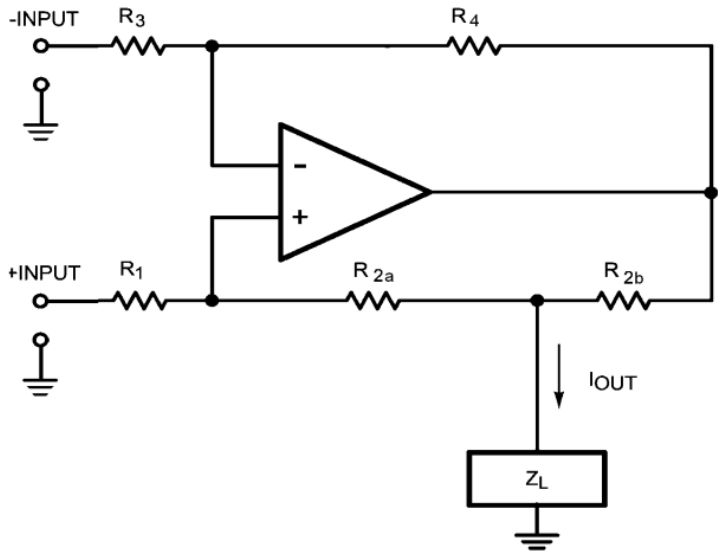

Figure 4.3 - Electrical schematic of the Improved Howland Current Pump (reproduced from Tabuenca (2009)).

The R_2 resistor is split in two, with different values, but the sum of both should still maintain the resistor bridge balance. Therefore, the R_{2b} resistor may assume values as small as 100 Ω, while the R_{2a} should be kept rather high in other to conserve power. Knowing this, the output current i_{out} through the load and the output impedance R_o are given by:

$$i_{out} = \frac{(R_{2a} + R_{2b})/R_1}{R_{2b}} V_{in} \tag{5}$$

$$R_o = \frac{R_3 R_{2b}(R_1 + R_{2a})}{R_4 R_1 - R_3(R_{2a} + R_{2b})} \tag{6}$$

In theory, if the resistors are perfectly matched, infinite output impedance is achieved. However, this does not happen in practical implementations, due to the resistors tolerance, which, according to Pease (2008), should not exceed 0.1%. Another option is to replace the R_1 resistor with a potentiometer, allowing the adjustment of the resistors mismatch (Franco, 2002; Ross *et al.*, 2003).

4.3. Methodology

4.3.1. Participants

A group of ten individuals, six male and four female, recruited from local university students with 24±3.3 years old, body mass of 69.1±12.2 kg and 1.74±0.10 m in height participated in this study. None of the participants had a history of circulatory and/or nervous disturbance, as well as recent skin lesions.

4.3.2. Materials

4.3.2.1. Impedance Measuring Circuit

An electronic circuit, capable of injecting current into the body and measuring the resulting voltage drop, was implemented in order to measure skin-electrode impedance. The followed approach was to develop a circuit capable of measuring both magnitude and phase of the impedance, as well to provide the most reliable data through a previous circuit calibration.

In Figure 4.4 is depicted the developed current injector, comprising an IHCP, and two instrumentation amplifiers responsible for measuring voltage drops. The IHCP is based on a LM324AN integrated circuit (IC) and a resistors bridge, converting the voltage signal from the signal generator into a 100 µA amplitude current signal that is driven by a control resistor $R\_Control$ to an electrode and injected into the body, here represented as R_Body, or through the calibration resistor R_Calib, depending on the switch state. The $Signal\_Generator$ used was an analog Topward function generator 8110.

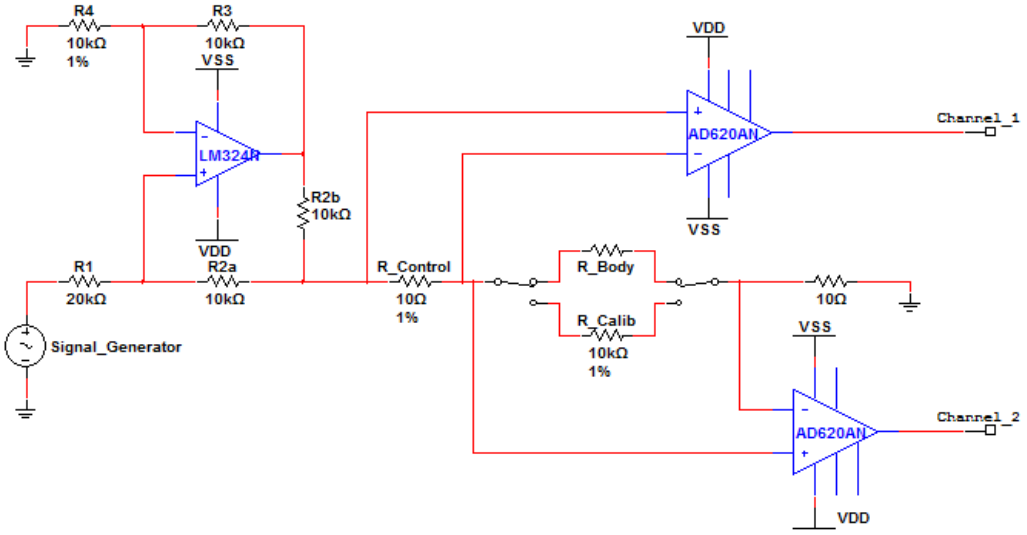

Figure 4.4 - Electronic schematic of the developed current injector based on the IHCP.

The two AD620AN were chosen to measure the voltage drops due to their very high input impedance that prevents the occurrence of leakage currents into the IC. By measuring the resulting voltage amplitude at $Channel\_2$, and according to Ohm's Law, it is possible to calculate the skin-electrode impedance magnitude. The phase shift introduced by the skin-electrode interface can also be obtained by the difference of the voltage phase to the current phase, which can be measured at $Channel\_2$ and $Channel\_1$, respectively.

To ensure its proper operation, the circuit allows calibration using the calibration resistor R_Calib and a trimmer in place of R_{2a}. By changing the switch state, the current flows through R_Calib instead of the body, and R_{2a} can be trimmed to adjust R_0. Since R_Calib has

a known value, $R_0 = \infty$ is achieved when the voltage drop on this resistor is proportional to the expected current.

4.3.2.2. Evaluated Electrodes

Three sets of electrodes with distinct characteristics and shapes were evaluated, including standard silver-chloride electrodes and two models of textile electrodes, one for ECG and another for EMG recordings.

The silver-chloride standard electrodes used as reference were the auto-adhesive SX-30 model of Dormo&Blayco (Telic S.A., Spain), with a solid gel film over a 1 cm^2 circular sensory area. The ECG textile electrodes were manufactured with a knitting technique and a mixture of Bekintex stainless steel and elastane, with a linear density of 20 tex, in a rectangular shape with a sensory area of 26 cm^2. Since this electrode has a higher area and ductility, a soft foam strip has been sewn behind the electrode to provide some volume and improve the skin contact through a cushioning effect, as proposed by Ottenbacher (2004).

(a) (b) (c)

Figure 4.5 -The three electrodes used in the study: (a) the standard silver-chloride electrode, (b) the ECG textile electrode with a rectangular sensory area, and (c) the EMG textile electrode with a rectangular sensory area.

The EMG textile electrodes were also knitted, using a mixture of 80% silver-plated polyamide (Elitex) with 20% Lycra and a linear density of 23.5 tex, having a sensory area of 1 cm^2 and a 2 cm centre-to-centre distance between electrodes.

4.3.3. Measurement Setup

Consecutive measurements were conducted to compare the skin-electrode impedance magnitude and phase of the three electrodes under evaluation. For this purpose, an experimental setup was developed which included skin preparation, electrodes placement, control of the exerted pressure, and the impedance measurement itself.

No special skin preparation was performed besides cleaning it with 70% ethylic alcohol, after which the electrodes were placed on the right ventral forearm with a distance of 2 cm

centre-to-centre. Although textile electrodes can operate without conductive gel, a thin layer of conductive gel (Quick Eco-Gel, Lessa S.A., Spain) was applied in order to provide similar contact conditions between the skin and the textile electrode to those of the standard electrodes. Measurements were conducted two minutes after placing the electrode on the skin and a sphygmomanometer cuff was used to maintain a constant pressure of 2.67 kPa (20 mmHg). Subjects were asked to sit and keep still during the measurement procedure so that muscular movement would not cause waveform artefacts.

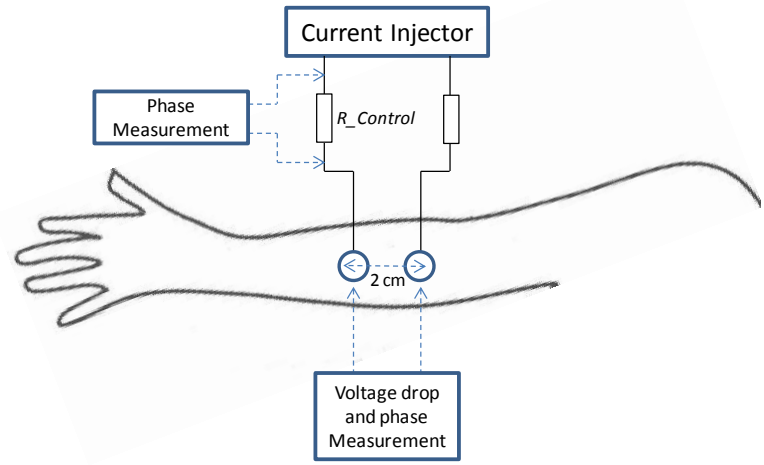

Figure 4.6 - Schematic of the impedance measurement apparatus.

Current was injected using the circuit depicted in Figure 4.4, which generated a 100 µA amplitude sinusoidal current signal from 15 to 1000 Hz. Calibration was performed before measurements by setting the voltage signal generator at a frequency of 100 Hz and trimming R_{2b}. After this two electrodes of the same type were used to create a closed circuit which allowed the current to travel from one electrode to another through the skin. The voltage signals from $Channel\_1$ and $Channel\_2$ were acquired with a NI-USB6211 (National Instruments, TX, USA), with a 16 bit resolution and a sampling frequency of 42 kSamples/s. The experimental setup used to measure the impedance's magnitude and phase is depicted in Figure 4.6.

4.4. Results and Discussion

By comparing both the impedance magnitude and phase shift caused by the skin-electrode impedance, it is possible to infer if the textile electrodes have similar values and behaviour across frequencies, which would allow them to record physiological signals with quality and waveform distortion similar to the standard electrodes.

Beginning with the assessment of the impedance magnitude versus frequency, it is possible to observe a similar decreasing trend in all the electrodes, which would be expected considering the frequency dependency of the skin model presented in 3.1. Comparing the resulting data depicted in Figure 4.7, it can be seen that the standard electrodes show much

higher magnitude than the textile electrodes. In the lowest frequencies standard electrodes have a magnitude higher than 200 kΩ, decreasing down to 13.6 kΩ at higher frequencies, showing a sharper transition than that observed in the textile electrodes.

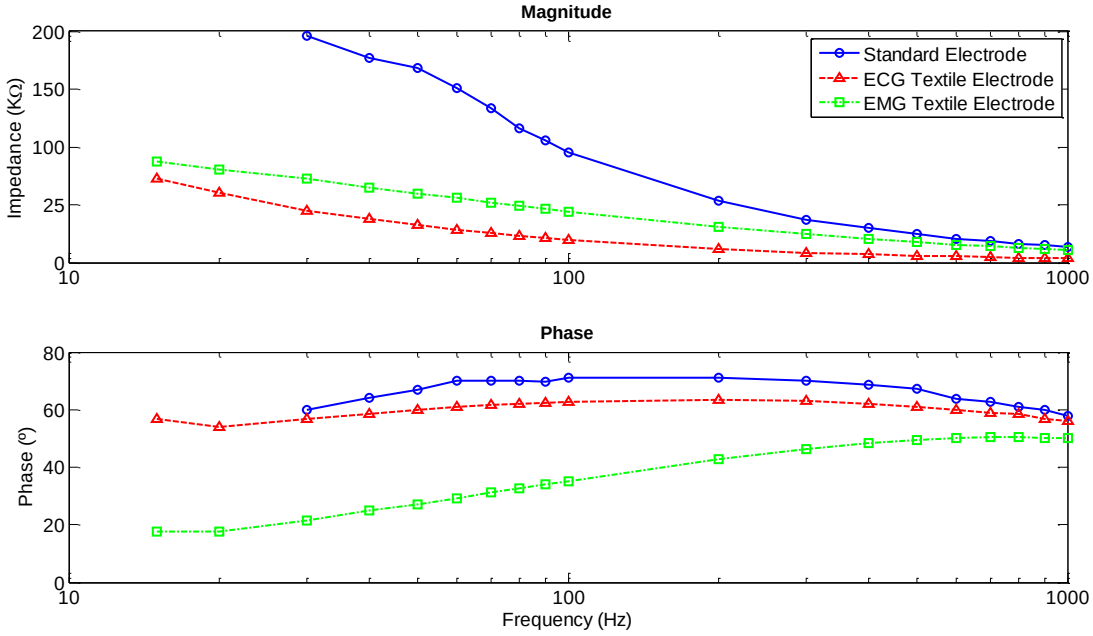

Figure 4.7 - Skin-electrode impedance versus time in terms of magnitude and phase.

The phase shift introduced by the electrodes is very distinct from one electrode to another, although there is substantial resemblance of the ECG textile electrodes with the standard electrodes. However, while the ECG textile electrodes have a more consistent behaviour over the frequency range, the standard electrodes show a phase step between 60º and 90º, and a sudden phase decrease at 500 Hz. In turn, the EMG textile electrodes show lower values of phase shifting over the whole frequency range and a linear tendency to stabilize around 50º.

If the size of each electrode is taken into account, results became more expressive since the impedance magnitude of the standard electrodes at 100Hz is 95.5 kΩ/cm^2 while the ECG and EMG textile electrodes have values of 752 Ω/cm^2 and 44.2 kΩ/cm^2, respectively. Although the ECG electrodes are made of stainless steel, which usually has higher impedance than silver and especially than silver-chloride, the larger area reduces it to a value lower than the other electrodes.

Table II - Average magnitude and angle of the impedance at four frequencies for all the evaluated electrodes.

	50 Hz		**100 Hz**		**500 Hz**		**1000 Hz**	
Electrode	Z (kΩ)	φ (Deg)	Z (kΩ)	φ (Deg)	Z (kΩ)	φ (Deg)	Z (kΩ)	φ (Deg)
Silver-Chloride	167.9	66.8	95.5	71	24.5	67.4	13.7	57.7
ECG Textile	32.3	59.9	19.6	62.7	5.9	61.1	3.6	55.9
EMG Textile	59.9	27.2	44.2	35.2	17.8	50.2	11.2	50.3

4.5. Conclusions

Skin-electrode impedance measurements have shown that there are differences between standard and textile electrodes. This was expected, since the textile electrodes were manufactured with different materials, methods and sizes. The standard electrodes, were expected to show the lowest impedance magnitude and phase, however that happened with the textile electrodes.

The collected data shows that textile electrodes are capable of achieving lower impedance values than the standard electrodes in all the frequencies from 15 Hz to 1000 Hz, what would make them suitable to impedance sensitive measurements.

Chapter 5

Validation of textile electrodes for electrocardiogram measurements at rest

5.1. Introduction

Electrode's characteristics, such as impedance, polarization and the electrical properties of the transducer material can cause morphological and time distortions to the recorded signal. Since the textile electrodes are manufactured with different materials and techniques than the standard electrodes it is necessary to study how these differences reflect themselves in the measured signal.

This work aims at validating the use of textile electrode for measuring cardiac potentials at rest. Marozas (2011) listed some of the most common properties used to characterize electrodes, which includes skin-electrode impedance, the variation of this impedance over time, visual comparison of the signals recorded with the electrodes under investigation and reference electrodes, biocompatibility and skin response, correlation analysis, signal-to-noise ratio, detectability of ECG waves, power spectrum density, and the electrode's electrical properties. Taking into account the above properties, ECG recordings were performed using simultaneously the ECG textile electrodes and the standard silver-chloride electrodes described in 4.3.2.2. The resulting data, in addition to the skin-electrode impedance evaluation performed in Chapter 4, were used to compare the usability of the ECG textile electrodes to record cardiac potentials in a similar manner to the reference silver-chloride electrodes.

5.2. Methodology

5.2.1. Participants

Physiological ECG recordings were performed with a group of fifteen healthy participants, six male and nine female, recruited from local university students with no history of cardiac conditions. They were 24±3.6 years old, body mass of 66±9.8 kg and 1.69±0.09 m in height.

All volunteers were informed of the study objectives and the experimental protocol to be used, after which they had the possibility to familiarize themselves with the experimental setup and the electrodes to be used.

5.2.2. Materials

The standard silver-chloride electrodes used as reference were the auto-adhesive SX-30 model of Dormo&Blayco (Telic S.A., Spain), with a solid gel film over a 1 cm^2 circular sensory area. The ECG textile electrodes were manufactured with a knitting technique and a mixture of Bekintex stainless steel and elastane, with a linear density of 20 tex, in a rectangular shape with a sensory area of 26 cm^2. The textile electrodes were embedded in a sleeveless single size jersey, with the first electrode placed over the manubrium, the second over the fifth intercostal space of the midaxillary line and the reference electrode over the iliac crest. Both electrodes are displayed in Figure 4.5.

Since the ECG is a low amplitude signal, during the physiological measurements both sets of electrodes were coupled to a two-stage amplifier (Gonçalves *et al.*, 2006). The first stage pre-amplified the signal 100 times with a CMRR larger than 110 dB, while at the second an amplification of 11 times was performed, in a total amplification of 1100 times. The ECG amplified signals were then recorded using a BIOPAC MP100 (BIOPAC Systems Inc., CA, USA) with a 16 bit resolution and 1000 Hz sampling frequency.

5.2.3. Measurement Setup

No special skin preparation was performed before placing the electrodes besides cleaning it with 70% ethylic alcohol, after which each volunteer was asked to wear the textile electrodes jersey and the standard electrodes were placed. Due to the inability of placing both the standard and textile electrodes on the exact same location, they were carefully placed as near as possible in order to prevent morphological changes. The relative placement of the electrodes and the overall measurement setup is depicted in Figure 5.1. Since the measuring and recording system only allowed one reference electrode, the textile electrodes were used as reference.

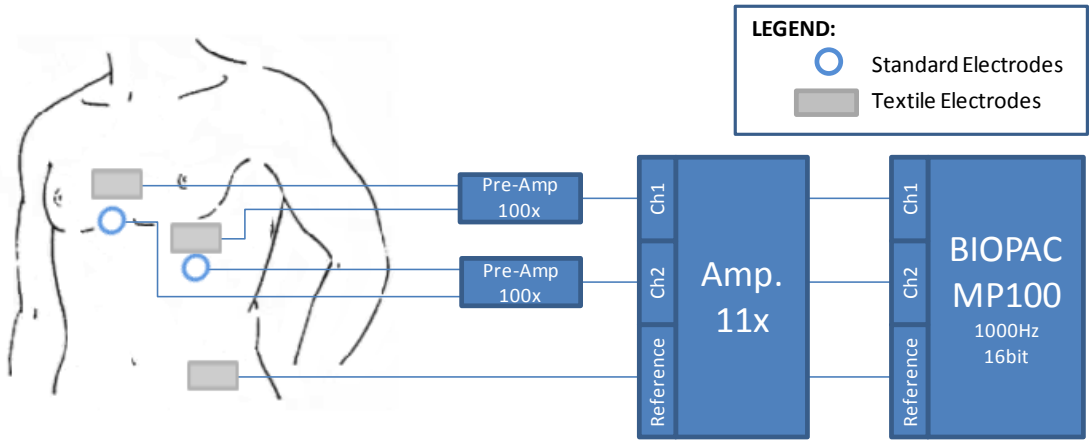

Figure 5.1 - Summary of the experimental setup mounted.

A thin layer of conductive gel (Quick Eco-Gel, Lessa S.A., Spain) was applied on the textile electrodes, and volunteers sat comfortably on a chair for at least two minutes, after which a five minutes recording was performed.

5.2.4. Data Analysis

Raw data was digitally filtered after acquisition using Matlab 7.9.0 (MathWorks, MA, USA). This process included the DC component removal, a 1-100 Hz zero-phase Butterworth bandpass filter (-80 dB/decade) to restrict the signal frequencies to those with physiological relevance, and a zero-phase 50 Hz notch filter (-80 dB/decade) to remove the power-line interference. In order to evaluate the performance of the textile electrodes in measuring ECG with respect to the standard silver-chloride electrodes, a set of morphological, time and frequency analysis was performed.

Morphological analysis intends to assess the variation on the ECG signal shape resulting from the different electrodes characteristics. This analysis included the overlapping of both ECG signals and their visual inspection, after which a Bland-Altman diagram of a single complete representative cardiac cycle of each subject was plotted to assess their measurement agreement. In addition, similarities between signals were verified through correlation and the Root Mean Square Error (RMSE). The measurement of Signal-to-Noise Ratio (SNR) was used as a signal quality parameter.

The different physical characteristics, such as size and skin-electrode impedance, could be responsible for introducing time shifts into the recorded signals. Therefore, through a comparison of time variables, it is possible to assess if temporal differences occur between standard and textile electrodes. The interval between consecutive R-waves (IRR) of both signals were calculated and correlated. Afterward, this interval was averaged (AVRR) and along with the standard deviation (SDRR) and the maximum difference between IRR (dIRR), was used to compare their overall similarities. Once again, a Bland-Altman diagram was plotted using the IRR to verify the agreement between the R-waves intervals of both signals.

Power Spectrum Density (PSD) was used to quantify the power distribution across the frequency spectrum and quantify how much a given frequency is expressed in a signal. The frequency analysis included a one-sided PSD plotted using the Welch method, with a 256 points Hamming window and 50% overlap. The resulting PSD from both signals was overlapped and visually inspected.

The Matlab algorithms used in the data analysis were developed expressly for these tasks and can be viewed in Appendix A.

5.3. Results

During standard ECG measurements, electrodes are usually placed according to the Einthoven Triangle, with an electrode over the left and right shoulder, and the third on the right leg. This derivation is used due to its good immunity to motion artefacts caused by trunk movements (Enzo Pasquale *et al.*, 2005). However, since the ECG textile electrodes under evaluation were design to be used in a sensorised garment for swimming and other sports practice, electrodes placed on the left and right shoulder would experience substantial movement due to the arms movements. So, by shifting the electrodes into a more stable position on the chest it is expected to minimize motion artefacts, being this the reason why a less conventional derivation was chosen.

Data from two participants were excluded; the first due to a poor electrode placement, resulting in a morphological distorted signal that could not be analysed, and the second due to a previously unknown cardiac condition. The data collected from the remaining participants were processed and analysed as described in 5.2.4, without any constraints.

Several participants stated that the textile electrodes were comfortable to use, not noticing any difference between the electrode and the remaining shirt fabric.

5.3.1. Morphological Comparison

Through a visual comparison it was intended to verify if there were any particular features that differentiated signals recorded with both electrodes. In order to facilitate a direct comparison, signals were overlapped on the same graph.

Since the textile electrodes were embedded in a jersey their relative position over the chest may have changed between participants. This may have led to differences in the ECG signals of some of the participants, as seen in Figure 5.2. Despite this occurrence, the standard electrodes were always placed as near as possible to the textile electrodes, in order to record an ECG signal with the closest derivation possible. This way, even having differences between participants, the signals from the textile and standard electrodes should be identical, what indeed happened.

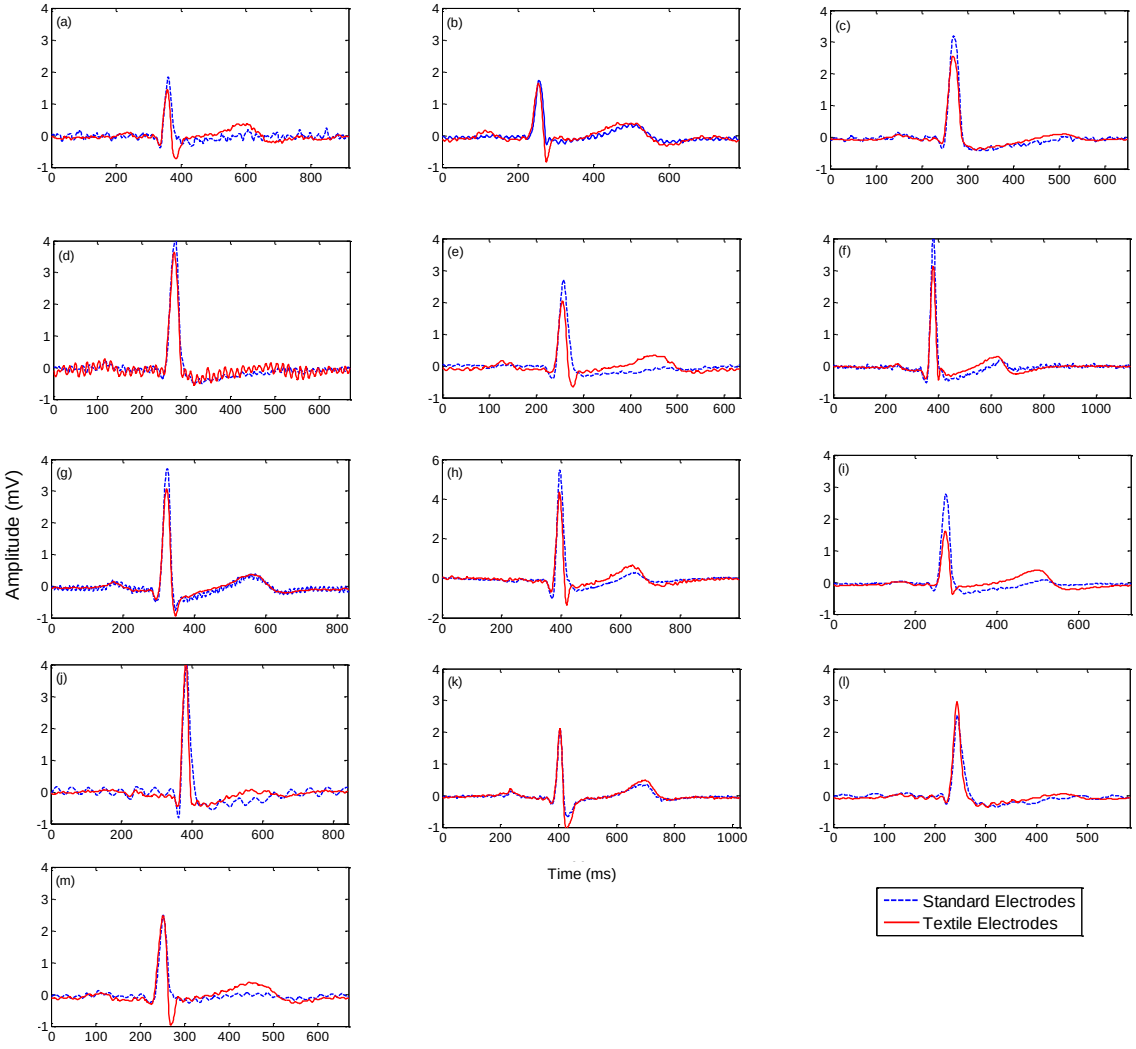

Figure 5.2 - Sample of one complete cycle from each participant of the study.

A four seconds sample from a best case scenario signal was selected and is depicted in Figure 5.3. At first glance, signals seem to match both in duration and amplitude, except for the R-wave, which is shorter in the textile electrode signal, and the higher noise in the standard electrode's signal. More accurate information can be obtained from a single cardiac cycle, containing a complete systolic and diastolic phase, since this allows the observation of these differences in more detail. Observing the complete cardiac cycle, it is now possible to see that the standard signal's thicker aspect is caused by a superimposed 100 Hz sinusoidal signal possibly caused by the 50 Hz power line second harmonic.

Although neither period nor amplitude measurements for each wave were carried out, by observing Figure 5.4 it is safe to say that all the waves have identical periods, that is clearly seen with the P and the T-waves, being the differences restricted to some waves amplitude. The most noteworthy differences are related with the QRS complex which has lower amplitude in both the Q and R-waves while the S-wave, in turn, has a more prominent depression than the corresponding wave in the standard electrode. The same morphological differences seen in Figure 5.4 are present in Figure 5.2.

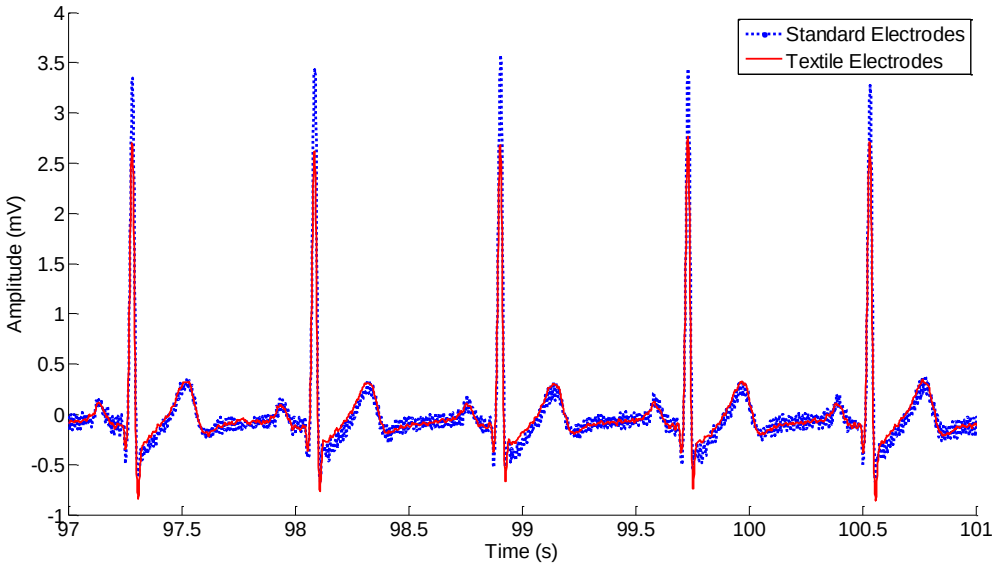

Figure 5.3 - Overlapping signals recorded with both sets of electrodes.

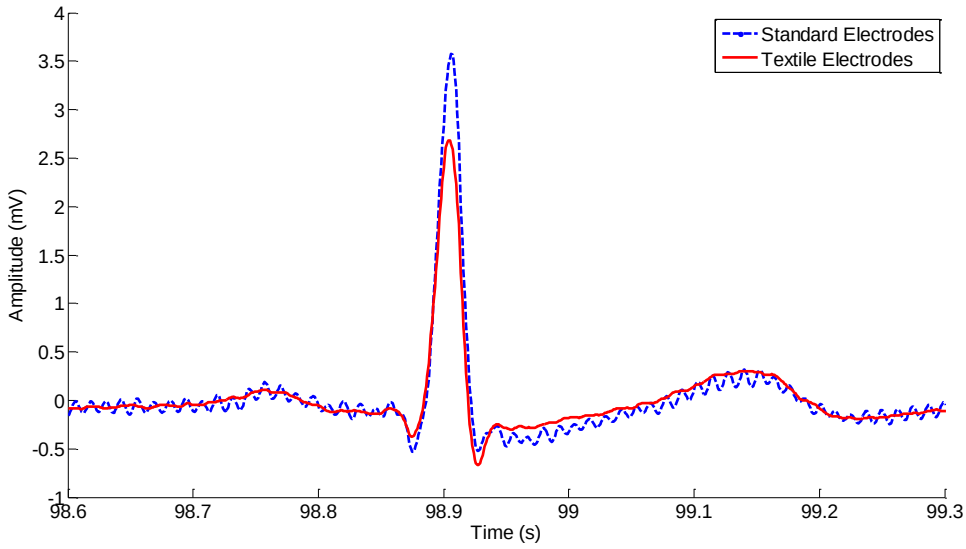

Figure 5.4 - Representative complete cardiac cycle with both diastolic and systole phases.

The presence of noise is clearer in the standard electrode's signal, however some of the ECG signals recorded with textile electrodes also show the presence of the power line noise. The reason why noise is not seen in some of the measurements could be related, along with different measurement conditions, with the amplitude of the signals, since noise is more easily detected in higher amplitude signals. To infer about this issue the SNR can be measured using the following mathematical expression:

$$SNR = 20 \log \frac{A_{signal}}{A_{noise}} \tag{7}$$

where A_{signal} is the signal amplitude and A_{noise} the noise amplitude. Since the isoelectric region of an ECG represents a moment when there is no cardiac electropotentials being

generated, it should have a zero value amplitude, being any other value different than zero a consequence of noise contamination. By comparing this amplitude with the R-wave amplitude it's possible to calculate the SNR. Adapting equation (7) to this situation, and assuming that the noise amplitude present in the isoelectric region is the same that contaminates all the ECG waves, we have that:

$$SNR = 20 \log \frac{A_{wave} - A_{noise}}{A_{noise}} \tag{8}$$

Calculating the SNR for each R-wave of each signal, and averaging the result, a SNR of 29.5±2.23 dB from the standard electrodes and 24.09±3.03 dB from the textile electrodes is obtained.

By using correlation analysis and RMSE it is possible to assess the linear relation between signals and how much they differ from each other. When signals recorded with both electrodes where correlated, a mean r coefficient of 0.87 and a standard deviation of 0.10 was obtained. This result, together with the small standard deviation indicates a strong linear relation between signals. On the other hand, when calculating the average RMSE from all the signals, a result of 6.87 μV is obtained. Since BIOPAC MP100 has a 16 bit (n) resolution, and worked with a ±10 V amplitude range ($\pm V$), each quantization step (Q) is given by:

$$Q = \frac{\pm V}{2^n} \tag{9}$$

$$Q = \frac{20}{2^{16}} = 305\ \mu V \tag{10}$$

As proven by equation (10), the average RMSE value is smaller than the quantization step of BIOPAC MP100 and therefore negligible. Since the correlation coefficient is not enough to assess data agreement, and the RMSE proved to be negligible, another method is necessary to assess the point-by-point agreement. By plotting the difference of each point from the standard and textile electrodes against their mean, a scatter plot known as Bland-Altman diagram can be obtained. The agreement between measurements would then be evaluated by the number of the diagram's points that were within the 95% confidence interval, delimited by ±2 SD of the difference.

The Bland-Altman diagram used to assess the point-by-point agreement between a single representative cardiac cycle of each subject is depicted in Figure 5.5. Although this diagram appears to have a considerable number of pointes outside the 95% confidence interval, they actually only represent 3.75% of all the points, being most of them clustered around the mean. The points outside the confidence interval result from differences that some participants showed in the descending R-wave pattern. In these cases they present an R-wave with a duration that, although the same as those measured with standard electrodes, has a more abrupt downward slope.

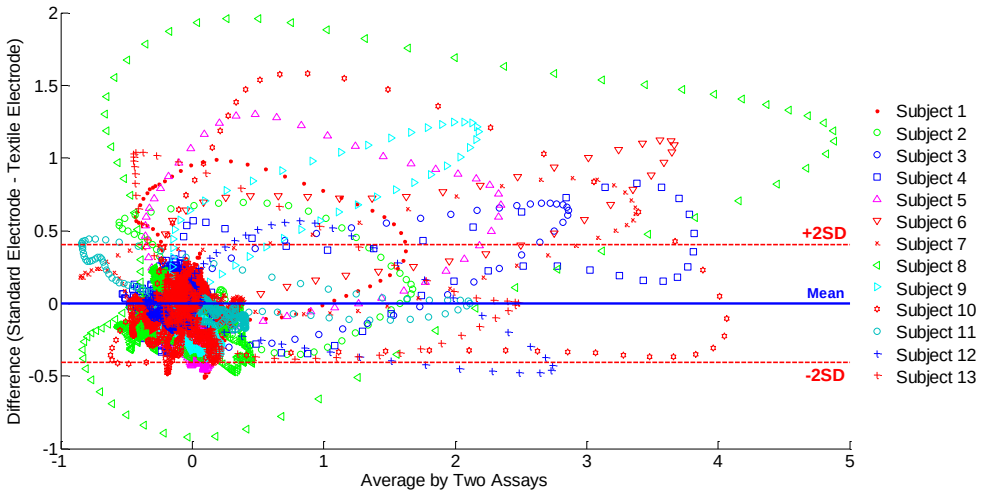

Figure 5.5 - Bland-Altman diagram from a complete representative cardiac cycle of each participant.

5.3.2. Time Analysis of the RR Interval

In a healthy person, cardiac potentials are generated in a quasi-periodic manner. However, the period between consecutive R-waves is not constant, changing with breathing and heart rhythm. During five minutes more than 300 IRRs are expected, which allows to verify if, with the course of time, noticeable differences appear between the standard's and the textile's electrodes IRRs. By plotting all the measured IRRs with the standard electrodes against the IRRs from the textile electrodes, it is possible to have a graphical representation allowing the visualization of the data distribution.

A total of 5307 IRRs from each electrode's signal were obtained and used to plot Figure 5.6. With the naked eye it can be seen that the IRRs have a very strong linear dependency, which is proved by a correlation coefficient of $r = 0.99$.

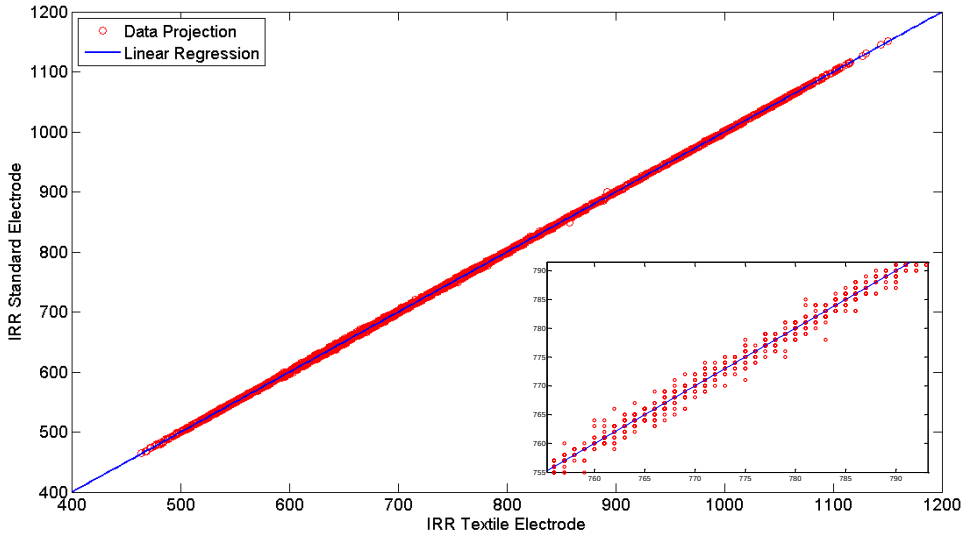

Figure 5.6 – Plotting of the standard electrodes IRRs versus the textile electrodes IRRs. In the inset it can be seen an amplified segment.

The high correlation results from the close proximity of the IRRs to the regression line, as can be seen in the inset of Figure 5.6. Indeed, the regression line does not distinguish from the identity line of both distributions. This can be explained by the analysis of Table III, which shows that the AVRR and SDRR of each signal are exactly the same for each subject, 732±146 ms, with differences between corresponding IRRs that do not exceed 9 ms. As stated by Bland & Altman (1986), the regression analysis and the correlation coefficient is not enough to assess data agreement. The Bland-Altman diagram using the IRRs of both the standard and textile signals is depicted in Figure 5.7. This diagram shows there is a good agreement between signals since the majority of points are located inside the confidence interval. Although there are some points outside this interval, they only represent less than 3.7% of the total IRRs plotted. The mean of the difference has a zero value, and the confidence interval has a value of ±2.34 ms, which are in accordance with the values of Table III. The farthest point from the confidence interval represents a 9 ms difference between IRR from both signals.

Table III - Comparison between the AVRR, SDRR and maximum dIRR from signals recorded with standard and textile electrodes.

Subject #	Standard Electrode		Textile Electrode		Maximum dIRR (ms)
	AVRR (ms)	SDRR (ms)	AVRR (ms)	SDRR (ms)	
1	746	61	746	61	5
2	776	25	776	25	5
3	651	40	651	40	4
4	652	32	652	32	6
5	561	50	561	50	2
6	988	62	988	62	2
7	757	66	757	66	3
8	977	87	977	87	2
9	750	59	750	59	2
10	761	59	761	59	2
11	980	63	980	63	9
12	550	20	550	20	1
13	701	61	701	61	2
Mean	757	52	757	52	3

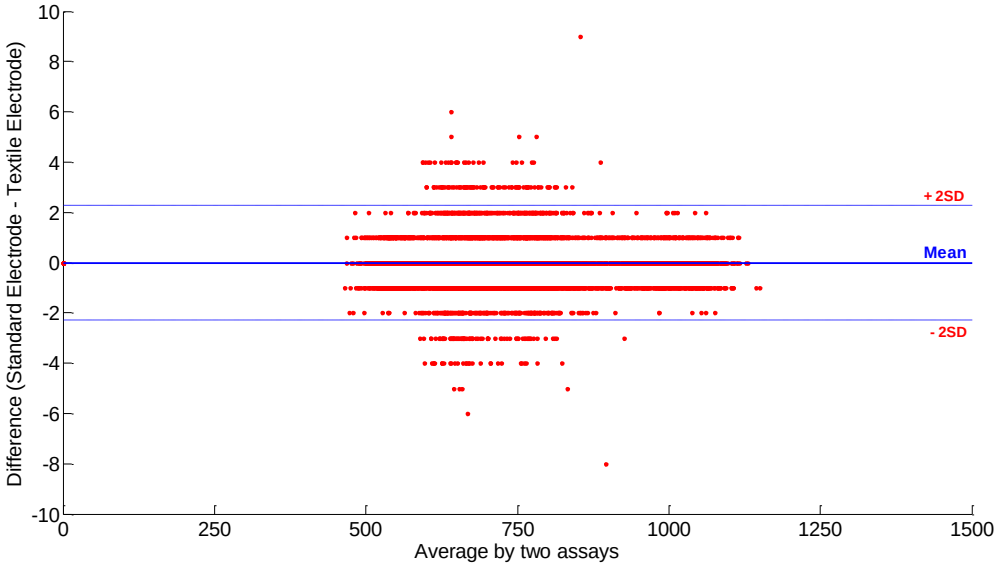

Figure 5.7 - Bland-Altman diagram of the IRR from each participant.

5.3.3. Power Spectrum Density

The PSD signals of each subject obtained via the Welch Method were averaged and normalized to their maximum intensity. A grey band, representing a 95% confidence interval, was obtained from the ±2 SD of the standard electrode's PSD signals, and overlapped to both the PSD. Through visual inspection of Figure 5.8 it is apparent that both signals show a similar spectral behaviour, especially between 1 Hz and 50 Hz, where the majority of the ECG spectral content lies. This is supported by the close proximity of both signals and the smaller confidence interval, which indicates a smaller standard deviation on this region. Between 50 Hz and 100 Hz, an increase in the standard deviation is noticeable, however the textile electrode PSD signal remains well inside the confidence interval.

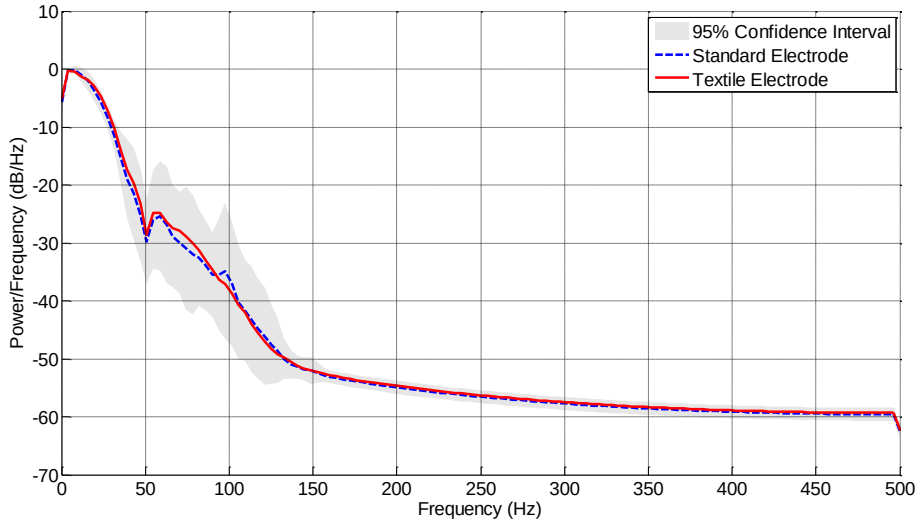

Figure 5.8 - Representation of the averaged PSD for both signals, and the 95% confidence interval shown in grey.

The band-pass filter, with an upper cut-off frequency of 100 Hz, made both signals show a very close trajectory from this frequency up to 500 Hz, as result of the attenuation provided by the filter. It is important to highlight that the 50 Hz centred valley is the result of the notch filter used to remove the power-line interference. As previously referred, in certain situations the occurrence of 50 Hz harmonics, is noticed by the presence of its second harmonic at 100 Hz in some of the measurements, in particular in the signals recorded with the standard electrodes. This is now clearly seen in the power spectrum plot.

5.4. Discussion

Although the ECG measurements were conducted at rest, the textile electrodes were more vulnerable to signal drift due to small movements of the torso, as for instance, during breathing. It was found that the cushioning effect provided by the soft foam material sewn behind the electrodes as proposed by Ottenbacher (2004) was fundamental to provide a good contact with the skin, resulting in fewer observations of these occurrences.

Since the standard electrodes were positioned below the textile electrodes in the frontal plane, the cardiac potentials were measured with the same angle, but from a slightly different position, which can explain the amplitude differences. Similar results were reported by Marozas (2011), who noticed that even a 1.5 cm distance between electrode's position have a significant impact in the recorded signal, revealing amplitude differences in both the QRS complex and the T-wave. Looking at a best case scenario as the signals of Figure 5.3, the textile electrodes can record a waveform where one can easily distinguish all the waves that constitute the ECG.

One particular aspect regarding the differences between signals is that textile electrodes seem to be more immune to the power-lines 50 Hz noise and its harmonics. Although measures were taken to reduce noise, like the use of shielded cables, limitation of noise sources, the use of a 50 Hz notch-filter and a high attenuation digital bandpass filter, this was not enough to reduce the noise power to unnoticeable levels. It should be noted that since the textile electrodes were not customized to work with press studs like the standard electrodes do, they used common conductive cables about 10 cm long, after which they were connect to the shielded cables. The standard electrodes, in turn, were directly connected to the shielded cables. Therefore, one would expect the standard electrodes to be more immune to electrical noise however this does not seem to have occurred. This does not mean that the 50 Hz noise and its harmonics are not present in the signals, but its expression is rather lower in the textile electrode's signal than in the standard electrodes signal. According to Puurtinen (2006), when using textile electrodes with hydrogel there is a significant noise drop with the increasing of the electrode area. Since the textile electrodes used in the ECG recordings had a 26 cm^2 sensory area it is possible that the substantially higher area of this electrode has contributed to the lower incidence of noise.

With the impedance data obtained in Figure 4.7, it was also expected that the signals recorded with textile electrodes had a higher SNR, however this did not happen. The textile electrodes showed a smaller average SNR than the standard electrodes, which is in accordance with results reported by Catrysse (2004) and with the values presented by Lee (2008). When comparing the results obtained by Lee (2008) using the same method as the one used here, not only the values are similar, but also shows a difference of 5 dB to 13 dB in favour of the standard electrodes. This could be related to some uncontrolled constraints related to the electrode impedance during the ECG recordings. All the participants used the same single size sensory shirt, which caused different electrode pressure against each participant's skin, in addition, the larger area of the textile electrodes made it more difficult to apply the electrolytic gel evenly through its entire surface, which could have contributed to higher impedances in some measurements. Moreover, no measurements to infer the skin-electrode impedance prior to the ECG recordings were carried out, making it impossible to know how low the textile electrodes impedance was at the moment of the recordings, and how the chest hair influenced the overall impedance and therefore the signal quality. Despite its quality, signals recorded with both sets of electrodes seem to be identical to each other, with minor differences that do not compromise the measurement of the cardiac rhythm, as emphasized by the good agreement between signals. It is possible to observe all the ECG waves in both signals, and there were no reported differences in their period. The smaller R-wave amplitude in the textile electrode did not compromise the capability of peak detection and therefore the heart rate and heart rate variability estimation.

Signals recorded from textile electrodes may present temporal shifts when compared to signals from standard electrodes. To assess if this indeed happens, a set of temporal analysis was performed. In order to preserve the signal phase with which the signals were recorded, all filtering procedures used a zero-phase filter. The regression analysis showed a strong linear relationship between the IRR measured from both signals, which was reinforced by the equal values of AVRR and SDRR. Some authors have suggested that when calculating the difference between IRR measured with two different systems, differences greater than 20 ms (Gamelin *et al.*, 2006) or 50 ms (Marchant-Forde *et al.*, 2004) should be considered an error. The maximum dIRR returned an average value of 3 ms and did not exceeded 9 ms, which is not only small, considering it represents a difference less than 0.4%, as it does not meet the error criteria described above. Identical difference values were reported by Lee (2008). The Bland-Altman diagram showed a good agreement between IRRs, being the percentage of outliers the same as in the point-by-point Bland-Altman diagram performed to assess the agreement between single representative cardiac cycles, 3.7%. These results allow to state that the differences in the R-wave amplitude and form, plus the smaller impedance phase of the textile electrodes do not generate temporal distortion in the signal.

Finally, the power distribution of each frequency revealed that the textile electrodes power distribution is very similar to that of the standard electrodes, especially in the frequencies below 50 Hz. The textile electrode PSD signal follows the standard electrode PSD

signal closely, always inside the confidence interval, even having a smaller width in this region. The question of the prevalence of the 100 Hz noise in the standard electrode's signals is here highlighted, since it is perfectly seen a slightly higher power peak in this frequency, and it has a very wide confidence interval.

5.5. Conclusions

In this chapter, a comprehensive study of the morphological, time and power properties of the ECG textile electrodes was performed and compared against those of the standard silver-chloride electrodes. This comparison was focused on the morphological and time aspects, since they are the most used in clinical context and in the spectral content in order to assess the power-frequency distribution.

Considering the data obtained after its analysis, substantial differences between electrodes were not found, indicating its use for measuring cardiac potentials at rest is feasible, and it can be used as a reliable alternative to the traditional silver-chloride electrodes.

Further studies should be performed in order to assess the textile electrode's ability to measure cardiac potentials in activities requiring higher cardiac effort, its immunity to motion artefacts especially during exercise, as well as longer recordings to verify if polarization effects do occur, and its possible influence in the recorded signal.

Chapter 6

Validation of textile electrodes for electromyography

6.1. Introduction

The electromyography signal (EMG) is the result of the capture of the electrical effect of the recruitment of different muscular fibres with different properties, thus making the measurement of EMG variables a challenge in terms of reproducibility between subjects and even within the same subject. According to Merletti (2004) some of the anatomical, physical and methodological factors that may affect the EMG variables include (1) the thickness of the subcutaneous tissue layer, (2) the depth of the sources within the muscle, (3) the inclination of the detection system with respect to the muscle fibre orientation, (4) the length of the fibres, (5) the location of the electrodes over the muscle, (6) the filters used, (7) the inter-electrode distance, (8) the electrode shape and size, (9) crosstalk with nearby muscles, and (10) the estimators used for EMG variables computation. So, if one wants to record an EMG signal with two pairs of electrodes simultaneously, a careful muscle choice and electrode placement is necessary, so that even measuring different muscle fibres the overall EMG signal would be similar.

In this chapter, a validation study of the use of textile EMG electrodes in comparison to standard silver-chloride electrodes was performed. Signals from both sets of electrodes were recorded simultaneously during isometric contraction with three different sub-maximal loads. The resulting signals were evaluated in terms of morphologic resemblance, power frequency spectrum, and time-frequency power distribution to determine if there are significant differences between the two types of electrodes.

6.2. Methodology

6.2.1. Muscle Selection

Considering the variables that affect EMG signal, as described by Merletti (2004), a set of criteria was established to assist the choice of the muscle where the validation measurements were going to be performed. Therefore, two sets of criteria were established, one regarding locations issues (a-c) and the other muscle characteristics (d-f): (a) the muscle should be located in a easily accessible area where clothing is not a constraint, (b) the area should have a low subcutaneous tissue layer, (c) it should have as few body hair as possible (d) the muscle fibres orientation should be easily detected, (e) the muscle should be large enough to accommodate two pairs of electrodes, (f) it should be an area with few other muscles, with which crosstalk may occur. In terms of location, the best muscles are those in the upper and lower limbs, since they are easily accessible while using a t-shirt or shorts. Considering the locations issues, the muscle that best fit these criteria is the *rectus femoris*. However, its characteristics make it not eligible since there are other muscles in the vicinity that could contribute to the occurrence of crosstalk, the region where it locates has a higher subcutaneous layer in woman (Browning *et al.*, 2006), and men usually have abundant body hair in the lower limbs. In addition *rectus femoris* muscle is penniform, making it difficult to detect the fibres orientation. The best candidate appears to be the *biceps brachii* since it meets all the location criteria. By being relatively large, the fibres orientation being fusiform, and because there are no other muscles in the vicinity, the muscle criteria are also met. To reinforce this choice, Merletti (2004) stated that this muscle presented a good repeatability during isometric voluntary contractions.

6.2.2. Participants

Muscular isometric voluntary contraction recordings were performed with a group of 10 healthy participants, five male and five female, recruited from local university students. All participants were right-handed, with no history of neuromuscular constrains, 25±3 years old, body mass of 65±10 kg and 1.69±0.11 m in height.

Volunteers were informed of the study objectives and the experimental protocol, after which they had the possibility to familiarize themselves with the experimental setup and the electrodes to be used.

6.2.3. Materials

The standard silver-chloride electrodes used as reference were the auto-adhesive SX-30 model of Dormo&Blayco (Telic S.A., Spain), with a solid gel film over a 1 cm^2 circular sensory

area. The EMG textile electrodes were manufactured through a knitting technique, using a mixture of 80% silver-plated polyamide (Elitex) with 20% Lycra and a linear density of 23.5 tex. Each EMG sensor comprises two 1 cm^2 rectangular shaped electrodes with a 2 cm centre-to-centre distance. Both electrodes used are displayed in Figure 4.5. Due to the lack of auto-adhesive properties of the textile electrodes, they were sewn into a semi-rigid foamed material (plastazote) and fixed to the skin with the help of an adjustable elastic band.

(a) (b)

Figure 6.1 – The (a) textile electrodes sewn in the plastazote and (b) fixated against the skin.

Maximum isometric force was assessed with a Globus Ergo Meter Load Cell (Globus Italia, Italy). Since the EMG is a low amplitude signal, during the physiological measurements both sets of electrodes were coupled to a two-stage amplifier (Gonçalves *et al.*, 2006). The first stage pre-amplified the signal 100 times with a CMRR larger than 110 dB, while at the second an amplification of 11 times was performed, in a total amplification of 1100 times. The EMG amplified signals were then recorded using a BIOPAC MP100 (BIOPAC Systems Inc., CA, USA) with a 16 bit resolution and 1000 Hz sampling frequency.

6.2.4. Measurement Setup

Before the electrodes placement, skin was cleaned with 70% ethylic alcohol and slightly abraded with a piece of cotton until redness. After this, electrodes were placed perpendicular to the muscle fibres on the *biceps brachii* belly, and the reference electrode was attached to the elbow. Due to the inability of placing both the standard and textile electrodes on the same place, and to prevent substantial differences in the recorded signal, they were carefully placed as near as possible, as shown in Figure 6.2. A thin layer of 0.1 mL of conductive gel (Quick Eco-Gel, Lessa S.A., Spain) was applied on each textile electrode to provide them with similar skin contact conditions to those of the standard electrodes.

Figure 6.2 - Standard and textile electrodes position on the *biceps brachii*.

The pressure exerted by the textile electrodes against the skin was not standardized, but the elastic band was adjusted to keep a good and comfortable skin contact, at the same time.

Participants were asked to sit on a rigid armless chair with the right elbow flexed at 90º and the forearm supinated, as described by Oliveira (2009) and Linz (2007). The relative placement of the electrodes, the participant's posture and the overall measurement setup is depicted in Figure 6.3.

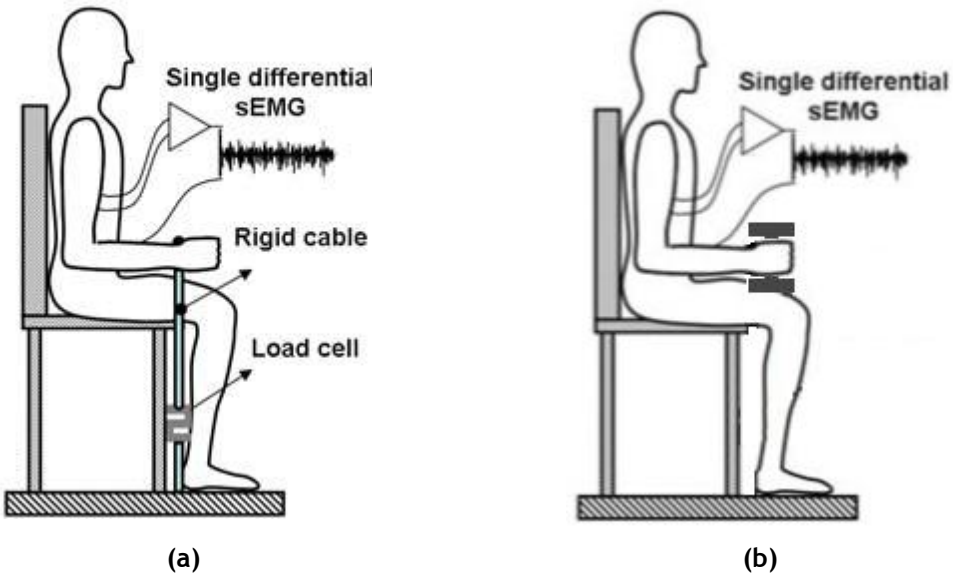

Figure 6.3 - Measuring setup for the (a) MVC and (b) the sub-maximal isometric contractions. Adapted from Oliveira (2009).

Three maximum voluntary contractions (MVC) attempts with ten seconds of duration and at least two minutes of rest in between were performed with strong verbal encouragement. During each MVC attempt, the maximum isometric force was measured with a load cell. After a resting period of at least three minutes, isometric sub-maximal contractions were

performed holding dumbbells against gravity, with loads representing 20%, 50% and 80% of the MVC. For each sub-maximal load three repetitions of five seconds were carried out, followed by at least two minutes of rest, and between loads at least three minutes of rest was given. The order in which the dumbbells were provided to the participants was randomized.

6.2.5. Data Analysis

Raw data was digitally filtered after acquisition using Matlab 7.9.0 (MathWorks, MA, USA). This process included the DC component removal and a 20-500 Hz zero-phase Butterworth bandpass filter (-80 dB/decade) to restrict the signal frequencies to those with physiological relevance. No 50 Hz notch filter was used in order to preserve as much EMG information as possible. Afterwards, a full wave rectification of the filtered signal was carried out, and its Root Mean Square (RMS) envelope, was calculated with a 150 samples smoothing window. The resulting envelopes of each electrode were then normalized by the corresponding MVC value.

To evaluate the performance of the textile electrodes in measuring EMG with respect to the standard silver-chloride electrodes, a set of morphological, frequency, and time-frequency analysis was performed. Morphological analysis intended to assess the similarities between the textile and standard electrode's RMS envelopes patterns using different loads. This analysis included the overlapping of both envelopes and their visual inspection, after which the Root Mean Square Error (RMSE) between envelopes was calculated to infer about how much they differ from each other. The Teager-Kaiser Energy Operator (TKEO) was used to automatically detect an envelope's onset and offset by detecting a sudden change in the signal's amplitude and frequency, with the aid of a threshold level (Th) applied to the TKEO output, and defined by:

$$Th = u_0 + j.o_0 \tag{11}$$

where u_0 and o_0 represent the mean and standard deviation of the TKEO output when there is no muscle activity, and j is a variable determined empirically and ranging from 1 to 10. The onset and offset time is determined when the TKEO output exceeds the threshold level (Xiaoyan Li, 2005). The TKEO algorithm was used over the RMS envelopes using a threshold level of $j = 1$ and whenever the automatic detection failed, manual detection with the aid of the threshold was performed. Next the envelope's peak (pRMS) and the envelope's integral (iRMS) was calculated. Since the EMG activation period, i.e., the time interval between the onset and the offset is not exactly the same in every measurement, all the iRMS were time-normalized (Hildenbrand & Noble, 2004). The presence of noise was measured by the Signal-to-Noise Ratio (SNR) obtained from the MVC data, being the result for each participant an average of the three repetitions.

Power Spectrum Density (PSD) was used to quantify the overall power distribution across the frequency spectrum and how much a given frequency was expressed in a signal. The frequency analysis included a one-sided PSD plotted using the Welch method, with a 256

points Hamming window, 50% overlapping and normalized by its maximum. The resulting PSD from both signals was overlapped and visually inspected, while the average power differences were calculated by subtracting the textile electrode PSD signal to the standard electrode PSD for each sub-maximal load. The median frequency (MDF) was also obtained to quantify the power distribution of each PSD signal.

The time-frequency analysis was performed through Short Time Fourier Transform (STFT) spectrograms of a representative signal from each load and participant. The STFT of the signals measured with the standard and the textile electrodes were computed with a Hanning window of 127 points and normalized to their absolute maximum. The difference between the standard electrodes normalized STFT and the normalized textile STFT was calculated to help detecting differences. The instantaneous median frequency (IMF) was also calculated and compared for the standard and textile signals PSD.

The Matlab algorithms used in the data analysis were developed expressly for these tasks and can be viewed in Appendix B.

6.2.6. Statistical Analysis

Descriptive statistical analysis with mean, standard deviation, minimum and maximum value of each variable under study was performed. In order to evaluate if there were significant differences between measures, between the standard and the textile electrodes and between the sub-maximal loads when measuring the pRMS, the iRMS, the MDF and the RMSE, an ANOVA for repeated measures test was carried out. These statistic procedures were performed using SPSS Statistics 18 (IBM, NY, USA), with a probability level of 0.05 and following the Greenhouse-Geisser line in order to guarantee the data homogeneity. Data normality was verified using the Shapiro-Wilk normality test. Agreement between the standard and textile electrodes measurements of the pRMS, the iEMG and the MDF for each of the sub-maximal loads were also assessed using Bland-Altman diagrams to that end.

6.3. Results

6.3.1. Morphological Comparison

One of the main concerns when using textile electrodes is their fixation and contact with the skin. In this study, the textile electrodes were fastened against the skin using an elastic band that was responsible for keeping them in position. Although there was no attempt to control the pressure that the elastic band exerted, it was always fastened by the same person, trying to impose the same pressure. After measurements with each participant, it was found that the electrodes imprinted themselves on the skin as a result of the pressure

they exerted. Figure 6.4 shows a good example of the imprints left by both sets of electrodes.

Figure 6.4 - Imprints of the textile and standard electrodes on the skin.

The standard electrode left two concentric circular imprints, caused by the circular sensory area (inner circle) and by the adhesive band (outer circle). As a result of the adhesive glue in use on this type of electrodes, irritated skin can be seen as a reddish coloration on the outer circle. The textile electrode imprints, although more noticeable due to the marks left by the cables and the plastazote's edges, does not seem to have caused any kind of skin irritation, and it did not left any glue residues.

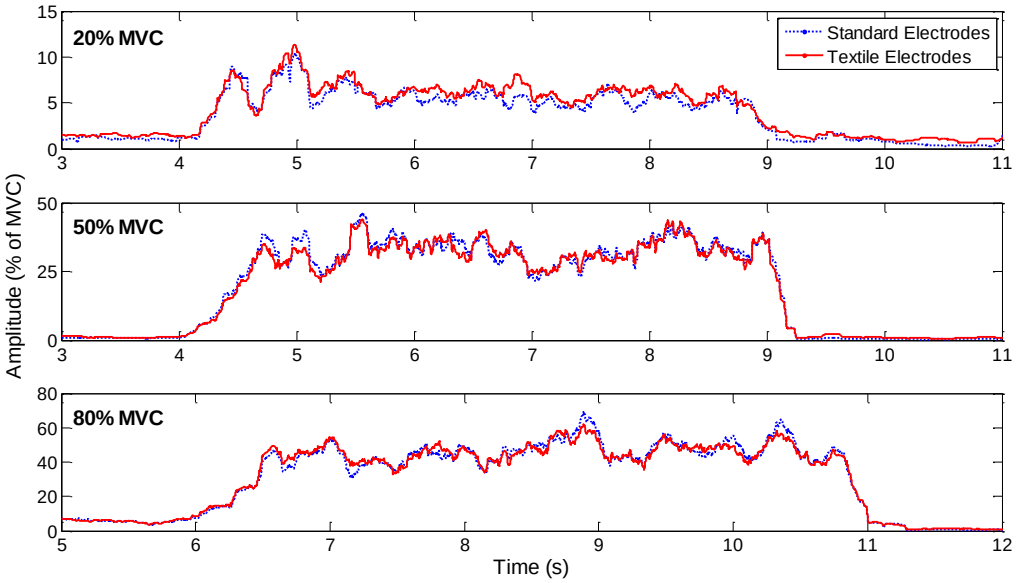

Figure 6.5 - An example of an EMG signal recorded using both sets of electrodes.

Table IV - Root Mean Square Error between the standard and textile electrodes at each sub-maximal load.

	RMSE		
	20% MVC (%MVC)	50% MVC (%MVC)	80% MVC (%MVC)
Mean	3.6	9.3	7.9
Standard Deviation	3.2	9.5	4.9
Minimum	0.8	1.2	1.9
Maximum	11.5	31.5	22.1

The imprints left by both types of electrodes suggest that they had good contact with the skin. They also show how closely they were placed on the muscle belly and that they had the same orientation regarding the muscle fibres. Therefore, it was expected that the resulting EMG signals were similar enough for an effective pattern comparison. By computing the RMS envelope, the abrupt changes characteristic of the EMG signal were smoothed, and it could be used as an EMG approximation, allowing an easier observation of its pattern. In Figure 6.5, a representative example of the envelopes obtained for each load can be seen.

Although there are some amplitude and behaviour differences between the standard and the textile electrode envelopes, they seem to coincide in most of their features, especially in the isoelectric line and in the envelope's onset and offset. This is particularly noticeable in the beginning and ending of the 50% MVC and 80% MVC load envelopes. During the activation period, both envelopes have identical patterns which are denoted by the coincidence of several peaks. During the 20% MVC signal, it can be seen that the first two peaks were well replicated by the textile electrode's envelope, but some variations did occur during the rest of the envelope. During the 50% MVC and 80% MVC, the textile electrode's envelope kept a closely matched pattern along the entire standard electrode's envelope.

Further analysis of how much the standard and textile electrode's differed or resembled, to each other, was analysed by calculating the RMSE between their envelopes. The results presented in Table IV reveal that the mean RMSE value becomes higher with the increase of the sub-maximal load, and that the standard deviation shares the same behaviour. The higher RMSE value has occurred at the 50% MVC, reaching to 31.5% MVC.

Noise may play a significant role in the envelope's amplitude and masking the EMG signal, since the noise amplitude is also accounted when the envelope is calculated. Once the isoelectric lines of both electrode's envelope seem to have identical amplitude, this would indicate that both types of electrodes have the same susceptibility to noise. To infer about this, the SNR was calculated using the envelope of the three MVC attempts, because they were the measurements with the highest recorded amplitudes, and using the following equation:

$$SNR = 20\log_{10}\frac{RMS_{EMG} - RMS_{noise}}{RMS_{noise}} \quad (12)$$

where RMS_{EMG} refers to the average RMS envelope amplitude, and RMS_{noise} to the average RMS amplitude of the isoelectric line during the three seconds before the EMG onset. The SNR results, summarized in Table V, show that the average difference between the noise content of the signals measured using either the standard or the textile electrodes is just one decibel. However, the standard deviation and the difference between the maximum and minimum of each type of electrodes reveal that the textile electrodes signal have a higher variation range than the standard electrodes.

Table V - Signal-to-noise ratio of the standard and textile electrodes.

	SNR		
	Standard Electrodes (dB)	**Textile Electrode (dB)**	**Absolute difference between electrodes (dB)**
Mean	23.4	22.4	1.0
Standard Deviation	4.6	5.6	1.0
Minimum	16.9	13.5	3.4
Maximum	36.3	37.5	1.2

The pRMS is an indicator of the muscle maximal activation, and it is obtained from the maximum amplitude value of the RMS envelope. Descriptive statistical analysis between the standard and textile electrodes, shown in Table VI, reveals that the standard electrodes have a higher pRMS value along all the sub-maximal loads, and that the difference between electrodes tends to grow with the increase of the sub-maximal loads. This is also valid on the standard deviation of both electrodes. When observing the minimum and maximum values, it can be seen that standard electrodes have a higher variation, but in terms of minimum values, differences between electrodes are almost non-existent.

The ANOVA statistical analysis showed that there were no differences between measurements ($p=0.48$) and neither between the measurements and the electrodes ($p=0.75$), which indicates that both types of electrodes are capable of measuring similar values for pRMS. In addition, no differences were found between each measurement and the sub-maximal loads ($p=0.49$). Since the sub-maximal loads represent different percentages of the maximum voluntary contraction, it was expected to observe differences between each load; however no statistical differences between 50% MVC and 80% MVC were found ($p=0.72$). This may indicate that the pRMS values were too similar in both sub-maximal isometric contractions. Finally, no differences were found between each electrode type measurements at different sub-maximal loads ($p=0.97$), which indicates that for the same load, both electrodes made similar measurements.

Table VI – Comparison of the peak values of the RMS envelope between the standard and textile electrodes.

Sub-maximal load	Type of Electrodes	pRMS Mean (%MVC)	Standard Deviation (%MVC)	Minimum (%MVC)	Maximum (%MVC)
20% MVC	Standard Electrodes	16.10	6.99	6.90	38.10
	Textile Electrodes	14.16	4.74	7.10	26.90
	Difference between electrodes	1.93	2.25	-0.20	11.20
50% MVC	Standard Electrodes	41.22	23.04	2.60	91.70
	Textile Electrodes	36.42	16.61	2.60	63.00
	Difference between electrodes	4.79	6.44	0.00	28.70
80% MVC	Standard Electrodes	60.33	29.03	4.50	127.80
	Textile Electrodes	52.80	23.55	4.80	106.60
	Difference between electrodes	7.53	5.48	-0.30	21.20

Agreement between the pRMS measures performed with the standard and the textile electrodes was assessed by Bland-Altman diagrams for each sub-maximal load, as depicted in Figure 6.6. The positive bias of the Bland-Altman diagram mean shows that the standard electrodes generally have higher peak amplitude, which becomes higher with the increase of the sub-maximal loads. The limits of agreement, established by the ±2 SD, determine that the data points inside them represent a pair of measures with good agreement. Knowing this, just a few data points can be found outside this limit, which account for 10% (at 20% MVC), 13.3% (at 50% MVC) and 6.7% (at 80% MVC) of the total data points. Nevertheless, the values of the limits of agreement represent considerably higher differences between electrodes, which can be explained by an abnormal amplitude of the textile electrodes showed by some subjects. This explains why most of the data points are located around the mean, and only some of them approach the limits of agreement. Altogether, the pRMS from both types of electrodes have a good agreement, even considering the high variability that some data pairs have shown.

In Figure 6.7 is depicted a representative sample of a detected onset and offset using TKEO, which was simultaneously overlapped on the filtered signal and on the RMS envelope in order to verify if the TKEO output did really correspond to the onset and offset. With the envelope's onset and offset detected, it is possible to proceed with the iRMS calculation, which is a time-dependent variable. By integrating the envelope delimited between the onset and the offset period, it is possible to quantify its area during the period of muscle activation.

A brief descriptive statistical analysis can be found in Table VII, where it is shown that for the 20% MVC sub-maximal load, both electrodes iRMS are very close to each other, revealing that they have similar areas. A close similarity is also verified at 80% MVC. As previously with the pRMS data, the minimum values for each sub-maximal load show very small differences, being the 80% MVC the only exception.

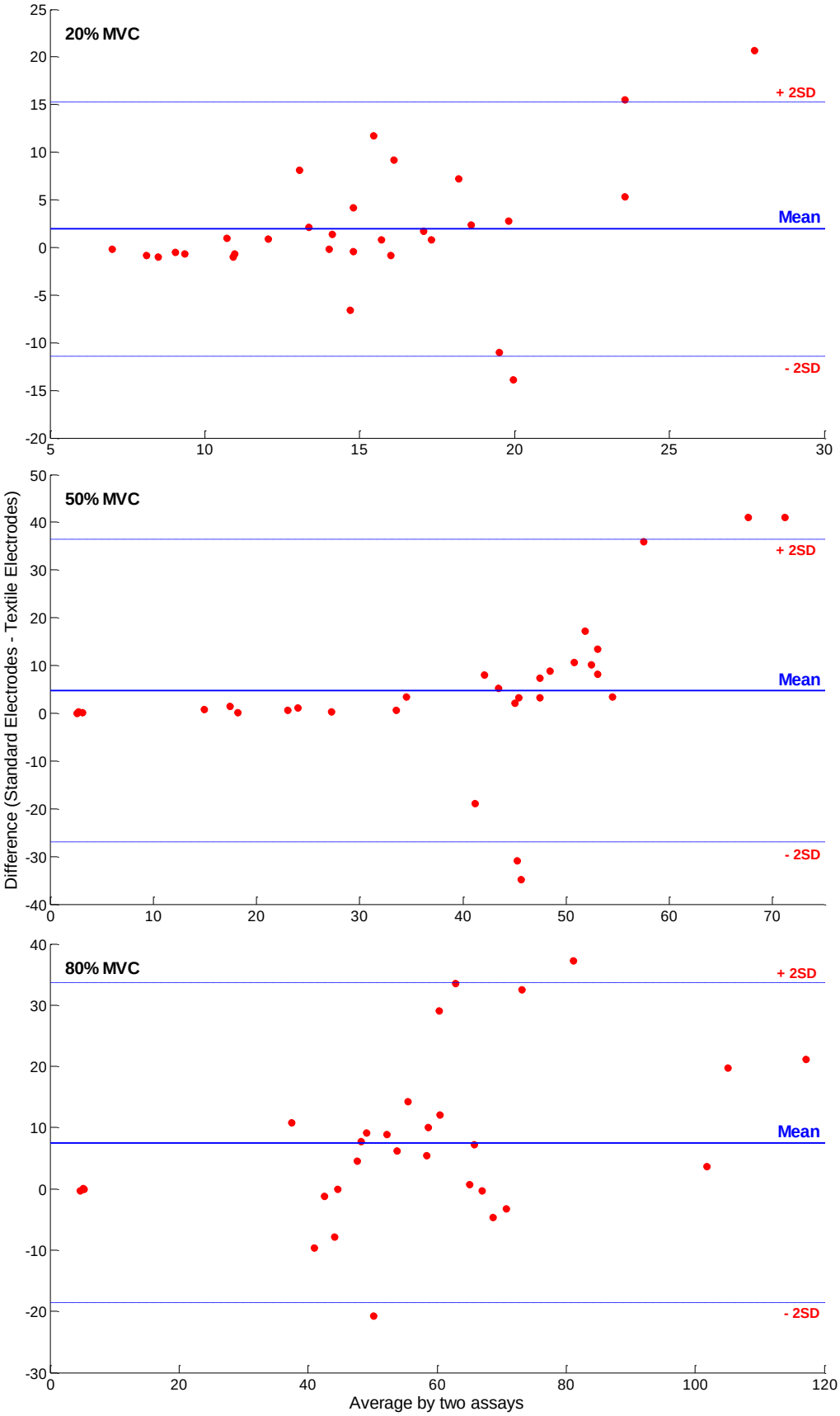

Figure 6.6 - Bland-Altman diagram of the pRMS values for each load.

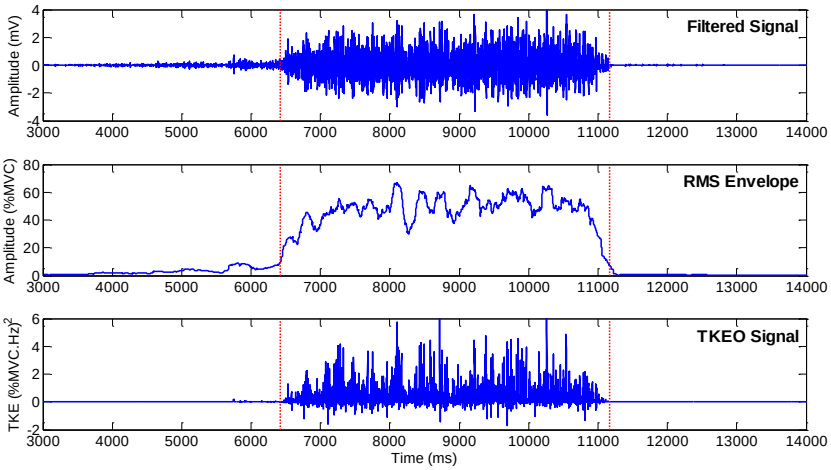

Figure 6.7 - Output of the onset and offset detection using the TKEO, and comparison with the filtered signal and the RMS envelope.

The ANOVA statistical analysis revealed that there were no differences between measurements (p=0.58), and neither between the measurements and the electrodes (p=0.83), which indicates that both types of electrodes are capable of measuring similar values of iRMS. No differences were found between each measurement and the sub-maximal loads (p=0.65).

Further information about the iRMS of each electrode type at different sub-maximal loads can be obtained from the agreement assessment performed by the Bland-Altman diagram, as depicted in Figure 6.8. The data points scattering pattern over the diagrams is very similar to that of the pRMS, indicating there is a close relationship between the pRMS and the iRMS. Even the data points outside the limits of agreement have equal values, representing 10% (at 20% MVC), 13.3% (at 50% MVC) and 6.7% (at 80% MVC) of the total data points. The bias of the mean show that the standard electrodes tend to have higher values than the textile electrodes, and that the mean difference between the two types of electrodes is roughly the same along the difference of sub-maximal loads.

Table VII – Comparison of the integral values for the RMS envelope between the standard and textile electrodes.

Sub-maximal load	Type of Electrodes	iRMS Mean (%MVC.s)	Standard Deviation(%MVC.s)	Minimum (%MVC.s)	Maximum (%MVC.s)
20% MVC	Standard Electrodes	9.66	3.97	4.10	21.50
	Textile Electrodes	8.77	3.23	4.80	19.20
	Difference between electrodes	0.89	0.74	-0.70	2.30
50% MVC	Standard Electrodes	29.01	15.73	9.50	65.00
	Textile Electrodes	24.46	8.98	9.30	41.20
	Difference between electrodes	4.55	6.75	0.20	23.80
80% MVC	Standard Electrodes	38.39	14.14	23.40	80.40
	Textile Electrodes	35.09	11.29	19.50	66.20
	Difference between electrodes	3.30	2.85	3.90	14.20

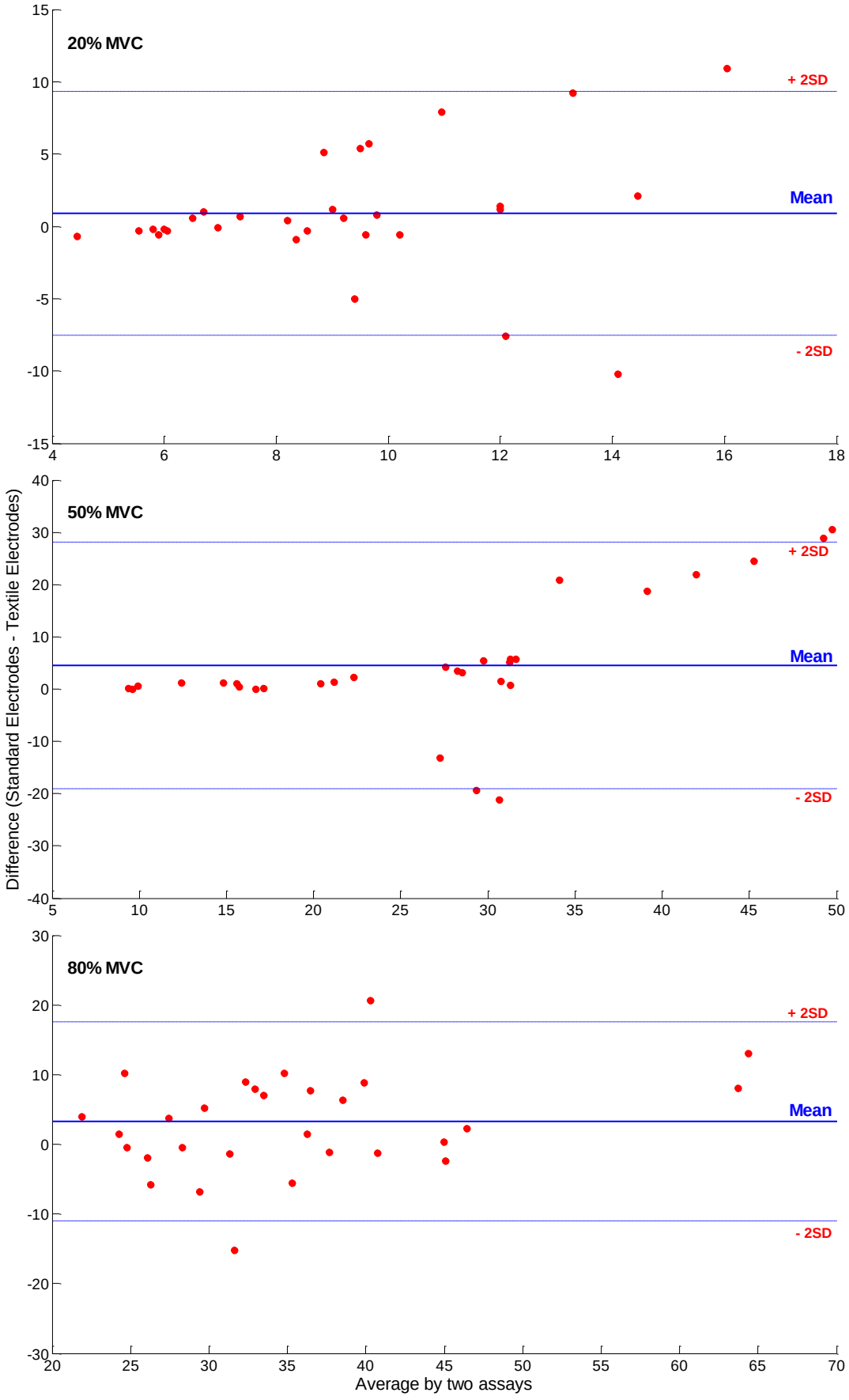

Figure 6.8 - Bland-Altman diagram of the RMS integral value for each load.

6.3.2. Frequency Analysis

A representative sample of three Welch periodograms, representing the overall power distribution of the standard and textile electrodes for each sub-maximal load, is depicted in Figure 6.10. It is possible to notice some clear differences between the standard and textile signals, like the presence of noise peaks on the textile signal at 200 Hz and 400 Hz, caused by the power-line harmonics, and a high power peak in the textile signal near the 450 Hz.

Unlike other electrophysiological signals, as for instance the ECG, the EMG signals have a spectral content that shows large variations between repetitions and subjects, due to the recruitment of different muscle fibres. Thus, comparing the standard and textile electrodes PSD from difference subjects during different measurements is not feasible. The difference plots, depicted in Figure 6.10, represent the differences between PSD signals for each sub-maximal load, allowing an easier observation of how much the two signals differ from each other, and at which frequencies are these differences more pronounced.

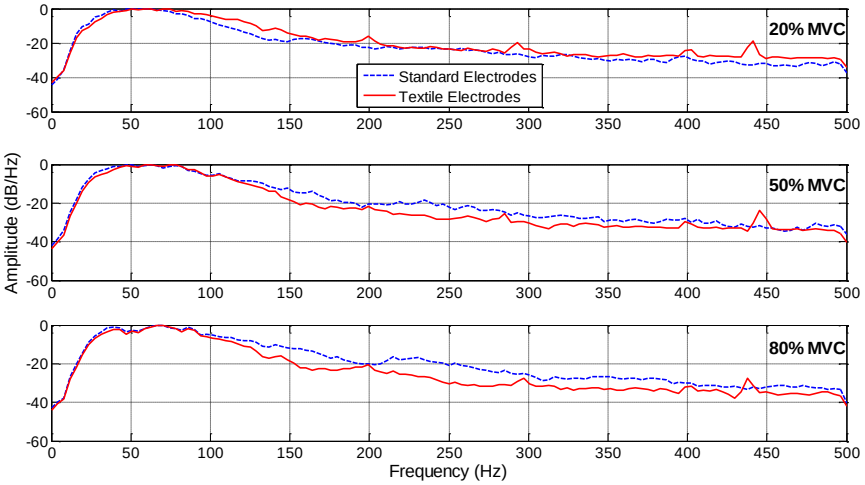

Figure 6.9 – Representative examples of a PSD signal for each load.

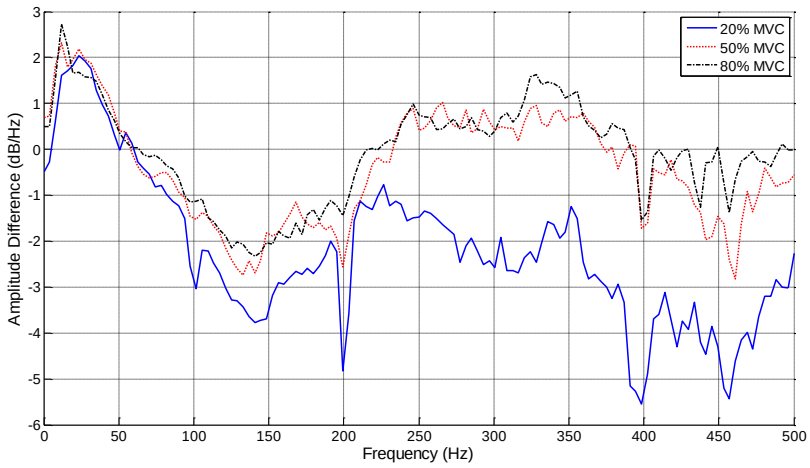

Figure 6.10 - Average power differences between the standard and textile electrodes PSD signals for each load.

With the average power differences, it can be seen that for each sub-maximal load the difference between signals have a large variation depending on the frequency. During isometric contraction at 20% MVC, the PSD from the textile electrodes have power amplitude substantially lower than that of the standard electrodes, as evidenced by the negative value of the difference plot. When the sub-maximal load is increased to 50% MVC and 80% MVC, the difference patterns become similar, and they start to vary around zero.

One thing that Figure 6.10 makes clear is that the 50 Hz power-line noise was recorded by both types of electrodes, as denoted by the zero difference value at this frequency. However, the textile electrode show a higher susceptibility to the 50 Hz harmonics, especially to the second, fourth and eighth harmonics, as evidences by the negative peaks at 100 Hz, 200 Hz and 400 Hz, respectively. It should be noticed that since a notch filter was not used, the 50 Hz noise is present in both signals. This is reinforced by Figure 6.11 which reveals that the PSD standard deviation around 50 Hz decreased to a minimal difference for all sub-maximal loads. At the rest of the spectrum the standard deviation does not show any abnormal value, which emphasizes that for the same sub-maximal load there is not a frequency, or frequency interval, with substantial differences between subjects and measurements.

According to Costa (2010), the MDF is the frequency that divides the power spectrum in two halves with the same power content, thus making it suitable to assess if the power content of the standard and textile electrodes is similar. To this end, the MDF was calculated using the following mathematical expression:

$$MDF = \frac{1}{2}\sum_{i=1}^{M} P_i \tag{13}$$

where, P_i is the power at the frequency of i Hz, and M is the highest frequency considered.

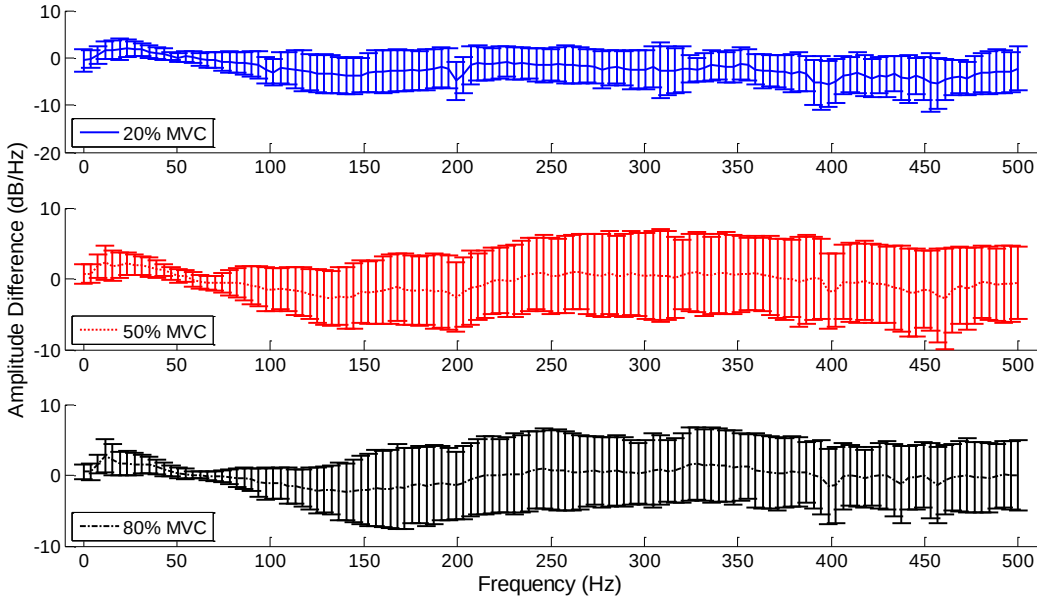

Figure 6.11 - Average differences between the standard and textile electrodes PSD signals for each load, and the corresponding standard deviation for each frequency.

Table VIII – Comparison of the integral values for the RMS envelope between the standard and textile electrodes.

Sub-maximal Load	Type of Electrode	Median Frequency Mean (Hz)	Standard Deviation (Hz)	Minimum (Hz)	Maximum (Hz)
20% MVC	Standard Electrodes	316	6	300	326
	Textile Electrodes	313	9	290	324
	Difference between electrodes	3	-3	10	2
50% MVC	Standard Electrodes	324	8	305	339
	Textile Electrodes	324	7	313	335
	Difference between electrodes	0	1	-8	4
80% MVC	Standard Electrodes	325	6	312	334
	Textile Electrodes	327	7	317	344
	Difference between electrodes	-3	-1	-5	-10

The MDF descriptive statistical analyses of Table VIII show that its values are very close to each other, as suggested by the small differences between the mean MDF and the almost equal standard deviation of both electrode types. With the exception of the 50% MVC sub-maximal load, the standard electrodes normally have smaller differences between the minimum and maximum values than the standard electrodes.

ANOVA statistical analysis revealed that there were no statistically significant differences between measurements ($p=0.21$), and neither between the measurements and the electrodes ($p=0.63$), which indicates that both types of electrodes are capable of measuring similar MDF values. For each sub-maximal load, the measures were also not different ($p=0.71$), but since there were no statistically significant differences between the MDF measures at 50% MVC and 80% MVC ($p=0.72$), this suggests that MDF values between these loads are very similar. Differences between measurements performed with the two types of electrodes at the different sub-maximal loads did not reveal significant differences ($p=0.68$).

Agreement between measures performed with the two types of electrodes was assessed with the help of Bland-Altman diagrams for each sub-maximal load. The results depicted in Figure 6.12 show that the MDF have higher agreement than the other parameters previously presented, with only 3.3% (at 20% MVC and 50% MVC) and 10% (at 80% MVC) of the data points out of the confidence interval. The bias of the diagram's mean also showed that, at 20% MVC, the standard electrodes measure higher values of MDF, but this tends to change with the increase of the sub-maximal load, being the textile electrodes the ones that measure higher values at 80% MVC. In addition, the limits of agreement appear to remain constant throughout the different sub-maximal loads.

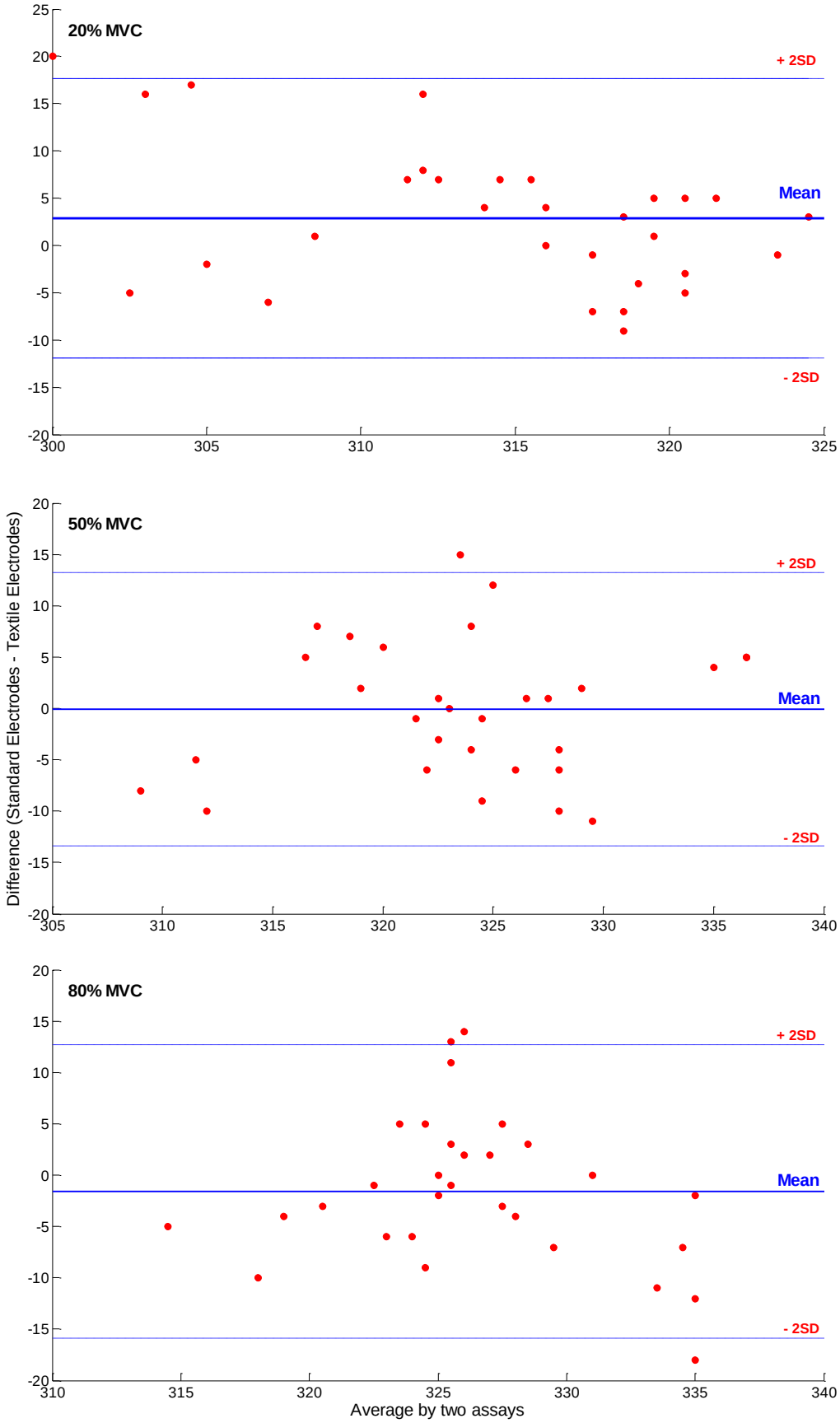

Figure 6.12 - Bland-Altman diagram of the median frequencies for each load.

6.3.3. Time-Frequency Analysis

Frequency analysis of the EMG signals revealed the overall differences and similarities of the signals measured with both types of electrodes. However, the PSD plots used to obtain that information lack time description. To this end, time-frequency analysis returns power and frequency information to a given time period, allowing the assessment of which frequencies were active at that moment. The instantaneous median frequency (IMDF) was used to give an idea of how power was distributed along each moment during the muscle activation. According to Merletti (2004), the IMDF can be given by:

$$IMDF = \int_0^{IMDF(t)} P(t,\omega)d\omega = \int_{IMDF(t)}^{\infty} P(t,\omega)d\omega \tag{14}$$

and it represents the frequency at which the power integral defined between zero and the IMDF equals the power integral between the IMDF and the final frequency. All the STFT analysis had as output a figure containing the spectrogram of the standard and textile electrodes, a spectrogram of the difference between the standard and textile electrodes, the IMDF of both electrodes and their RMS envelope. The spectrograms obtained from the recorded data reveal that the majority of the power content is beneath 300 Hz, and that the highest power value is under 100 Hz. In the 20% MVC spectrogram depicted in Figure 6.13, it is possible to see that the moments of high power roughly coincided between both electrodes. The difference spectrogram shows there are some differences, but they are not greater than 30%. The IMDF from both types of electrodes show some variation, but in the overall aspect they coincide.

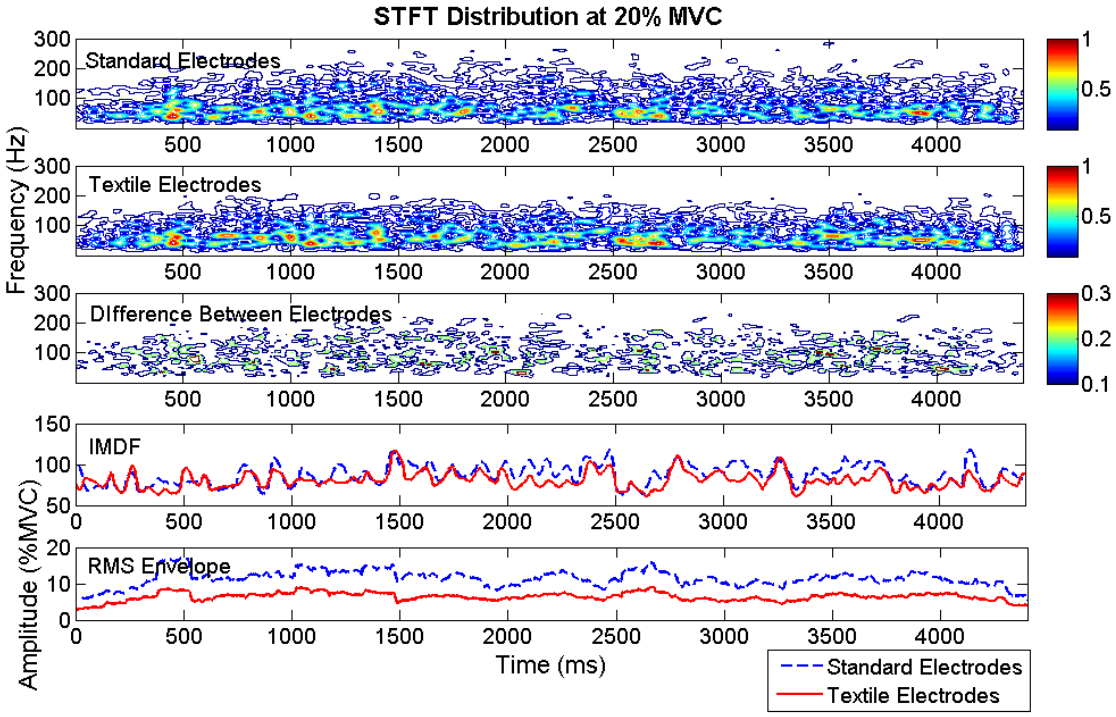

Figure 6.13 - Spectrogram and IMDF of the EMG measured with the standard and the textile electrodes at 20% MVC.

In the 50% MVC, the spectrograms of Figure 6.14 show the higher power moment located around 1500 ms in both electrodes. When observing the power differences it can be seen that they are very small, typically in the range of 10% to 20%, and that at 1500 ms there are not big differences at the frequency where the high power activation occurred. A similar situation can be seen between 2500 ms and 3000 ms. The textile electrode's IMDF, at 50% MVC, showed a considerable decrease after 1000 ms, which is in accordance with the PSD analysis where it can be found smaller MDF values for this electrode. Despite this, the IMDF pattern remains similar between electrodes.

The 80% MVC spectrograms of Figure 6.15 show more high power activation moments along the contraction period in both the standard and textile electrodes. The most noticeable difference is the standard electrodes having power distributions above 200 Hz, while the textile electrodes have its power distributed well beneath this frequency. Observing the difference spectrogram, there are no significant differences at the moments of higher power, and the IMDF plots show a good correspondence between electrodes. Once again the first 500 ms are the period where the IMDF have the closest match.

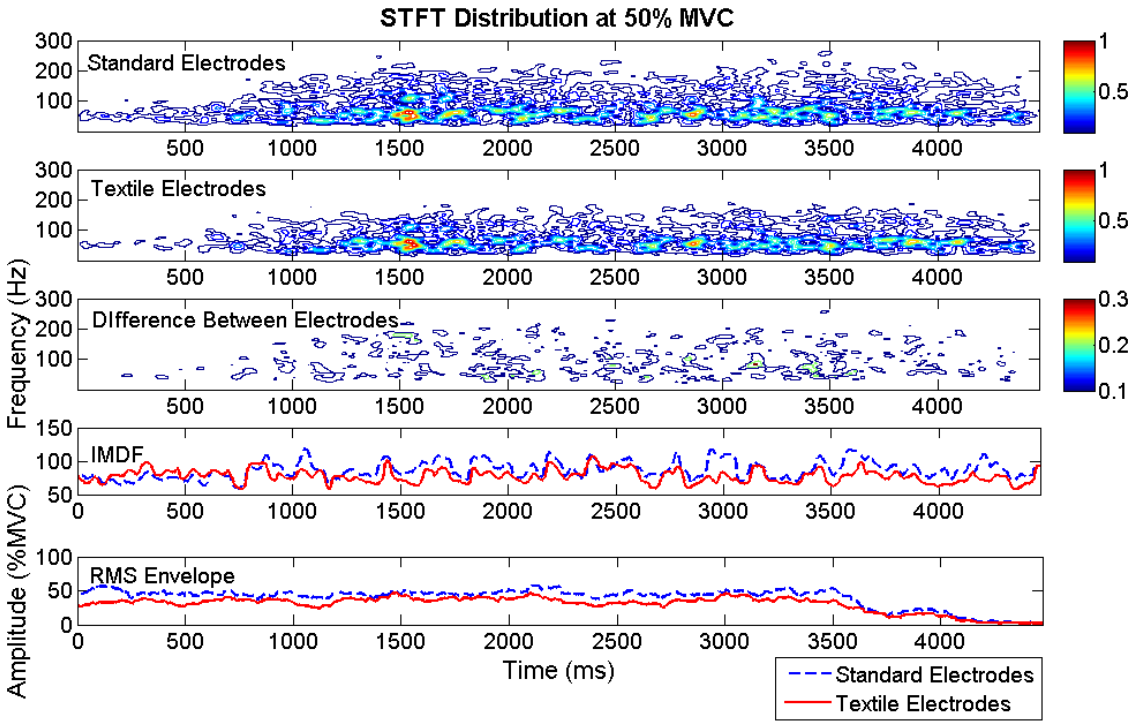

Figure 6.14 - Spectrogram and IMDF of the EMG measured with the standard and the textile electrodes at 50% MVC.

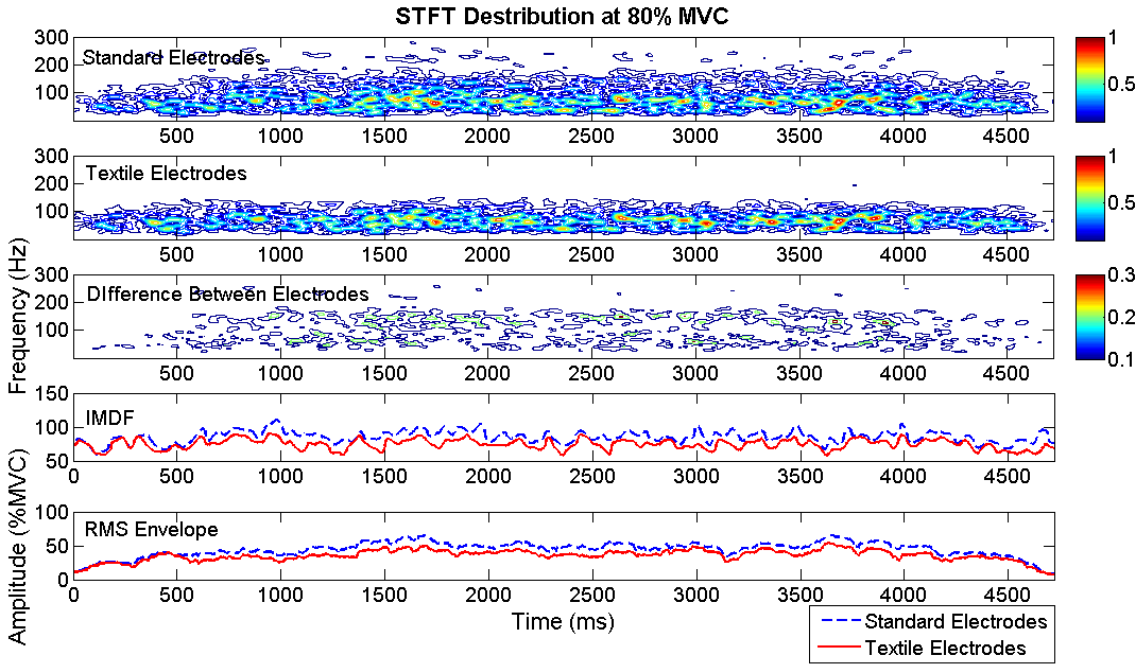

Figure 6.15 - Spectrogram and IMDF of the EMG measured with the standard and the textile electrodes at 80% MVC.

6.4. Discussion

During the study undertaken to validate the use of textile electrodes for measuring the EMG traces of isometric voluntary contractions on the *biceps brachii*, it became evident that the textile electrodes imprinted themselves on the skin, leaving a mark that could be seen after their removal. According to Marozas (2011), the presence of imprints suggests a good contact between the electrodes and the skin, reducing the probability of the electrode changing position. In addition, the textile electrodes did not leave any sign of skin irritation caused either by the conductive gel or any kind of adhesive. These are desirable outcomes when using textile electrodes, since they are in agreement with the philosophy of being completely passive and do not cause any kind of damage to the user.

The morphological analysis of the signal was intended to observe if there were any significant pattern differences between the signals measured by the standard and textile electrodes. The need of such assessment is related with two concerns: the different shape of the electrodes and their simultaneous placement on the *biceps brachii*. According to Hermes (2000), the difference in shape of the standard and textile electrodes would not be a problem because the state of the art showed that there is not much difference between electrodes with different shapes as long as the total area is similar. This did in fact occur with the textile electrodes under validation, since they had a sensory area equal to the standard electrodes. Therefore, the only concern that remained was the difference in the electrode placement. The careful selection of the muscle where the electrodes were placed, the b*iceps brachii* revealed to be a muscle large enough to accommodate two pairs of electrodes over its

muscle belly. When qualitatively compared, signals recorded with both types of electrodes did not show any decisive difference between their overall patterns, even being placed a few centimetres apart. The RMSE between the envelopes of each type of electrode presented small differences that do not jeopardize the textile electrode ability to measure identical patterns. Nevertheless, some participants showed higher amplitude difference between the standard and textile electrode signal, which is reflected in the higher standard deviation of the RMSE values. The noise evaluation performed by the SNR calculation of both signals revealed a small average difference, when compared with the results obtained by authors like Chan (2010) and Laferriere (2011), that also compared non-standard electrodes with standard electrodes for EMG applications. These results indicate that both electrodes have a similar susceptibility to the power-line noise, at 50 Hz, since the frequency analysis of the textile electrodes showed a higher incidence of some other noise harmonics. Nevertheless, the synergetic influence of the 50 Hz noise and its harmonics on the textile electrode only caused an average decrease of one decibel, what in practical terms is almost negligible.

The need to ascertain about some other parameters that usually are targeted in EMG studies, led to the analysis of the maximum value of each of the electrode's envelope. The textile electrodes seem to be capable of measuring the pRMS values, but with smaller amplitudes than the standard electrodes, which can be explained by the practical impossibility of placing each pair of electrodes on the exact same muscle location. The small distance between pair of electrodes, even If they are both in the muscle belly, is enough to cause amplitude differences between the recorded signals (Beck *et al.*, 2008; Rainoldi *et al.*, 2000). The pRMS results support this statement, since the standard electrodes predominantly present higher amplitude than the textile electrodes along all the sub-maximal loads. Although the minimum value for each electrode is very similar, the maximum value shows a big difference in favour of the standard electrode. Despite the lower pRMS mean, the low standard deviation shows that the textile electrodes have a smaller variation than the standard electrodes when measuring this variable.

Several methods are available to performed an EMG envelope onset and offset detection, having Reaz (2006) and Staude (2001) summarized some of the most common methods, for instance the single-threshold method, the double threshold methods, and the model-based statistical approaches. Although being very popular and providing a good visual aid, the single-threshold method depends too much on the threshold chosen by the user, causing missed detections (Thexton, 1996). The double threshold allows a higher detection probability and it can be adapted to the specificities of each signal, but Lanyi (2004) found that this method was too complex, it has a high computational cost and is not too sensitive. In addition, these methods show several degrees of sensitivity according to the signal's noise. The model-based statistical approach provide higher detection rate and higher accuracy than other methods (Staude *et al.*, 2001), but unfortunately it requires a greater computational effort, and when some of the signal's properties are not previously know, it may have a decrease in performance. The TKEO appears as a trade-off between the simplicity of the

threshold methods, the accuracy of the model-based statistical methods, and the immunity to noise (Solnik *et al.*, 2008). By using this method of detection, it was possible to accurately detect the envelope's onset even in measures where the true onset was masked by an amplitude increase that did not corresponded to EMG activity, as can be seen in

Figure 6.7, thus making the iRMS calculation more reliable. By performing the iRMS normalization in function of the activation time it was possible to compensate small variations of the activation time, and thereby compare the area beneath each envelope during the same period of time. The iRMS data show that standard electrodes have a greater area beneath the envelope at all the sub-maximal loads than the textile envelopes, which is in accordance with the results of the pRMS. Even the Bland-Altman diagram distribution is very similar to that of the pRMS, denoting a very close relationship between these two variables. The small difference in terms of mean and standard deviation, and the identical range established by the minimum and maximum values reveal that the standard and textile electrodes measure EMG signals identically. The results provided by the ANOVA statistical analysis ensured that the measurements performed with both types of electrodes at different sub-maximal loads do not have differences.

Frequency analysis was used to analyse the power-frequency content of the signals measured by both types of electrodes. With the data obtained from this analysis, it was observed that the PSD signals had a similar pattern and that the noise frequency, typically present at 50 Hz, was present in both types of electrodes as evidenced by both the Figure 6.10 and Figure 6.11. However, some of the 50 Hz harmonics also appeared, but only in the textile electrodes. This situation can be related with the fact that some adaptions had to be done to enable the connection of the textile electrode with the shielded cables that led the measured signal to the amplifier. While the standard electrodes had a press stud enabling a direct connection with the shielded cable, the textile electrodes did not have this type of connection, being necessary to use regular conductive cables, without any type of shielding to establish a connection interface. This way, the standard electrodes had a direct and shielded connection with the amplifier while the textile electrode's signals had to be transmitted first through a 15 centimetres unshielded cable before getting into the shielded cable. This could have been enough to introduce some of the 50 Hz harmonics only in the textile signal. Considering this, it is difficult to say if the extra noise present in this signal was caused by a higher sensitivity to noise by the textile electrode but, considering the SNR, the noise harmonics do not bring substantial increase in the overall noise. The mean frequency (MNF) and the median frequency (MDF) of a PSD are two variables that provide some basic information about the power-spectrum of a signal, and they usually are reported together. To the purposes of this study only MDF was chosen for comparison, since it is less affected by additive noise, especially those at high frequencies, as the noise harmonics verified on the textile electrode PSD (Merletti & Parker, 2004). The MDF difference between electrodes showed a variation of only three Hertz on all the sub-maximal loads, which is rather small and does not bring any practical constraint. Further, a more detailed analysis of

the power-frequency distribution along the activation period was carried out using STFT. When high power frequencies occurred, both electrodes measured them at the same moment, and their differences in value were relatively small, normally representing a 20% difference between electrodes. Since both electrode's STFT showed good temporal synchronism when measuring high power activation, and the IMF had a similar pattern, it is safe to say that they measured identical power-spectrum at the same time. The overall electrode's PSD differences are thereby more related with their displacement over the muscle belly than with differences in the textile electrode measuring capabilities.

6.5. Conclusions

Several variables normally used to describe the EMG signal characteristics in terms of morphology (pRMS, iRMS, SNR and RMSE), frequency (PSD and MDF), and the power-frequency distribution over time (STFT) were used to compare the measuring capability of the textile electrodes comparatively to the standard electrodes.

Morphological analysis revealed that the textile electrodes are capable of measuring signals with similar patterns but with smaller amplitude, as result of the fact that both electrodes where placed simultaneously on the muscle and thereby amplitudes differences are expected.

The overall noise content was not too different between electrodes, being the higher noise content of the textile electrodes not visually noticeable in its corresponding signal. The frequency analysis showed that this was due to the presence of noise harmonics, but further studies should be conducted in order to verify if this was caused by the electrodes themselves or the interface arrangement. Although there were some overall power differences between PSD signals, they did not represented a substantial difference since the MDF data showed small variations. With the STFT analysis, it became evident that both electrodes measured the higher power-spectrum activation at the same time, and with small differences.

The textile electrodes here studied have a good measuring performance, allowing the measurement of EMG signals identical to the standard electrodes. Thereby, the textile electrodes could be used as a reliable alternative to the standard silver-chloride electrodes in EMG measurement applications with no expense of signal quality, pattern alterations or substantial power-spectrum differences.

Chapter 7

7.1. General Discussion

The electrical properties of the two types of textile electrodes being validated revealed that their material and size were fundamental in providing lower impedance values than the standard electrode. The ECG textile electrode was manufactured using stainless steel, which usually has high impedance, but its higher sensory area reduced the overall impedance allowing it to have the smallest impedance per square centimetre. The EMG textile electrodes, where manufactured with yarns coated with silver, and even presenting an equal sensory area but different shape than the standard electrodes it achieves smaller impedance values.

Both textile electrodes had the problem of fixation, however this was successfully solved using tight cloth in the case of the ECG and an elastic band in the case of the EMG. This allowed a good contact with the skin, but unstable at the same time, letting each small movement cause motion artefacts. These were easily eliminated during the filtration phase of the data processing, but they revealed a susceptibility to motion artefacts by the textile electrodes.

When measuring physiological signals, both textile electrodes presented signals that resembled those obtained with standard electrodes in terms of morphology, time period and frequency content. The ECG data revealed that even with some morphological differences caused by the different electrode placement, each ECG wave period was similar in both electrode's signal, the IRR was exactly the same and the PSD pattern was very similar. With the EMG data this degree of similarity was not possible due to its weak reproducibility. However, it was possible to observe that the EMG pattern of both textile and standard electrodes coincided in several points along the activation phase. The analysis of time-dependent variables like the iRMS was more difficult due to the necessity of detecting the envelope's onset and offset. The use of the TKEO method provided an automatic detection, that allowed a better precision in determine the moments at which the muscle was active.

Both ECG and EMG textile electrodes had a very similar and close resemblance with the standard electrode PSD signals, which suggests that the electrodes are capable of measuring the corresponding physiological signals without causing severe attenuations or amplifications at specific frequency band, preserving the entire frequency range of interest of each signal.

7.2. General Conclusions

Two types of textile electrodes for ECG and EMG measuring applications were presented and validated through comparison with standard silver-chloride electrodes, and their electrical characteristics evaluated by mean of skin-electrode impedance.

The ECG analysis showed that the cardiac waves measured by the ECG textile electrodes are identical to those measured by the standard electrodes, and they do not present any severe temporal and frequency differences. Similar outcome was found in the EMG textile electrodes that were capable of measuring a closely matched pattern with the standard electrode. In addition, this textile electrode did not show significant differences in terms of power-spectrum, or time-frequency spectrum distribution when using different sub-maximal loads.

Some usability considerations can be drawn, since it became evident that textile electrodes have to struggle with the issue of keeping a good skin contact, which is rather difficult when using adhesive bands is not an option. However, if good contact conditions are met, it is possible to measure signals with good quality, in a comfortable manner and without causing any kind of skin irritation. This is particularly true in relation to the EMG textile electrodes, were good skin contact and an almost equal SNR were found.

Results thus suggest that both types of textile electrodes are eligible to be used as an alternative to the standard textile electrodes in rest and isometric measurements, as long as good skin contact is provided.

References

Al-Obaidi, A. A. & M. Meribout (2011). A new enhanced Howland voltage controlled current source circuit for EIT applications. GCC Conference and Exhibition (GCC), 2011 IEEE.

Anliker, U., J. A. Ward, et al. (2004). "AMON: a wearable multiparameter medical monitoring and alert system." Information Technology in Biomedicine, IEEE Transactions on **8**(4): 415-427.

Ariyatum, B., R. Holland, et al. (2005). "The future design direction of smart clothing development." Journal of the Textile Institute **96**(4): 199 - 210.

Baba, A. & M. J. Burke (2008). "Measurement of the electrical properties of the ungelled ECG electrodes." International Journal of Biology and Biomedical Engineering **2**(3): 89-97.

Beck, T. W., T. J. Housh, et al. (2008). "The effects of electrode placement and innervation zone location on the electromyographic amplitude and mean power frequency versus isometric torque relationships for the vastus lateralis muscle." Journal of Electromyography and Kinesiology **18**(2): 317-328.

Beckmann, L. & et al. (2010). "Characterization of textile electrodes and conductors using standardized measurement setups." Physiological Measurement **31**(2): 233.

Benito-Lopez, F., S. Coyle, et al. (2010). Sweat-on-a-chip: Analysing sweat in real time with disposable micro-devices. Sensors, 2010 IEEE.

Bifulco, P., M. Cesarelli, et al. (2011). A wearable device for recording of biopotentials and body movements. Medical Measurements and Applications Proceedings (MeMeA), 2011 IEEE International Workshop on.

Bland, M. J. & D. G. Altman (1986). "Statistical methods for assessing agreement between two methots of clinical measurement." The Lancet **327**(8476): 307-310.

Bonfiglio, A. & D. E. Rossi (2010). Wearable Monitoring Systems, Springer.

Borges, L. M., A. Rente, et al. (2008). Overview of progress in Smart-Clothing project for health monitoring and sport applications. Applied Sciences on Biomedical and Communication Technologies, 2008. ISABEL '08. First International Symposium on.

Bourdon, L., S. Coli, et al. (2005). First results with the wealthy garment electrocardiogram monitoring system. Computers in Cardiology, 2005.

Bouwstra, S., L. Feijs, et al. (2009). Smart Jacket Design for Neonatal Monitoring with Wearable Sensors. Wearable and Implantable Body Sensor Networks, 2009. BSN 2009. Sixth International Workshop on.

Brady, S., L. E. Dunne, et al. (2005). Garment-based monitoring of respiration rate using a foam pressure sensor. Wearable Computers, 2005. Proceedings. Ninth IEEE International Symposium on.

Browning, R. C., E. A. Baker, et al. (2006). "Effects of obesity and sex on the energetic cost and preferred speed of walking." Journal of Applied Physiology **100**(2): 390-398.

Catrysse, M., R. Puers, et al. (2004). "Towards the integration of textile sensors in a wireless monitoring suit." Sensors and Actuators A: Physical **114**(2-3): 302-311.

Chan, A. D. C. & E. D. Lemaire (2010). Flexible dry electrode for recording surface electromyogram. Instrumentation and Measurement Technology Conference (I2MTC), 2010 IEEE.
Chan, A. Y. K. (2008). Biomedical Device Technology: Principles And Design, Charles C. Thomas.
Chen, D. X., X. Deng, et al. (2010). "Comparison of three current sources for single-electrode capacitance measurement." **81**(3).
Collins, G. E. & L. J. Buckley (1996). "Conductive polymer-coated fabrics for chemical sensing." Synthetic Metals **78**(2): 93-101.
Coosemans, J., B. Hermans, et al. (2005). Integrating wireless ECG monitoring in textiles. Solid-State Sensors, Actuators and Microsystems, 2005. Digest of Technical Papers. TRANSDUCERS '05. The 13th International Conference on.
Coosemans, J., B. Hermans, et al. (2006). "Integrating wireless ECG monitoring in textiles." Sensors and Actuators A: Physical **130–131**(0): 48-53.
Costa, M. V., L. A. Pereira, et al. (2010). Fourier and wavelet spectral analysis of EMG signals in maximal constant load dynamic exercise. Engineering in Medicine and Biology Society (EMBC), 2010 Annual International Conference of the IEEE.
Coyle, S., K.-T. Lau, et al. (2010). "BIOTEX: biosensing textiles for personalized healthcare management." Trans. Info. Tech. Biomed. **14**(2): 364-370.
Coyle, S., D. Morris, et al. (2009). Textile sensors to measure sweat pH and sweat-rate during exercise. Pervasive Computing Technologies for Healthcare, 2009. PervasiveHealth 2009. 3rd International Conference on.
De Rossi, D., A. D. Santa, et al. (1997). Dressware: wearable piezo- and thermoresistive fabrics for ergonomics and rehabilitation. Engineering in Medicine and Biology Society, 1997. Proceedings of the 19th Annual International Conference of the IEEE.
Di Rienzo, M., P. Meriggi, et al. (2010). "Textile Technology for the Vital Signs Monitoring in Telemedicine and Extreme Environments." Information Technology in Biomedicine, IEEE Transactions on **14**(3): 711-717.
Di Rienzo, M., F. Rizzo, et al. (2007). MagIC: a Textile System for Vital Signs Monitoring. Advancement in Design and Embedded Intelligence for Daily Life Applications. Engineering in Medicine and Biology Society, 2007. EMBS 2007. 29th Annual International Conference of the IEEE.
Di Rienzo, M., F. Rizzo, et al. (2005). A textile-based wearable system for vital sign monitoring: applicability in cardiac patients. Computers in Cardiology, 2005.
Dittmar, A., R. Meffre, et al. (2005). Wearable Medical Devices Using Textile and Flexible Technologies for Ambulatory Monitoring. Engineering in Medicine and Biology Society, 2005. IEEE-EMBS 2005. 27th Annual International Conference of the.
Dunne, L. E., P. Walsh, et al. (2006). Design and Evaluation of a Wearable Optical Sensor for Monitoring Seated Spinal Posture. Wearable Computers, 2006 10th IEEE International Symposium on.
El-Sherif, M., L. Bansal, et al. (2007). "Fiber optic sensors for detection of toxic and biological threats." Sensors **7**(12): 3100-3118.
Enzo Pasquale, S., A. Gemignani, et al. (2005). "Performance evaluation of sensing fabrics for monitoring physiological and biomechanical variables." Information Technology in Biomedicine, IEEE Transactions on **9**(3): 345-352.
Fabrice, A., P. M. Schmitt, et al. (2005). "Flexible technologies and smart clothing for citizen medicine, home healthcare, and disease prevention." Information Technology in Biomedicine, IEEE Transactions on **9**(3): 325-336.
FEUP. (2010). "PROLIMB - Sensorização Electrónica para a Profilaxia de Patologias dos Membros Inferiores." Retrieved 27 July, 2012, from http://sigarra.up.pt/feup/projectos_geral.mostra_projecto?P_ID=1527.
Franco, S. (2002). Design with operational amplifiers and analog integrated circuits, McGraw-Hill.
Gamelin, F. X., S. Berthoin, et al. (2006). "Validity of the Polar S810 Heart Rate Monitor to Measure R-R Intervals at Rest." Medicine & Science in Sports & Exercise **38**(5): 887-893.

Gibbs, P. & H. H. Asada (2004). Wearable conductive fiber sensor arrays for measuring multi-axis joint motion. Engineering in Medicine and Biology Society, 2004. IEMBS '04. 26th Annual International Conference of the IEEE.

Gilsoo, C., J. Keesam, et al. (2011). "Performance Evaluation of Textile-Based Electrodes and Motion Sensors for Smart Clothing." Sensors Journal, IEEE **11**(12): 3183-3193.

Giorgino, T., F. Lorussi, et al. (2006). Posture Classification via Wearable Strain Sensors for Neurological Rehabilitation. Engineering in Medicine and Biology Society, 2006. EMBS '06. 28th Annual International Conference of the IEEE.

Gonçalves, P., S. Pereira, et al. (2006). "Underwater electromyograph system and his dialog with other instrumentation." Revista Portuguesa de Ciências do Desporto **6**(Supl.1): 21.

Gopalsamy, C., S. Park, et al. (1999). "The Wearable Motherboard™: The first generation of adaptive and responsive textile structures (ARTS) for medical applications." Virtual Reality **4**(3): 152-168.

Gruetzmann, A., S. Hansen, et al. (2007). "Novel dry electrodes for ECG monitoring." Physiological Measurement **28**(11): 1375.

Harris, M. & J. Habetha (2007). The MyHeart project: A framework for personal health care applications. Computers in Cardiology, 2007.

Hermens, H. J., B. Freriks, et al. (2000). "Development of recommendations for SEMG sensors and sensor placement procedures." Journal of Electromyography and Kinesiology **10**(5): 361-374.

Hildenbrand, K. & L. Noble (2004). "Abdominal Muscle Activity While Performing Trunk-Flexion Exercises Using the Ab Roller, ABslide, FitBall, and Conventionally Performed Trunk Curls." Journal of athletic training **39**(1): 37-43.

Hui, Z., T. Xiaoming, et al. (2011). Textile-structured human body surface biopotential signal acquisition electrode. Image and Signal Processing (CISP), 2011 4th International Congress on.

INESCTEC. (2011). "PROLIMB Electronic Sensing for the Prophylaxis of Lower Limb Pathologies (2010-2013)." Retrieved 27 July, 2012, from http://oet.inescporto.pt/page4/PosterProLimb.pptx.

Isaacson, D. (1986). "Distinguishability of Conductivities by Electric Current Computed Tomography." Medical Imaging, IEEE Transactions on **5**(2): 91-95.

Ishijima, M. (1997). "Cardiopulmonary monitoring by textile electrodes without subject-awareness of being monitored." Medical and Biological Engineering and Computing **35**(6): 685-690.

Khandpur, R. S. (2003). Handbook of Biomedical Instrumentation. New Delhi, Tata McGraw-Hill Publishing Company Limited.

Kirstein, T., D. Cottet, et al. (2005). Wearable computing systems - electronic textiles. Wearable electronics and photonics T. Xiaoming. Boca Raton, FL, CRC Press**:** 177-197.

Koncar, V. (2005). "Optical Fiber Fabric Displays." Opt. Photon. News **16**(4): 40-44.

Laferriere, P., E. D. Lemaire, et al. (2011). "Surface Electromyographic Signals Using Dry Electrodes." Instrumentation and Measurement, IEEE Transactions on **60**(10): 3259-3268.

Langereis, G., L. de Voogd-Claessen, et al. (2007). ConText: Contactless Sensors For Body Monitoring Incorporated In Textiles. Portable Information Devices, 2007. PORTABLE07. IEEE International Conference on.

Lanyi X., A. A. (2004). An improved method for muscle activation detection during gait. Canadian Conference of Electrical and Computer Engineering. **1:** 357-360.

Lay-Ekuakille, A. & S. C. Mukhopadhyay (2010). Wearable and Autonomous Biomedical Devices and Systems for Smart Environment: Issues and Characterization, Springer.

Lee, I. B., S. C. Shin, et al. (2008). Comparison of conductive fabric sensor and Ag-AgCl sensor under motion artifacts. Engineering in Medicine and Biology Society, 2008. EMBS 2008. 30th Annual International Conference of the IEEE.

Lim, H. (2009). "Smart underwear for diabetic patients." Journal of textile and apparel, technology and management **6**(1).

Lind, E. J., S. Jayaraman, et al. (1997). "A sensate liner for personnel monitoring applications." Acta Astronautica **42**(1-8): 3-9.

Linti, C., H. Horter, et al. (2006). Sensory baby vest for the monitoring of infants. Wearable and Implantable Body Sensor Networks, 2006. BSN 2006. International Workshop on.
Linz, T., L. Gourmelon, et al. (2007). Contactless EMG sensors embroidered onto textile. 4th International Workshop on Wearable and Implantable Body Sensor Networks (BSN 2007). S. Leonhardt, T. Falck and P. Mähönen, Springer Berlin Heidelberg. **13:** 29-34.
Loriga, G., N. Taccini, et al. (2005). Textile Sensing Interfaces for Cardiopulmonary Signs Monitoring. Engineering in Medicine and Biology Society, 2005. IEEE-EMBS 2005. 27th Annual International Conference of the.
Luprano, J. (2009). "BIOTEX: Bio-sensing textile for health management." Retrieved 15 April, 2012, from http://www.biotex-eu.com/default.htm.
Marchant-Forde, R. M., D. J. Marlin, et al. (2004). "Validation of a cardiac monitor for measuring heart rate variability in adult female pigs: accuracy, artefacts and editing." Physiology & Behavior **80**(4): 449-458.
Marozas, V., S. Daukantas, et al. (2011). "A comparison of conductive textile-based and silver/silver-chloride gel electrodes in exercise electrocardiogram recordings." Journal of Electrocardiology **44**(2): e57-e58.
Merletti, R. & P. A. Parker (2004). Electromyography: Physiology, Engineering, and Noninvasive Applications. Hoboken, New Jearsey, IEEE/John Wiley & Sons.
Merritt, C. R. (2008). Electronic Textile-based Sensors and Systems for Long-term Health Monitoring, North Carolina State University.
Mestrovic, M. A., R. J. N. Helmer, et al. (2007). Preliminary study of dry knitted fabric electrodes for physiological monitoring. Intelligent Sensors, Sensor Networks and Information, 2007. ISSNIP 2007. 3rd International Conference on.
Morris, D., S. Coyle, et al. (2009). "Bio-sensing textile based patch with integrated optical detection system for sweat monitoring." Sensors and Actuators B: Chemical **139**(1): 231-236.
Noury, N., A. Dittmar, et al. (2004). VTAMN - A Smart Clothe for Ambulatory Remote Monitoring of Physiological Parameters and Activity. Engineering in Medicine and Biology Society, 2004. IEMBS '04. 26th Annual International Conference of the IEEE.
Oliveira, L. F., T. T. Matta, et al. (2009). "Effect of the shoulder position on the biceps brachii EMG in different dumbbell curls." Journal of Sports Science and Medicine **8**: 24-29.
Ottenbacher, J., S. Romer, et al. (2004). Integration of a Bluetooth based ECG system into clothing. Wearable Computers, 2004. ISWC 2004. Eighth International Symposium on.
Pandian, P. S., K. Mohanavelu, et al. (2008). "Smart Vest: Wearable multi-parameter remote physiological monitoring system." Medical Engineering & Physics **30**: 466-477.
Paradiso, R. & D. De Rossi (2006). Advances in textile technologies for unobtrusive monitoring of vital parameters and movements. Engineering in Medicine and Biology Society, 2006. EMBS '06. 28th Annual International Conference of the IEEE.
Paradiso, R., G. Loriga, et al. (2005). "A wearable health care system based on knitted integrated sensors." Information Technology in Biomedicine, IEEE Transactions on **9**(3): 337-344.
Pease, R. A. (2008). A Comprehensive Study of the Howland Current Pump, National Semiconductor Application Note 1515.
Pola, T. & J. Vanhala (2007). Textile Electrodes in ECG Measurement. Intelligent Sensors, Sensor Networks and Information, 2007. ISSNIP 2007. 3rd International Conference on.
Puurtinen, M. M., S. M. Komulainen, et al. (2006). Measurement of noise and impedance of dry and wet textile electrodes, and textile electrodes with hydrogel. Engineering in Medicine and Biology Society, 2006. EMBS '06. 28th Annual International Conference of the IEEE.
Rainoldi, A., M. Nazzaro, et al. (2000). "Geometrical factors in surface EMG of the vastus medialis and lateralis muscles." Journal of Electromyography and Kinesiology **10**(5): 327-336.
Rattfalt, L., M. Chedid, et al. (2007). Electrical Properties of Textile Electrodes. Engineering in Medicine and Biology Society, 2007. EMBS 2007. 29th Annual International Conference of the IEEE.
Reaz, M., M. Hussain, et al. (2006). "Techniques of EMG signal analysis: detection, processing, classification and applications." Biological Procedures Online **8**(1): 11-35.

Rocha, L. A. & J. H. Correia (2006). Wearable Sensor Network for Body Kinematics Monitoring. Wearable Computers, 2006 10th IEEE International Symposium on.
Rosell, J., J. Colominas, et al. (1988). "Skin impedance from 1 Hz to 1 MHz." Biomedical Engineering, IEEE Transactions on **35**(8): 649-651.
Ross, A. S., G. J. Saulnier, et al. (2003). "Current source design for electrical impedance tomography." Physiological Measurement **24**(2): 509.
Salazar, A. J., A. S. Silva, et al. (2010). An initial experience in wearable monitoring sport systems. Information Technology and Applications in Biomedicine (ITAB), 2010 10th IEEE International Conference on.
Salvo, P., F. Di Francesco, et al. (2010). "A Wearable Sensor for Measuring Sweat Rate." Sensors Journal, IEEE **10**(10): 1557-1558.
Schwartz, S. J. P., Alex (1999). The Smart Vest: Towards a Next Generation Wearable Computing Platform.
Solnik, S., P. DeVita, et al. (2008). "Teager–Kaiser Operator improves the accuracy of EMG onset detection independent of signal-to-noise ratio." Acta of Bioengineering and Biomechanics **10**(2): 65-68.
Staude, G., C. Flachenecker, et al. (2001). "Onset Detection in Surface Electromyographic Signals: A Systematic Comparison of Methods." EURASIP Journal on Advances in Signal Processing **2001**(2): 867853.
Stiz, R. A., P. Bertemes, et al. (2009). "Wide Band Howland Bipolar Current Source using AGC Amplifier." Latin America Transactions, IEEE (Revista IEEE America Latina) **7**(5): 514-518.
Suh, M., K. E. Carroll, et al. (2010). "Critical Review on Smart Clothing Product Development." Journal of textile and apparel, technology and management **6**(4).
Sung, M., R. DeVaul, et al. (2004). Shiver motion and core body temperature classification for wearable soldier health monitoring systems. Wearable Computers, 2004. ISWC 2004. Eighth International Symposium on.
Tabuenca, J. A. (2009). Multichannel Bioimpedance Measurement. Electronic Engineering, Tampere University of Technology. **Master Thesis:** 69.
Tao, X. (2001). Smart technology for textiles and clothing. Smart Fibres, Fabrics and Clothing T. Xiaoming. Boca Raton, FL, CRC Press: 1-6.
Textronic. (2008). "Textronics, Inc. Receives FDA Clearance on Textile Electrode." Retrieved 12, April, 2011, from http://www.textronicsinc.com/press/textronics-inc-receives-fda-clearance-on-textile-electrode.
Thexton, A. J. (1996). "A randomisation method for discriminating between signal and noise in recordings of rhythmic electromyographic activity." Journal of Neuroscience Methods **66**(2): 93-98.
Tröster, G. (2005). The Agenda of Wearable Healthcare. International Medical Informatics Association: Ubiquitous Health Care Systems. R. Haux and C. A. Kulikowski. Stuttgart, Schattauer: 125-138.
Van Langenhove, L. & C. Hertleer (2004). "Smart clothing: a new life." International Journal of Clothing Science and Technology **16**(1/2): 63-72.
Weber, J. L., D. Blanc, et al. (2003). VTAM - a new "biocloth" for ambulatory telemonitoring. Information Technology Applications in Biomedicine, 2003. 4th International IEEE EMBS Special Topic Conference on.
Webster, J. G. & J. W. Clark (2009). Medical Instrumentation: Application and Design, John Wiley & Sons.
Wijesiriwardana, R. (2006). "Inductive fiber-meshed strain and displacement transducers for respiratory measuring systems and motion capturing systems." Sensors Journal, IEEE **6**(3): 571-579.
Xiaoyan Li, A. S. A. (2005). Muscle Activity Onset Time Detection Using Teager-Kaiser Energy Operator. Engineering in Medicine and Biology Society, 27th Annual International Conference. IEEE. Shanghai, China: 7549 - 7552
Xu, P. J., H. Zhang, et al. (2008). "Textile-structured electrodes for electrocardiogram." Textile Progress **40**(4): 183 - 213.
Yuxiang, Y., W. Jue, et al. (2006). "Design and preliminary evaluation of a portable device for the measurement of bioimpedance spectroscopy." Physiological Measurement **27**(12): 1293.

Appendix A

1. Algorithm Structure

The developed algorithm to process and analyse the ECG data is distributed in routines responsible for particular tasks, which are then used by the main algorithm to present results to the user. The chart of Figure A. 1 describes how the various routines work along with the main algorithm.

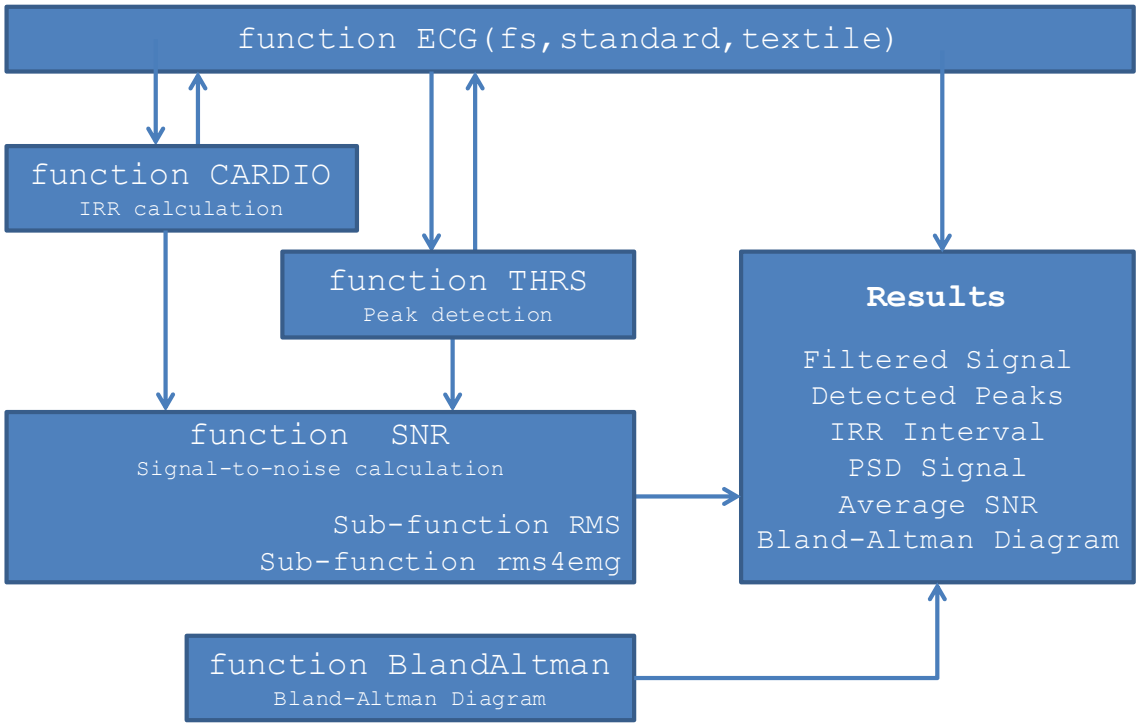

Figure A. 1 – Descriptive chart of the processing and analysis algorithm used with the ECG data and its articulation with the various routines

2. ECG Processing and Analysis

```
function [bandBP,bandBS]=ECG(fs,BIOPAC,BIOSWIM)

%%
%INICIALIZATION
close all;clc;clf;hold off;

%%
%DC-COMPONENT REMOVAL
BIOPAC=BIOPAC-mean(BIOPAC);
BIOSWIM=BIOSWIM-mean(BIOSWIM);

%%
%FILTERING
fnyq=fs/2;
fc_rejeita = [48/fnyq,52/fnyq];
fc_banda = [5/fnyq,100/fnyq];

%Zero phase distortion with square magnitude
[f,e] = butter(2,fc_rejeita,'stop');
notchBP=filtfilt(f,e,BIOPAC);
notchBS=filtfilt(f,e,BIOSWIM);

[f,e] = butter(4,fc_banda);
bandBP=filtfilt(f,e,notchBP);
bandBS=filtfilt(f,e,notchBS);
fprintf('Filtering: DONE\n');

%Signals Correlation
corr_ecg=corr(bandBP,bandBS);
fprintf('Factor de correlação do ECG: %f\n',corr_ecg);

%%
%TIME VARIABLES
time_bp=[0:1/fs:(length(bandBP)-1)*(1/fs)];    %valores temporais
time_bs=[0:1/fs:(length(bandBS)-1)*(1/fs)];    %valores temporais

%%
%PEAKS & CARDIAC VARIABILITY
[R_loc_bp,R_val_bp]=THRS(1000,bandBP);
[R_loc_bs,R_val_bs]=THRS(1000,bandBS);

[RR_bp]=CARDIO(1000,R_loc_bp);
[RR_bs]=CARDIO(1000,R_loc_bs);

fprintf('Peaks detected: DONE\n');
fprintf('Cardiac Variability: DONE\n');

%%
%FREQUENCY ANALYSIS
[PSD_bp,freq]=pwelch(bandBP,hamming(512),[],[],fs,'onesided');
PSD_bp=20*log10(PSD_bp);
[PSD_bs,freq]=pwelch(bandBS,hamming(512),[],[],fs,'onesided');
PSD_bs=20*log10(PSD_bs);
fprintf('PSD: DONE\n');
```

```
%%
%RESULTS
%Signals Visual Comparison
figure(1)
set(gcf,'Color','white')
subplot(3,1,1), plot(time_bp,bandBP);hold on;
      plot(R_loc_bp/fs,R_val_bp,'.r');
      axis([0 max(time_bp) min(bandBP) max(bandBP)]);
subplot(3,1,2), plot(time_bs,bandBS,'r');hold on;
      plot(R_loc_bs/fs,R_val_bs,'.b');
      axis([0 max(time_bs) min(bandBS) max(bandBS)]);
subplot(3,1,3), plot(time_bp,bandBP,'-b');hold on;
      plot(time_bs,bandBS,'r');hold on;
      plot(R_loc_bp/fs,R_val_bp,'.r');hold on;
      plot(R_loc_bs/fs,R_val_bs,'.b');

%IRR Tachogram
figure(2)
set(gcf,'Color','white')
      plot(RR_bp(1,(2:end)),RR_bp(2,(2:end)),'ob');hold on;
      plot(RR_bp(1,(2:end)),RR_bp(2,(2:end)),'b');
      plot(RR_bs(1,(2:end)),RR_bs(2,(2:end)),'.r');hold on;
      plot(RR_bs(1,(2:end)),RR_bs(2,(2:end)),'r');
xlabel('Number of beats','FontSize',12);
ylabel('RR Interval (ms)','FontSize',12);hold off;

%Frequency Spectrum Comparison
figure(3)
set(gcf,'Color','white')
      plot(freq,PSD_bp);hold on;
      plot(freq,PSD_bs,'r')
title(['Power Spectrum Density of EMG sampled at ',
num2str(fs),'Hz',],'FontSize',12, 'FontWeight', 'bold');
legend('BIOPAC System PSD','BIOSWIM System PSD');
xlabel('Frequency (Hz)');
ylabel('Power/Frequency (dB/Hz)');
grid on

end
```

2.1. Peak Detection

```
function [R_loc,R_val]=THRS(fs,bandECG)

t=1/fs:1/fs:length(bandECG)/fs; %time vector
n=60;
l=length(bandECG);
r=bandECG;

s=(r>0.5*max(r)); %70% thresholding
i=1;
picos=[];
while i<=length(s)
    if s(i)==0
        i=i+1;
    else
        v=[];
        while s(i)==1
```

```
            v=[v i];
            i=i+1;
        end
        [y j]=max(r(v));
        picos=[picos [y;v(j)]];
    end
end

R_loc=picos(2,:);
R_val=picos(1,:);
end
```

2.2. IRR Calculation

```
function [RR]=CARDIO(fs,picos)

%Variables inicialization
input = [];
RR=[];

for i=2:length(picos)
        input = [input ((picos(i)-picos(i-1)))];
end

RR(1,:)=[1:1:length(input)+1];

for i=1:length(input)
    RR(2,i+1)=input(i);
end

end
```

2.3. Signal-to-Noise Ratio Calculation

```
function [SNR]=SNR(signal,fs,IRR,R_loc)

env=RMS(signal,fs,31);
alfa=0.567;
beta=0.272;
dif1=alfa.*IRR(2,:);
dif2=beta.*IRR(2,:);
l=length(IRR);

%%
%Isoelectric line boundaries detection
for i=1:1:length(dif1)
      T(i)=R_loc(i)-dif1(i);
      P(i)=R_loc(i)-dif2(i);
end

%%
%SNR Calculation
for j=1:1:length(T)
      medias(j)=mean(env(T(j):P(j)));
      R_val(j)=env(R_loc(j));
```

```
end

for k=2:1:l
      SNR(k-1)=20*log10((R_val(k)-medias(k))/medias(k));
end

%%
%Plot of the envelope signals and marked boundaries
figure;
      plot(env);
      hold on;

for i=1:1:length(R_loc)
      line([R_loc(i) R_loc(i)],[-1 1.5],'color','red');
end

for i=2:1:(length(dif1)-1)
      line([T(i) T(i)],[-1 1.5],'color','green');
      line([P(i) P(i)],[-1 1.5],'color','green');
end

%%
%Resulting mean SNR of the signal
SNRm=mean(SNR)
```

2.3.1. Envelope of the ECG signal

```
% ------------------------------------------------------------------
% RMS Envelope Calculation
%
% Written by:
% Prof. Leandro Machado
% Faculty of Sports of the University of Porto, Portugal
% ------------------------------------------------------------------

function env = RMS(EMG,fs,inttempo)

convolmaxs=zeros(1,4);
ts=1/fs;
time=[0:ts:(length(EMG)-1)*ts];
meio=floor(abs(inttempo/2));
inttempo=2*meio;

for i=1:4
    npt=length(EMG);
    nv=npt-inttempo;
    superRMS=zeros(npt,1);
    abs2rms=EMG.*EMG; %EMG já é um sinal abs
    for ip=1:nv
        iinf=ip;
        isup=ip+inttempo-1;
        superRMS(ip+meio)=rms4emg(time,abs2rms,iinf,isup,inttempo);
    end
    env=superRMS;
end

end
```

```
function valor=rms4emg(t,absx,iinf,isup,inttempo)

% Calculamos la integral de la señal rectificada en ese intervalo:
integrando1=(absx(iinf+1:isup)+absx(iinf:isup-1))./2;
integrando2=t(iinf+1:isup)-t(iinf:isup-1);

[fil1,col1]=size(integrando1);
[fil2,col2]=size(integrando2);

if col1~=col2
   integrando1=integrando1';
end

integral=sum(integrando1.*integrando2);
Tempo=t(isup)-t(iinf);

% Y por último, calculamos la AREMG:
valor=sqrt(integral/Tempo);
end
```

3. Bland-Altman Diagram

```
% ------------------------------------------------------------------
%
% Bland-Altman plot
%
% Bland Altam is a method of data plotting used in analysing the
%agreement between two different assays.
%
% Written by:
% Andrea Padoan
% University Hospital of Padua, Italy
% 12-13-2008
% Adapted by:
% Pedro Fonseca
% Faculty of Engineering, University of Porto, Portugal
% ------------------------------------------------------------------
% Please respect GNU General Public License agreement:
% Someone can distribute this program plus their own modifications.
% Thus, all enhancements and additions to this software must also be
% distributed as free software
% ------------------------------------------------------------------
% You must define data array before use the code. It must contain 3
%columns

function [funxy] = BlandAltman(data)

%%
%Variables optimization
funxy(:,1) = (data(:,2) + data(:,3))/2;  %poin mean between two
methods
funxy(:,2) = data (:,2) - data (:,3);    %point difference between two
methods

%Delete NaN if present. Bland Altman can't use missing values
funxy(any(isnan(funxy),2),:) = [ ];
```

```
%%
%Basic calculations
%Calculate mean of differences
diffmean = mean (funxy (:, 2))

%Calculate standard deviation of difference and confidence interval
sdev = std(funxy(:,2), 1)
twosdev = sdev * 2;

%Calculate max value of the mean
maxx = max (funxy (:, 1));

%Calculate max value of the difference
maxy = max (funxy (:, 2));
if (maxy < twosdev)
      maxy = twosdev;
end

%Add 1 sd to optimize graph
maxy = maxy + sdev;

%Min value of difference
miny = min (funxy (:, 2));
if (miny > -twosdev)
      miny = -twosdev;
end

%Subtract 1 sd to optimize graph
miny = miny - sdev;

%%
%Outliers calculation
a=find(funxy(:,2)>+2*sdev);
b=find(funxy(:,2)<-2*sdev);
c=length(a)+length(b);
l=length(funxy);
out=(c/l)*100;
fprintf('Percentage of outliers: %f\n',out);

%%
%Data plotting
%Scatterplot of funxy
figure (1);
scatter (funxy(:,1), funxy(:,2),'.r');
axis ([-5 maxx miny maxy]);
axis on;
hold on;

%Title and axis titles
title ('Bland-Altman plot');
xlabel ('Average by two assays');
ylabel ('Difference (Assay A - Assay B)');


%Draw 2*sdev line
line ([-5 maxx], [(twosdev+diffmean)
(twosdev+diffmean)],'LineStyle','--');
text (maxx, twosdev, '2SD ', 'Color', 'r' , 'FontSize', 12,
'FontWeight', 'bold');
```

```
line ([-5 maxx], [(diffmean-twosdev) (diffmean-twosdev)],
'LineStyle','--');
text (maxx, -twosdev, '-2SD', 'Color', 'r' , 'FontSize', 12,
'FontWeight', 'bold');

%Draw line as mean of differences
line ([-5 maxx], [diffmean diffmean],'LineStyle','-', 'LineWidth', 2);

%Add text 'mean'
text (maxx, diffmean, 'Mean', 'Color', 'b' , 'FontSize', 14,
'FontWeight', 'bold');

end
```

Appendix B

1. Algorithm Structure

The developed algorithm to process and analyse the EMG data is distributed in routines responsible for particular tasks. Contrary to what happened in Appendix A, the complexity of the variables under study and the computational cost of the spectrogram, requires the use of two main functions (EMG and TFA), as depicted in Figure B.1.

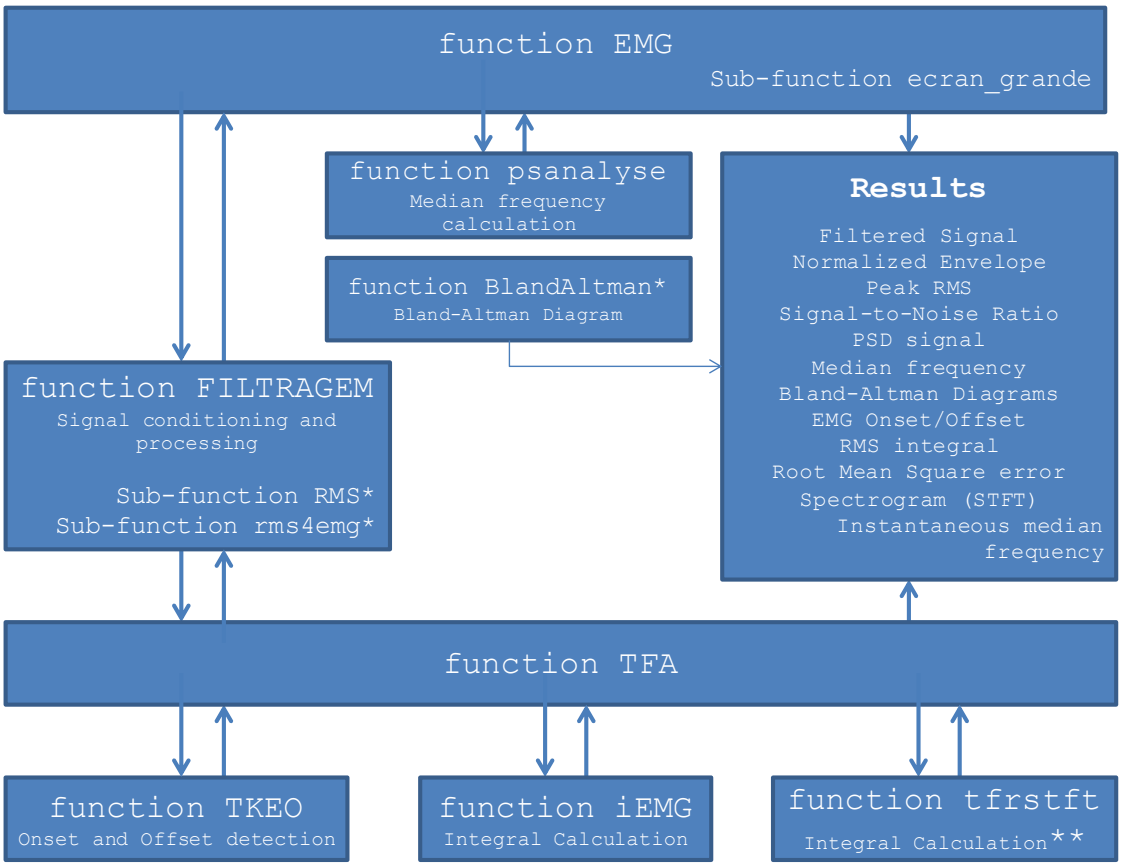

Figure B.1 - Descriptive chart of the processing and analysis algorithm used with the ECG data and its articulation with the various routines. The asterisk (*) refers to a function previously presented in Appendix A, and the double asterisk (**) to a function included in the Matlab Time-Frequency Toolbox.

2. EMG Processing and Analysis (function EMG)

```
function EMG(sujeito)

%%
%GLOBAL VARIABLES

%INICIALIZATION
clc;close all;
fs=1000;
fnyq=fs/2;
format('shortEng');
%%
%PROCESSING MVC FILES
fprintf('<<BEGINNING OF DATA PROCESSING>>\n\n');
fprintf('Load MVC files...\n\n');

%OPEN FILES
[~,pathname] = uigetfile('*.txt', 'Load MVC');
file1=strcat(pathname,sujeito,'_cvm1.txt');
file2=strcat(pathname,sujeito,'_cvm2.txt');
file3=strcat(pathname,sujeito,'_cvm3.txt');
CVM1=load(file1);
CVM2=load(file2);
CVM3=load(file3);
fprintf('BEGINNING OF MVC PROCESSING\n');

%MVC FILTERING
fprintf('Filtering MVC: ...');
[~,~,rmsCVM1_BP]=FILTRAGEM(fs,CVM1(:,1));
[~,~,rmsCVM2_BP]=FILTRAGEM(fs,CVM2(:,1));
[~,~,rmsCVM3_BP]=FILTRAGEM(fs,CVM3(:,1));
[~,~,rmsCVM1_BS]=FILTRAGEM(fs,CVM1(:,2));
[~,~,rmsCVM2_BS]=FILTRAGEM(fs,CVM2(:,2));
[~,~,rmsCVM3_BS]=FILTRAGEM(fs,CVM3(:,2));
fprintf('DONE!\n\n');

CVM_t_BP=vertcat(max(rmsCVM1_BP),max(rmsCVM2_BP));
CVM_t_BP=vertcat(CVM_t_BP,max(rmsCVM3_BP));
CVM_BP_M=max(CVM_t_BP);

CVM_t_BS=vertcat(max(rmsCVM1_BS),max(rmsCVM2_BS));
CVM_t_BS=vertcat(CVM_t_BS,max(rmsCVM3_BS));
CVM_BS_M=max(CVM_t_BS);

figure
ecran_grande
subplot(3,1,1),plot(rmsCVM1_BP); hold on; plot(rmsCVM1_BS,'r');
      title('MVC Envelopes: Select MVC onset and
offset','FontSize',12, 'FontWeight', 'bold');
      [x1,y1]=ginput(2);x1=round(x1);
subplot(3,1,2),plot(rmsCVM2_BP); hold on; plot(rmsCVM2_BS,'r');
      [x2,y2]=ginput(2);x2=round(x2);
subplot(3,1,3),plot(rmsCVM3_BP); hold on; plot(rmsCVM3_BS,'r');
      [x3,y3]=ginput(2);x3=round(x3);
      axis([0 length(rmsCVM1_BP) min(rmsCVM1_BP) max(rmsCVM1_BP)+10]);
close;
```

```
SNR_BP1=20*log10(mean(rmsCVM1_BP(x1(1):x1(2)))/mean(rmsCVM1_BP(x1(1)-
3000:x1(1))));
SNR_BP2=20*log10(mean(rmsCVM2_BP(x2(1):x2(2)))/mean(rmsCVM2_BP(x2(1)-
3000:x2(1))));
SNR_BP3=20*log10(mean(rmsCVM3_BP(x3(1):x3(2)))/mean(rmsCVM3_BP(x3(1)-
3000:x3(1))));
SNR_BS1=20*log10(mean(rmsCVM1_BS(x1(1):x1(2)))/mean(rmsCVM1_BS(x1(1)-
3000:x1(1))));
SNR_BS2=20*log10(mean(rmsCVM2_BS(x2(1):x2(2)))/mean(rmsCVM2_BS(x2(1)-
3000:x2(1))));
SNR_BS3=20*log10(mean(rmsCVM3_BS(x3(1):x3(2)))/mean(rmsCVM3_BS(x3(1)-
3000:x3(1))));

%%
fprintf('BEGINNING OF THE EMG PROCESSING\n');
%EMG SIGNALS

%LOAD FILES
f1=strcat(pathname,sujeito,'_20emg_1.txt');
f2=strcat(pathname,sujeito,'_20emg_2.txt');
f3=strcat(pathname,sujeito,'_20emg_3.txt');

f4=strcat(pathname,sujeito,'_50emg_1.txt');
f5=strcat(pathname,sujeito,'_50emg_2.txt');
f6=strcat(pathname,sujeito,'_50emg_3.txt');

f7=strcat(pathname,sujeito,'_80emg_1.txt');
f8=strcat(pathname,sujeito,'_80emg_2.txt');
f9=strcat(pathname,sujeito,'_80emg_3.txt');

emg20_1=load(f1);
emg20_2=load(f2);
emg20_3=load(f3);

emg50_1=load(f4);
emg50_2=load(f5);
emg50_3=load(f6);

emg80_1=load(f7);
emg80_2=load(f8);
emg80_3=load(f9);

fprintf('Filtering EMG: ...');

%EMGs FILTERING

[band20_BP1,~,rms20_BP1,time20_BP1]=FILTRAGEM(fs,emg20_1(:,1));
[band20_BP2,~,rms20_BP2,time20_BP2]=FILTRAGEM(fs,emg20_2(:,1));
[band20_BP3,~,rms20_BP3,time20_BP3]=FILTRAGEM(fs,emg20_3(:,1));
[band20_BS1,~,rms20_BS1,time20_BS1]=FILTRAGEM(fs,emg20_1(:,2));
[band20_BS2,~,rms20_BS2,time20_BS2]=FILTRAGEM(fs,emg20_2(:,2));
[band20_BS3,~,rms20_BS3,time20_BS3]=FILTRAGEM(fs,emg20_3(:,2));

[band50_BP1,~,rms50_BP1,time50_BP1]=FILTRAGEM(fs,emg50_1(:,1));
[band50_BP2,~,rms50_BP2,time50_BP2]=FILTRAGEM(fs,emg50_2(:,1));
[band50_BP3,~,rms50_BP3,time50_BP3]=FILTRAGEM(fs,emg50_3(:,1));
[band50_BS1,~,rms50_BS1,time50_BS1]=FILTRAGEM(fs,emg50_1(:,2));
[band50_BS2,~,rms50_BS2,time50_BS2]=FILTRAGEM(fs,emg50_2(:,2));
[band50_BS3,~,rms50_BS3,time50_BS3]=FILTRAGEM(fs,emg50_3(:,2));
```

```
[band80_BP1,~,rms80_BP1,time80_BP1]=FILTRAGEM(fs,emg80_1(:,1));
[band80_BP2,~,rms80_BP2,time80_BP2]=FILTRAGEM(fs,emg80_2(:,1));
[band80_BP3,~,rms80_BP3,time80_BP3]=FILTRAGEM(fs,emg80_3(:,1));
[band80_BS1,~,rms80_BS1,time80_BS1]=FILTRAGEM(fs,emg80_1(:,2));
[band80_BS2,~,rms80_BS2,time80_BS2]=FILTRAGEM(fs,emg80_2(:,2));
[band80_BS3,~,rms80_BS3,time80_BS3]=FILTRAGEM(fs,emg80_3(:,2));

fprintf('DONE!\n');

fprintf('Normalization: ...');

%MVC ENVELOPE NORMALIZATION
normRMS20_BP1=(rms20_BP1./CVM_BP_M)*100;
normRMS20_BP2=(rms20_BP2./CVM_BP_M)*100;
normRMS20_BP3=(rms20_BP3./CVM_BP_M)*100;
normRMS20_BS1=(rms20_BS1./CVM_BS_M)*100;
normRMS20_BS2=(rms20_BS2./CVM_BS_M)*100;
normRMS20_BS3=(rms20_BS3./CVM_BS_M)*100;

normRMS50_BP1=(rms50_BP1./CVM_BP_M)*100;
normRMS50_BP2=(rms50_BP2./CVM_BP_M)*100;
normRMS50_BP3=(rms50_BP3./CVM_BP_M)*100;
normRMS50_BS1=(rms50_BS1./CVM_BS_M)*100;
normRMS50_BS2=(rms50_BS2./CVM_BS_M)*100;
normRMS50_BS3=(rms50_BS3./CVM_BS_M)*100;

normRMS80_BP1=(rms80_BP1./CVM_BP_M)*100;
normRMS80_BP2=(rms80_BP2./CVM_BP_M)*100;
normRMS80_BP3=(rms80_BP3./CVM_BP_M)*100;
normRMS80_BS1=(rms80_BS1./CVM_BS_M)*100;
normRMS80_BS2=(rms80_BS2./CVM_BS_M)*100;
normRMS80_BS3=(rms80_BS3./CVM_BS_M)*100;
fprintf('DONE!\n\n');

figure(1)
ecran_grande;
subplot(3,1,1),plot(time20_BP1,normRMS20_BP1); hold on;
plot(time20_BP1,normRMS20_BS1,'r');
    title('EMG envelopes at 20% CVM','FontSize',12, 'FontWeight',
'bold');
    legend('Standard Electrodes','Textile Electrodes');
    xlabel('Time (s)');
    ylabel('Amplitude (%MVC)');
    axis([0 max(time20_BP1) 0 max(normRMS20_BP1)])

subplot(3,1,2),plot(time20_BP2,normRMS20_BP2); hold on;
plot(time20_BP2,normRMS20_BS2,'r');
    legend('Standard Electrodes','Textile Electrodes');
    xlabel('Time (s)');
    ylabel('Amplitude (%MVC)');
    axis([0 max(time20_BP2) 0 max(normRMS20_BP2)])

subplot(3,1,3),plot(time20_BP3,normRMS20_BP3); hold on;
plot(time20_BP3,normRMS20_BS3,'r');
    legend('Standard Electrodes','Textile Electrodes');
    xlabel('Time (s)');
    ylabel('Amplitude (%MVC)');
    axis([0 max(time20_BP3) 0 max(normRMS20_BP3)])
saveas(gcf,strcat(sujeito,'_20emg'),'jpg');
```

```
figure(2)
ecran_grande;
subplot(3,1,1),plot(time50_BP1,normRMS50_BP1); hold on;
plot(time50_BP1,normRMS50_BS1,'r');
    title('EMG envelopes at 50% CVM','FontSize',12, 'FontWeight',
'bold');
    legend('Standard Electrodes','Textile Electrodes');
    xlabel('Time (s)');
    ylabel('Amplitude (%MVC)');
    axis([0 max(time50_BP1) 0 max(normRMS50_BP1)])

subplot(3,1,2),plot(time50_BP2,normRMS50_BP2); hold on;
plot(time50_BP2,normRMS50_BS2,'r');
    legend('Standard Electrodes','Textile Electrodes');
    xlabel('Time (s)');
    ylabel('Amplitude (%MVC)');
    axis([0 max(time50_BP2) 0 max(normRMS50_BP2)])

subplot(3,1,3),plot(time50_BP3,normRMS50_BP3); hold on;
plot(time50_BP3,normRMS50_BS3,'r');
    legend('Standard Electrodes','Textile Electrodes');
    xlabel('Time (s)');
    ylabel('Amplitude (%MVC)');
    axis([0 max(time50_BP3) 0 max(normRMS50_BP3)])
saveas(gcf,strcat(sujeito,'_50emg'),'jpg');

figure(3)
ecran_grande;
subplot(3,1,1),plot(time80_BP1,normRMS80_BP1); hold on;
plot(time80_BP1,normRMS80_BS1,'r');
    title('EMG envelopes at 80% CVM','FontSize',12, 'FontWeight',
'bold');
    legend('Standard Electrodes','Textile Electrodes');
    xlabel('Time (s)');
    ylabel('Amplitude (%MVC)');
    axis([0 max(time80_BP1) 0 max(normRMS80_BP1)])

subplot(3,1,2),plot(time80_BP2,normRMS80_BP2); hold on;
plot(time80_BP2,normRMS80_BS2,'r');
    legend('Standard Electrodes','Textile Electrodes');
    xlabel('Time (s)');
    ylabel('Amplitude (%MVC)');
    axis([0 max(time80_BP2) 0 max(normRMS80_BP2)])

subplot(3,1,3),plot(time80_BP3,normRMS80_BP3); hold on;
plot(time80_BP3,normRMS80_BS3,'r');
    legend('Standard Electrodes','Textile Electrodes');
    xlabel('Time (s)');
    ylabel('Amplitude (%MVC)');
    axis([0 max(time80_BP3) 0 max(normRMS80_BP3)])
saveas(gcf,strcat(sujeito,'_80emg'),'jpg');

%%
fprintf('BEGINNING EMG FREQUENCY ANALYSIS\n');

fprintf('Frequency Analysis: ...\n');

[PSD20_BP1,freq]=pwelch(band20_BP1,hamming(256),[],[],fs,'onesided');
[PSD20_BP2,~]=pwelch(band20_BP2,hamming(256),[],[],fs,'onesided');
```

```
[PSD20_BP3,~]=pwelch(band20_BP3,hamming(256),[],[],fs,'onesided');
[PSD20_BS1,~]=pwelch(band20_BS1,hamming(256),[],[],fs,'onesided');
[PSD20_BS2,~]=pwelch(band20_BS2,hamming(256),[],[],fs,'onesided');
[PSD20_BS3,~]=pwelch(band20_BS3,hamming(256),[],[],fs,'onesided');

PSD20_BP1=10*log10(PSD20_BP1./max(PSD20_BP1));
PSD20_BP2=10*log10(PSD20_BP2./max(PSD20_BP2));
PSD20_BP3=10*log10(PSD20_BP3./max(PSD20_BP3));
PSD20_BS1=10*log10(PSD20_BS1./max(PSD20_BS1));
PSD20_BS2=10*log10(PSD20_BS2./max(PSD20_BS2));
PSD20_BS3=10*log10(PSD20_BS3./max(PSD20_BS3));

PSD_med20_BP1=psanalyse(freq,PSD20_BP1);
PSD_med20_BS1=psanalyse(freq,PSD20_BS1);
PSD_med20_BP2=psanalyse(freq,PSD20_BP2);
PSD_med20_BS2=psanalyse(freq,PSD20_BS2);
PSD_med20_BP3=psanalyse(freq,PSD20_BP3);
PSD_med20_BS3=psanalyse(freq,PSD20_BS3);

[PSD50_BP1,freq]=pwelch(band50_BP1,hamming(256),[],[],fs,'onesided');
[PSD50_BP2,~]=pwelch(band50_BP2,hamming(256),[],[],fs,'onesided');
[PSD50_BP3,~]=pwelch(band50_BP3,hamming(256),[],[],fs,'onesided');
[PSD50_BS1,~]=pwelch(band50_BS1,hamming(256),[],[],fs,'onesided');
[PSD50_BS2,~]=pwelch(band50_BS2,hamming(256),[],[],fs,'onesided');
[PSD50_BS3,~]=pwelch(band50_BS3,hamming(256),[],[],fs,'onesided');

PSD50_BP1=10*log10(PSD50_BP1./max(PSD50_BP1));
PSD50_BP2=10*log10(PSD50_BP2./max(PSD50_BP2));
PSD50_BP3=10*log10(PSD50_BP3./max(PSD50_BP3));
PSD50_BS1=10*log10(PSD50_BS1./max(PSD50_BS1));
PSD50_BS2=10*log10(PSD50_BS2./max(PSD50_BS2));
PSD50_BS3=10*log10(PSD50_BS3./max(PSD50_BS3));

PSD_med50_BP1=psanalyse(freq,PSD50_BP1);
PSD_med50_BS1=psanalyse(freq,PSD50_BS1);
PSD_med50_BP2=psanalyse(freq,PSD50_BP2);
PSD_med50_BS2=psanalyse(freq,PSD50_BS2);
PSD_med50_BP3=psanalyse(freq,PSD50_BP3);
PSD_med50_BS3=psanalyse(freq,PSD50_BS3);

[PSD80_BP1,freq]=pwelch(band80_BP1,hamming(256),[],[],fs,'onesided');
[PSD80_BP2,~]=pwelch(band80_BP2,hamming(256),[],[],fs,'onesided');
[PSD80_BP3,~]=pwelch(band80_BP3,hamming(256),[],[],fs,'onesided');
[PSD80_BS1,~]=pwelch(band80_BS1,hamming(256),[],[],fs,'onesided');
[PSD80_BS2,~]=pwelch(band80_BS2,hamming(256),[],[],fs,'onesided');
[PSD80_BS3,~]=pwelch(band80_BS3,hamming(256),[],[],fs,'onesided');

PSD80_BP1=10*log10(PSD80_BP1./max(PSD80_BP1));
PSD80_BP2=10*log10(PSD80_BP2./max(PSD80_BP2));
PSD80_BP3=10*log10(PSD80_BP3./max(PSD80_BP3));
PSD80_BS1=10*log10(PSD80_BS1./max(PSD80_BS1));
PSD80_BS2=10*log10(PSD80_BS2./max(PSD80_BS2));
PSD80_BS3=10*log10(PSD80_BS3./max(PSD80_BS3));

PSD_med80_BP1=psanalyse(freq,PSD80_BP1);
PSD_med80_BS1=psanalyse(freq,PSD80_BS1);
PSD_med80_BP2=psanalyse(freq,PSD80_BP2);
PSD_med80_BS2=psanalyse(freq,PSD80_BS2);
PSD_med80_BP3=psanalyse(freq,PSD80_BP3);
PSD_med80_BS3=psanalyse(freq,PSD80_BS3);
```

```
fprintf('DONE!\n\n');

figure(4)
ecran_grande;
subplot(311),plot(freq,PSD20_BP1);hold
on;plot(freq,PSD20_BS1,'r');grid on
    title('PSD distribution with 20%CVM','FontSize',12, 'FontWeight',
'bold')
    legend('Standard Electrodes','Textile Electrodes');
    xlabel('Frequency (Hz)');
    ylabel('Power/Frequency (dB/Hz)');
subplot(312),plot(freq,PSD20_BP2);hold
on;plot(freq,PSD20_BS2,'r');grid on
    legend('Standard Electrodes','Textile Electrodes');
    xlabel('Frequency (Hz)');
    ylabel('Power/Frequency (dB/Hz)');
subplot(313),plot(freq,PSD20_BP3);hold
on;plot(freq,PSD20_BS3,'r');grid on
    legend('Standard Electrodes','Textile Electrodes');
    xlabel('Frequency (Hz)');
    ylabel('Power/Frequency (dB/Hz)');
grid on
saveas(gcf,strcat(sujeito,'_PSD20'),'jpg');

figure(5)
ecran_grande;
subplot(311),plot(freq,PSD50_BP1);hold on;plot(freq,PSD50_BS1,'r');
grid on;
    title('PSD distribution with 50%CVM','FontSize',12, 'FontWeight',
'bold')
    legend('Standard Electrodes','Textile Electrodes');
    xlabel('Frequency (Hz)');
    ylabel('Power/Frequency (dB/Hz)');
subplot(312),plot(freq,PSD50_BP2);hold
on;plot(freq,PSD50_BS2,'r');grid on;
    legend('Standard Electrodes','Textile Electrodes');
    xlabel('Frequency (Hz)');
    ylabel('Power/Frequency (dB/Hz)');
subplot(313),plot(freq,PSD50_BP3);hold
on;plot(freq,PSD50_BS3,'r');grid on;
    legend('Standard Electrodes','Textile Electrodes');
    xlabel('Frequency (Hz)');
    ylabel('Power/Frequency (dB/Hz)');
grid on
saveas(gcf,strcat(sujeito,'_PSD50'),'jpg');

figure(6)
ecran_grande;
subplot(311),plot(freq,PSD80_BP1);hold on;plot(freq,PSD80_BS1,'r');
grid on;
    title('PSD distribution with 80%CVM','FontSize',12, 'FontWeight',
'bold')
    legend('Standard Electrodes','Textile Electrodes');
    xlabel('Frequency (Hz)');
    ylabel('Power/Frequency (dB/Hz)');
subplot(312),plot(freq,PSD80_BP2);hold on;plot(freq,PSD80_BS2,'r');
grid on;
    legend('Standard Electrodes','Textile Electrodes');
    xlabel('Frequency (Hz)');
    ylabel('Power/Frequency (dB/Hz)');
```

```
subplot(313),plot(freq,PSD80_BP3);hold on;plot(freq,PSD80_BS3,'r');
grid on;
    legend('Standard Electrodes','Textile Electrodes');
    xlabel('Frequency (Hz)');
    ylabel('Power/Frequency (dB/Hz)');
grid on
saveas(gcf,strcat(sujeito,'_PSD80'),'jpg');

%%
fprintf('<<END OF PROCESSING>>\n\n');

fprintf('<<RESULTS>>\n\n');

fprintf('SIGNAL-TO-NOISE RATIO\n');
fprintf('SNR BP1: %d\n',SNR_BP1)
fprintf('SNR BS1: %d\n',SNR_BS1)
fprintf('SNR BP2: %d\n',SNR_BP2)
fprintf('SNR BS2: %d\n',SNR_BS2)
fprintf('SNR BP3: %d\n',SNR_BP3)
fprintf('SNR BS3: %d\n',SNR_BS3)

fprintf('MAXIMUM RMS PEAK\n');
fprintf('Maximum RMS Peak at 0.2*MVC BP1: %f\n',max(normRMS20_BP1))
fprintf('Maximum RMS Peak at 0.2*MVC BS1: %f\n',max(normRMS20_BS1))
fprintf('Maximum RMS Peak at 0.2*MVC BP2: %d\n',max(normRMS20_BP2))
fprintf('Maximum RMS Peak at 0.2*MVC BS2: %d\n',max(normRMS20_BS2))
fprintf('Maximum RMS Peak at 0.2*MVC BP3: %d\n',max(normRMS20_BP3))
fprintf('Maximum RMS Peak at 0.2*MVC BS3: %d\n',max(normRMS20_BS3))
fprintf('Maximum RMS Peak at 0.5*MVC BP1: %d\n',max(normRMS50_BP1))
fprintf('Maximum RMS Peak at 0.5*MVC BS1: %d\n',max(normRMS50_BS1))
fprintf('Maximum RMS Peak at 0.5*MVC BP2: %d\n',max(normRMS50_BP2))
fprintf('Maximum RMS Peak at 0.5*MVC BS2: %d\n',max(normRMS50_BS2))
fprintf('Maximum RMS Peak at 0.5*MVC BP3: %d\n',max(normRMS50_BP3))
fprintf('Maximum RMS Peak at 0.5*MVC BS3: %d\n',max(normRMS50_BS3))
fprintf('Maximum RMS Peak at 0.8*MVC BP1: %d\n',max(normRMS80_BP1))
fprintf('Maximum RMS Peak at 0.8*MVC BS1: %d\n',max(normRMS80_BS1))
fprintf('Maximum RMS Peak at 0.8*MVC BP2: %d\n',max(normRMS80_BP2))
fprintf('Maximum RMS Peak at 0.8*MVC BS2: %d\n',max(normRMS80_BS2))
fprintf('Maximum RMS Peak at 0.8*MVC BP3: %d\n',max(normRMS80_BP3))
fprintf('Maximum RMS Peak at 0.8*MVC BS3: %d\n',max(normRMS80_BS3))

fprintf('MEDIAN FREQUENCIES\n');
fprintf('Median Frequency at 0.2*MVC BP1: %d\n',PSD_med20_BP1)
fprintf('Median Frequency at 0.2*MVC BS1: %d\n',PSD_med20_BS1)
fprintf('Median Frequency at 0.2*MVC BP2: %d\n',PSD_med20_BP2)
fprintf('Median Frequency at 0.2*MVC BS2: %d\n',PSD_med20_BS2)
fprintf('Median Frequency at 0.2*MVC BP3: %d\n',PSD_med20_BP3)
fprintf('Median Frequency at 0.2*MVC BS3: %d\n',PSD_med20_BS3)
fprintf('Median Frequency at 0.5*MVC BP1: %d\n',PSD_med50_BP1)
fprintf('Median Frequency at 0.5*MVC BS1: %d\n',PSD_med50_BS1)
fprintf('Median Frequency at 0.5*MVC BP2: %d\n',PSD_med50_BP2)
fprintf('Median Frequency at 0.5*MVC BS2: %d\n',PSD_med50_BS2)
fprintf('Median Frequency at 0.5*MVC BP3: %d\n',PSD_med50_BP3)
fprintf('Median Frequency at 0.5*MVC BS3: %d\n',PSD_med50_BS3)
fprintf('Median Frequency at 0.8*MVC BP1: %d\n',PSD_med80_BP1)
fprintf('Median Frequency at 0.8*MVC BS1: %d\n',PSD_med80_BS1)
fprintf('Median Frequency at 0.8*MVC BP2: %d\n',PSD_med80_BP2)
fprintf('Median Frequency at 0.8*MVC BS2: %d\n',PSD_med80_BS2)
fprintf('Median Frequency at 0.8*MVC BP3: %d\n',PSD_med80_BP3)
fprintf('Median Frequency at 0.8*MVC BS3: %d\n',PSD_med80_BS3)
```

```
RMS_CVM1(:,1)=rmsCVM1_BP;
RMS_CVM1(:,2)=rmsCVM1_BS;
RMS_CVM2(:,1)=rmsCVM2_BP;
RMS_CVM2(:,2)=rmsCVM2_BS;
RMS_CVM3(:,1)=rmsCVM3_BP;
RMS_CVM3(:,2)=rmsCVM3_BS;

RMS20_1(:,1)=normRMS20_BP1;
RMS20_1(:,2)=normRMS20_BS1;
RMS20_2(:,1)=normRMS20_BP2;
RMS20_2(:,2)=normRMS20_BS2;
RMS20_3(:,1)=normRMS20_BP3;
RMS20_3(:,2)=normRMS20_BS3;

RMS50_1(:,1)=normRMS50_BP1;
RMS50_1(:,2)=normRMS50_BS1;
RMS50_2(:,1)=normRMS50_BP2;
RMS50_2(:,2)=normRMS50_BS2;
RMS50_3(:,1)=normRMS50_BP3;
RMS50_3(:,2)=normRMS50_BS3;

RMS80_1(:,1)=normRMS80_BP1;
RMS80_1(:,2)=normRMS80_BS1;
RMS80_2(:,1)=normRMS80_BP2;
RMS80_2(:,2)=normRMS80_BS2;
RMS80_3(:,1)=normRMS80_BP3;
RMS80_3(:,2)=normRMS80_BS3;

PSD20_1(:,1)=PSD20_BP1;
PSD20_1(:,2)=PSD20_BS1;
PSD20_2(:,1)=PSD20_BP2;
PSD20_2(:,2)=PSD20_BS2;
PSD20_3(:,1)=PSD20_BP3;
PSD20_3(:,2)=PSD20_BS3;

PSD50_1(:,1)=PSD50_BP1;
PSD50_1(:,2)=PSD50_BS1;
PSD50_2(:,1)=PSD50_BP2;
PSD50_2(:,2)=PSD50_BS2;
PSD50_3(:,1)=PSD50_BP3;
PSD50_3(:,2)=PSD50_BS3;

PSD80_1(:,1)=PSD80_BP1;
PSD80_1(:,2)=PSD80_BS1;
PSD80_2(:,1)=PSD80_BP2;
PSD80_2(:,2)=PSD80_BS2;
PSD80_3(:,1)=PSD80_BP3;
PSD80_3(:,2)=PSD80_BS3;

end
```

2.1. Screen resizing

```
function ecran_grande

% ------------------------------------------------------------------
% Screen resizing
%
% Written by:
% Prof. Leandro Machado
% Faculty of Sports of the University of Porto, Portugal
% ------------------------------------------------------------------

scrsz=get(0,'ScreenSize');
h=gcf;
set(h,'Position',[scrsz(1)+5 scrsz(2)+70 scrsz(3)-10 scrsz(4)-150]);
figure(h)
clf
```

2.2. EMG Signals Filtering

```
function FILTRAGEM(fs,Sinal);

fnyq=fs/2;
fc_banda=[20/fnyq,499/fnyq];
timeSinal=[0:1/fs:(length(Sinal)-1)*(1/fs)];

%FILTERING
[f,e] = butter(2,fc_banda);
Sinal=filtfilt(f,e,Sinal);
bandSinal=Sinal-mean(Sinal);

%RECTIFICATION
absSinal=abs(bandSinal);

%ENVELOPE
rmsSinal=RMS(absSinal,fs,150);

end
```

2.3. Median Frequency

```
function psanalyse(freq,y)

% ------------------------------------------------------------------
% Median Frequency Calculation
%
% Written by: Brighton University, UK
% www.biomech.brighton.ac.uk/help/emg/psanalyse.m [Offline]
% Adapted by:Pedro Fonseca
% Faculty of Engineering of the University of Porto, Portugal
% ------------------------------------------------------------------


%Fourier Transform of Electromyographic (EMG) Signals
i=[];
%Interpolate to improve signal resolution
```

```
fi=[1:1:500];
yi = interp1(freq,y,fi);
yi=yi(1:497);%Remove NaN in the end of vector
r=0.5*sum(yi);

for n=1:1:497
    if sum(yi(1:n))<=r
        i=n;
        break
    end
end

mf=fi(i);

end
```

3. EMG Processing and Analysis (function TFA)

```
function TFA(sujeito,submax,trial)
close all;clf;
fs=1000;

%OPEN FILES
[~,pathname] = uigetfile('*.txt', 'Load files');
file=strcat(pathname,sujeito,'_',submax,'emg_',trial,'.txt');
cvm1=strcat(pathname,sujeito,'_cvm1.txt');
cvm2=strcat(pathname,sujeito,'_cvm2.txt');
cvm3=strcat(pathname,sujeito,'_cvm3.txt');
emg=load(file);
CVM1=load(cvm1);
CVM2=load(cvm2);
CVM3=load(cvm3);

%MVC FILTERING
[~,~,rmsCVM1_BP]=FILTRAGEM(fs,CVM1(:,1));
[~,~,rmsCVM2_BP]=FILTRAGEM(fs,CVM2(:,1));
[~,~,rmsCVM3_BP]=FILTRAGEM(fs,CVM3(:,1));
[~,~,rmsCVM1_BS]=FILTRAGEM(fs,CVM1(:,2));
[~,~,rmsCVM2_BS]=FILTRAGEM(fs,CVM2(:,2));
[~,~,rmsCVM3_BS]=FILTRAGEM(fs,CVM3(:,2));
fprintf('DONE!\n\n');

%MVC MAXIMUM
CVM_t_BP=vertcat(max(rmsCVM1_BP),max(rmsCVM2_BP));
CVM_t_BP=vertcat(CVM_t_BP,max(rmsCVM3_BP));
CVM_BP_M=max(CVM_t_BP);

CVM_t_BS=vertcat(max(rmsCVM1_BS),max(rmsCVM2_BS));
CVM_t_BS=vertcat(CVM_t_BS,max(rmsCVM3_BS));
CVM_BS_M=max(CVM_t_BS);

%EMG FILTERING AND NORMALIZATION
emg_BP=FILTRAGEM(1000,emg(:,1));
emg_BS=FILTRAGEM(1000,emg(:,2));

env_raw_BP=RMS(emg_BP,fs,150);
env_raw_BS=RMS(emg_BS,fs,150);
```

```
env_BP=(env_raw_BP./CVM_BP_M)*100;
env_BS=(env_raw_BS./CVM_BS_M)*100;

[onset,offset] = TKEO(emg_BP,env_BP,2);

%%
%iRMS CALCULATION
[iBP]=iEMG(fs,env_BP,onset,offset);
[iBS]=iEMG(fs,env_BS,onset,offset);
iBP=(iBP/(offset-onset))*1000;
iBS=(iBS/(offset-onset))*1000;
fprintf('iRMS VALUE\n');
fprintf(strcat('iRMS at  ', submax,'*MVC BP: %f\n'),iBP)
fprintf(strcat('iRMS at  ', submax,'*MVC BS: %f\n'),iBS)

%%
%RMSE CALCULATION
rmse=sqrt(sum((env_BP-env_BS).^2)/(offset-onset));

%%
%SHORT-TIME FOURIER TRANSFORM
%First trial
[tfr_BP,t,f] = tfrstft(emg_BP,onset:offset,fs,hanning(127),0);
[tfr_BS,t,f] = tfrstft(emg_BS,onset:offset,fs,hanning(127),0);
stf_BP=abs(tfr_BP(1:300,:));
stf_BS=abs(tfr_BS(1:300,:));
stf_BP=stf_BP/max(max(stf_BP));
stf_BS=stf_BS/max(max(stf_BS));
differ=abs(stf_BP-stf_BS);

%%
%INSTANTANEOUS MEDIAN FREQUENCY
for i=1:1:(offset-onset)
    medi_BP(i)=medi_stft(stf_BP(:,i));
end
for i=1:1:(offset-onset)
    medi_BS(i)=medi_stft(stf_BS(:,i));
end

%%
%PLOTS
figure(2)
subplot(511),contour(stf_BP,0:0.1:max(max(stf_BP))),colorbar;
title(strcat('STFT distribution with ',submax,'CVM'),'FontSize',12,
'FontWeight', 'bold')
    xlabel('Time (ms)');
    ylabel('Frequency (Hz)');
subplot(512),contour(stf_BS,0:0.1:max(max(stf_BS))),colorbar;
    xlabel('Time (ms)');
    ylabel('Frequency (Hz)');
subplot(513),contour(differ,0:0.1:max(max(differ))),colorbar;
    xlabel('Time (ms)');
    ylabel('Frequency (Hz)');
subplot(514),plot(medi_BP);hold on;plot(medi_BS,'r');
    legend('Standard Electrodes','Textile Electrodes');
    xlabel('Time (ms)');
    ylabel('Frequency (Hz)');
subplot(515),plot(env_BP(onset:offset));hold
on;plot(env_BS(onset:offset),'r');
```

```
    legend('Standard Electrodes','Textile Electrodes');
    xlabel('Time (ms)');
    ylabel('Amplitude (%MVC)');
saveas(gcf,strcat(sujeito,'_',submax,'stft_',trial),'jpg');
end
```

3.1. Detection of the onset and offset

```
function [onset,offset,t,tkeo] = TKEO(x,band,j,n)
% The Teager-Kaiser energy operator n'th order approximation. Omission
of n sets n=0
%x=signal
%j=threshold level

if nargin == 2
    n = 0;
end

%TKEO Signal
t = x(2:end-1).^2 - x(1:end-2).*x(3:end);

%Threshold
th=mean(t(100:1100)+j*std(t(100:1100)));
tkeo=RMS(t,1000,150);

act=[];
act=find(tkeo>th);
niveis=diff(act);
ponto=find(niveis>700);
on=act(1);
off=[];

for i=1:1:numel(niveis)
    if niveis(i)==1
            i=i+1;
    else
        if niveis(i)>1
            off=[off act(i)];
            on=[on act(i+1)];
        end
    end
end

onset=[];
offset=[];

for j=1:1:numel(off)
     if (off(j)-on(j))<1500
         0==0;
     else
         if (off(j)-on(j))>=1500
             onset=[onset on(j)];
             offset=[offset off(j)];
         end
     end
 end
```

```
%Present results
figure(100);
clf;
ecran_grande;
subplot(311),plot(x);hold on;
      line([1 numel(x)],[th th],'color','y');
      hold on;
      for i=1:numel(onset)
            line([onset(i) onset(i)],[0 max(x)],'color','r');
      end
      for i=1:numel(offset)
            line([offset(i) offset(i)],[0 max(x)],'color','g');
      end
      axis([0 numel(x) min(x) max(x)]);
      legend('RMS Envelope');
subplot(312),plot(band);hold on;
      line([1 numel(x)],[th th],'color','y');
      hold on;
      for i=1:numel(onset)
            line([onset(i) onset(i)],[0 max(band)],'color','r');
      end
      for i=1:numel(offset)
            line([offset(i) offset(i)],[0 max(band)],'color','g');
      end
      axis([0 numel(band) min(band) max(band)]);
      legend('Filtered EMG signal');

subplot(313),plot(t);
      hold on;
      for i=1:numel(onset)
            line([onset(i) onset(i)],[0 max(t)],'color','r');
      end
      for i=1:numel(offset)
            line([offset(i) offset(i)],[0 max(t)],'color','g');
      end
      axis([0 numel(t) min(t) max(t)]);
      legend('TKEO envelope signal');

choice='No';
while choice ~'Yes'
      choice = questdlg('Is the onset correct?', ...
    'Verify onset', ...
    'Yes','No','No');

switch choice
    case 'Yes'
        break
    case 'No'
        [loc_on y]=ginput(1);
        onset=[];
        onset(1)=loc_on(1);
        figure(100)
        subplot(311),
            for i=1:numel(onset)
                line([onset(i) onset(i)],[0 max(x)],'color','k');
            end
        axis([0 numel(x) min(x) max(x)]);
        subplot(312),
            for i=1:numel(onset)
                line([onset(i) onset(i)],[0 max(band)],'color','k');
            end
```

```
        axis([0 numel(band) min(band) max(band)]);
        subplot(313),
            for i=1:numel(onset)
                line([onset(i) onset(i)],[0 max(t)],'color','k');
            end
        axis([0 numel(t) min(t) max(t)]);
end
end

choice='No';
while choice ~'Yes'
choice = questdlg('Is the offset correct?', ...
    'Verify offset', ...
    'Yes','No','No');
% Handle response

switch choice
    case 'Yes'
        break
    case 'No'
        [loc_off y]=ginput(1);
        offset=[];
        offset(1)=loc_off(1);
        figure(100);
        subplot(311),
            for i=1:numel(offset)
                line([offset(i) offset(i)],[0 max(x)],'color','k');
            end
        axis([0 numel(x) min(x) max(x)]);
        subplot(312),
            for i=1:numel(offset)
                line([offset(i) offset(i)],[0 max(band)],'color','k');
            end
        axis([0 numel(band) min(band) max(band)]);
        subplot(313),
            for i=1:numel(offset)
                line([offset(i) offset(i)],[0 max(t)],'color','k');
            end
        axis([0 numel(t) min(t) max(t)]);
end

end

onset=round(onset);
offset=round(offset);

end
```

3.2. Integral calculation

```
function [iRMS]=iEMG(fs,sinal,onset,offset);

time=[0:1/fs:(length(sinal)-1)*(1/fs)];

for i=1:1:numel(onset)
iRMS(i)=trapz(time(onset(i):offset(i)),sinal(onset(i):offset(i)));
end

end
```